Fusion of dual frequency fully polarimetric data and hyperspectral data for enhanced land cover classification

SHENBAGA RAJAN VENKATACHALAPERUMAL

MARCH, 2016

ITC SUPERVISOR
Dr. Claudio Persello

IIRS SUPERVISOR
Mr. Vinay Kumar

Fusion of dual frequency fully polarimetric data and hyperspectral data for enhanced land cover classification

SHENBAGA RAJAN VENKATACHALAPERUMAL
Enschede, The Netherlands, March, 2016

Thesis submitted to the Faculty of Geo-Information Science and Earth Observation of the University of Twente in partial fulfilment of the requirements for the degree of Master of Science in Geo-information Science and Earth Observation.
Specialization: Geoinformatics

THESIS ASSESSMENT BOARD:
Chairperson : prof. dr. A. A. Voinov
External Examiner : Dr. Anup Kumar Das
ITC Professor : prof. dr. Ir. A. Stein
ITC Supervisor : Dr. C. Persello
IIRS Supervisor : Mr. Vinay Kumar

OBSERVERS:
ITC Observer : Dr. N.A.S. Hamm
ITC Observer : Dr. V. A. Tolpekin
IIRS Observer : Dr. S. K. Srivastav
IIRS Observer : Dr. Sameer Saran

DISCLAIMER

This document describes work undertaken as part of a programme of study at the Faculty of Geo-Information Science and Earth Observation of the University of Twente. All views and opinions expressed therein remain the sole responsibility of the author, and do not necessarily represent those of the Faculty.

DEDICATED TO ONE AND ALL WHO WERE ON THE SUCCESSFUL COMPLETION OF MY RESEARCH

ABSTRACT

Land cover classification using remotely sensed data is required for providing useful and authentic information about the land cover to solve many land, and related environmental problems. Sometimes individual satellite sensors due to their limitations are not sufficient to distinguish various land cover features. Therefore, the fusion of information from multiple sensors is necessary. Multi-sensor fusion enables an enhanced interpretation and land cover classification by combining the information obtained from different sources (sensors). In this research Hyperion and dual frequency fully polarimetric data, namely, the Radarasat 2 C-band and Advanced Land Observing Satellite – Phased Array type L-band Synthetic Aperture Radar (ALOS - PALSAR) were fused individually. The fusion was performed at three levels namely the pixel level, feature level, and the decision level. In the case of pixel level fusion, High pass filter, Wavelet and Gram-Schmidt fusion techniques were used. To extract features for Feature level fusion, kernel based principal component analysis from Hyperion and multicomponent scattering decomposition parameters from fully Polarimetric Synthetic Aperture Radar (PolSAR) data were used. A feature vector was formed from the features extracted from Hyperion and SAR datasets. One against all strategy of support vector machines was used in case of decision level fusion to decide the final class membership of the defined classes based on the membership values from the generated rule images of the classification. For the classification of the fused images and the individual datasets, the non-linear support vector machines based classification was used. To assess the accuracy, hold out method based cross validation was performed. The measures of accuracy which were taken into account were the overall accuracy, kappa and the individual class accuracies. From the obtained results, it was observed that the high pass filter fusion gave a better result for merging Polarimetric SAR (PolSAR) and hyperspectral data in comparison with the other pixel level fusion techniques used. Among the two pairs (Hyperion + ALOS PALSAR and Hyperion + Radarsat 2), the Hyperion and Radarsat 2 performed better. In the case of feature level fusion and decision level fusion, the Hyperion and ALOS PALSAR pair outperformed the Hyperion and Radarsat 2 pair regarding overall accuracy and kappa. A comparative study was done between the pairs that obtained the highest overall accuracy at three levels, and it was found that the Hyperion and ALOS PALSAR fusion at feature level was able to enhance the land cover classification and gave a better accuracy.

***Keywords**: Multi-sensor fusion, Pixel level, Feature level, Decision level, Support vector machines, Hyperspectral, PolSAR, Span*

ACKNOWLEDGEMENTS

Thanks to a great many people without whom this research work would not have been possible.

Firstly I would like to thank my parents, uncle, brother and my relatives for the encouragement and support they have given throughout my life.

I take immense pleasure to thank my IIRS supervisor Mr. Vinay Kumar for his valuable guidance and assistance he has rendered towards the completion of my research work. His constant support and encouragement meant a lot to me in successfully completing the research.

I would like to thank my ITC supervisor, Dr. Claudio Persello for the suggestions, comments, and remarks that he has given throughout my research work. I owe my sincere gratitude for helping me throughout.

I would like to thank Dr. S K Srivastav for giving valuable suggestions and making sure of proper research progress throughout for all the students. I would also like to thank Dr. Sameer Saran for the suggestions and support he has given for completing the course. I thank Dr. Nicholas Hamm for the support he has given during the course at ITC. I express my sincere gratitude to all the IIRS the ITC faculties for helping me to complete my modules successfully.

Special thanks to my M.Tech friends Gokul, Gokul Prasad, Arasu mani and Sanjay, M.Tech GID friends and Ponraj sir, and Kavita mam for their support and for the lively environment they have provided. Also special thanks to each and every one of my other M.Tech and PGD friends.

Last but not the least, I sincerely thank my MSc friends Aparna, Sayan, Amit, Solanki and Nitin, and Maral, Ipsit, Melkom, and Grace from ITC for the wonderful moments, encouragement and support.

Shenbaga Rajan V

TABLE OF CONTENTS

LIST OF FIGURES

LIST OF TABLES

1. INTRODUCTION

1.1. Background

Land cover classification is a salient application of remotely sensed data. It has its usage in land cover mapping, urban planning, forest cover monitoring, etc. Useful and authentic information about the land cover is required and significant to provide solutions and solve many environmental related problems (Townshend, Justice, Li, Gurney, & McManus, 1991). In remote sensing, in the case of complex urban and industrial areas, the natural vegetation cover and man-made materials appear spectrally similar in moderate resolution optical sensors and even high spatial resolution satellite sensors may not be sufficient to distinguish it (Borghys, Shimoni, Degueldre, & Perneel, 2007). Hence, the information extracted from those sensors are limited which in turn affects the land cover classification and the accuracy of it. This research deals with the fusion of dual frequency fully polarimetric Synthetic Aperture Radar (SAR) and hyperspectral data for the enhanced land cover classification.

Polarimetric SAR means that the RADAR (RAdioactive Detection And Ranging) sends and receives signal in different polarization channels. It measures the received backscatter signals and these signals correspond to different characteristics of the target object. Hence, the complete information about a target can be obtained using Polarimetric SAR. Significant advantages of RADAR are the longer wavelength property than the visible light and also not affected by the atmospheric interference. This property has made the RADAR to be used increasingly for the purpose of Earth Observation (Chandola, 2014). In the case of hyperspectral remote sensing or the imaging spectroscopy, the spectral resolution is the valuable property through which the spectrally similar objects can be differentiated. The term hyperspectral refers to spectra information which consists of a large number of contiguously spaced spectral bands. Each of these sensors provides different useful information which is complementary to each other.

.

Some of the man-made urban classes can be extracted using fully polarimetric Synthetic Aperture Radar (SAR) image based on the surface roughness, geometric and scattering properties of the objects. But in the case of interpretation of trees and vegetation, it is difficult using SAR imagery as the trees produce a bright backscatter as in buildings and identification of different vegetation types is also difficult (Borghys, Shimoni, & Perneel, 2007). The hyperspectral data are useful in extracting different vegetation classes due to the high spectral resolution. Therefore, information extraction from a single sensor does not provide an efficient solution.

It is necessary to make use of information from different sources for better interpretation and classification. The process of combining or merging information from different or multiple sources is termed as data fusion (Knödel et al., 2007). The data fusion preserves the primacy information and utilizes the interdependent information about the multiple sources (Li, Zhang, Zhao, & Shi, 2013). Here the sources are the different sensors. Fusion depends on the level of processing and results in the following approaches,

1. Pixel level data fusion,
2. Feature level data fusion and
3. Decision level data fusion (Pohl & Van Genderen, 1998).

As reviewed by Pohl & Van Genderen (1998) the data fusion levels are shown in the diagram (Figure 1.1) below.

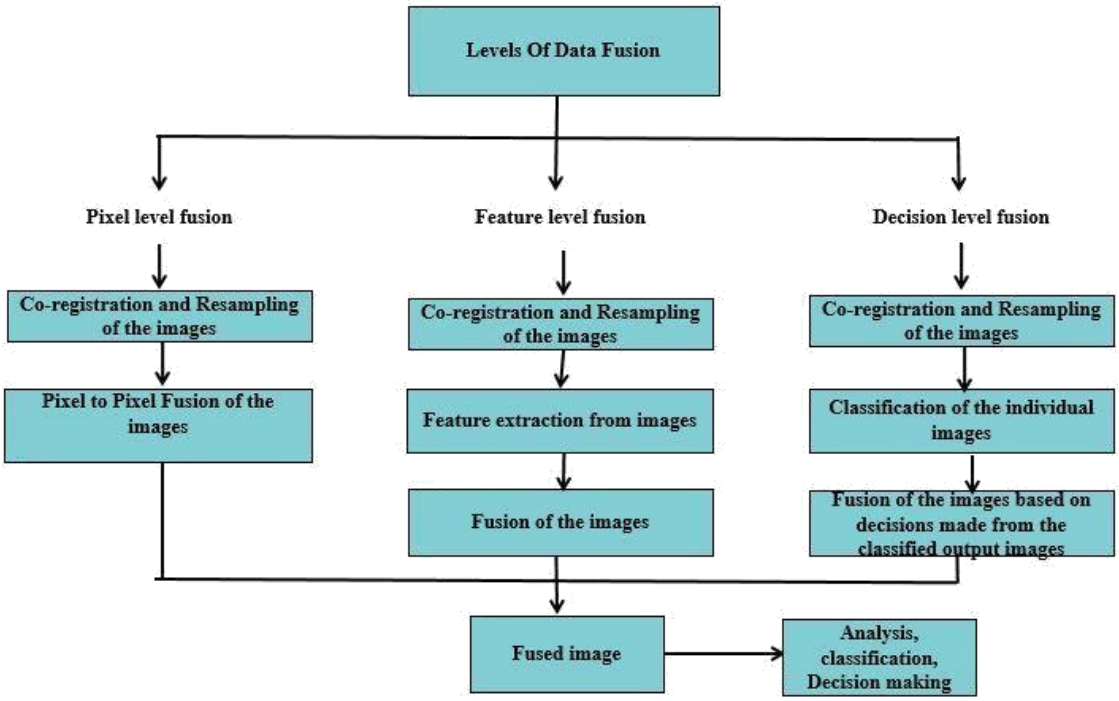

Figure 1-1 Levels of fusion

1.2. Motivation and Problem Statement:

Information extracted from the individual spaceborne remote sensing sensors are very limited when there is a low spectral, spatial resolution which in turn affects the land cover classification and also the accuracy of it. Fusion of images, as well as information from different sensors, have been found productive by improving the feature extraction and classification. The fused images contain more reliable information as the contents from multiple sources are combined. The PolSAR could provide information about urban and man-made targets using different parameters such as scattering information, textural properties, surface roughness, etc. Where as the hyperspectral data could provide the detailed information on the spectrally similar features. Fusion of the above sources could improve the interpretation of features and the classification..

1.3. Research objectives

The objective of this research is to enhance and improve the land cover classification accuracy by the fusion of dual frequency fully polarimetric SAR and hyperspectral data

1.3.1. Sub Objectives:

- ✓ Extraction of polarimetric parameters (Multi component scattering model (MCSM) and Span) from the fully polarimetric data.
- ✓ To Perform Pixel level fusion of hyperspectral data with span data which is the total intensity backscatter image extracted from quadpol data and classification of the fused images
- ✓ To Perform feature and decision level fusion of hyperspectral data with polarimetric parameters extracted from quadpol data and classification of the fused results
- ✓ Comparative analysis of all classified results of the fused products

1.4. Research questions

- ✓ How multicomponent scattering model improves the feature extraction using fully polarimetric data?
- ✓ Which pixel level fusion technique could give a satisfactory result for fusing hyperspectral

data with span data extracted from quadpol data?

- ✓ How fusion of fully polarimetric SAR and hyperspectral data efficiently enhances the classification of urban and natural vegetation cover types?

- ✓ Which level of fusion and also which fully polarimetric SAR data along with hyperspectral data can give an enhanced land cover classification?

1.5. Innovation aimed at

- ✓ To make use of dual frequency fully polarimetric SAR data in the fusion process with the hyperspectral data.

- ✓ To use polarimetric parameters extracted from MCSM for the fusion process.

1.6. Thesis Structure

This thesis accounts for the work done so far for this particular research work in following chapters. A brief introduction about this research, objectives to be accomplished and research formulated based on the objectives are given in the *first* chapter. The *Second* chapter describes the previous work that has been done related to this work and the methods used. The *third* chapter explains about the study area and the dataset used, the *fourth* chapter explains about the methodology and the methods adopted, the *fifth* chapter explains about the results and discussion, and the *sixth* chapter is about the conclusions of the research and the recommendations for future work.

The following chapter is on a literature review of previous studies done and methods adopted by the researchers on data/image fusion.

2. LITERATURE REVIEW

This chapter is about the literature review on the multi-sensor image/data fusion, different levels of image/data fusion and the previous research works done on image/data fusion at various levels. Also, review on SVM classification and MCSM decomposition technique of SAR is given in the separate sections of this chapter

2.1. Multi- Sensor image fusion

Many satellite imageries have become available with the development of multiple types of remote sensing sensors on board satellites. Each sensor has its own advantage and disadvantage of acquiring and extracting information of the land features. Multiple sensor image fusion enables the extraction of useful information that is not possible to obtain from a single sensor (Dong, Zhuang, Huang, & Fu, 2009). The fused images may contain more reliable information as the images with different characteristics are combined (Pohl & Van Genderen, 1998). Also, the images used for the fusion vary in spatial, spectral characteristics and also with time. Hence provides a complete view of the features observed (Pohl, Munro, & van Genderen, 1997)

As reviewed by Pohl & Van Genderen (1998)there are several aspects to be looked at in the muti sensor data fusion. They are the objective/application of the user, selection of sensors based on their complementary characteristics like spatial, spectral and temporal resolutions, necessary pre-processing steps like geometric correction, resampling method, etc. and the most importantly the best fusion technique to be applied. Apart from these aspects, there are several other challenges faced by the researchers in multi-sensor fusion.

The challenges are the integration of more number of spectral bands which increases the processing complexity, high resolution images require higher geometric correction accuracy, the geometric and radiometric correction requirements, shadow features may appear due to different observation angles of the sensors (Pohl & van Genderen, 2014). Apart from the above challenges the selection of bands for the fusion process is one of the important considerations to be taken into account for the fusion process. The band selection comes into picture when some of the fusion processes take only three input bands for the processing, for example, Intensity Hue Saturation (IHS) fusion technique. As reviewed by Pohl & Van Genderen (1998)the band selection could be made by optimum index factor and the feature extraction to select the uncorrelated components could be done using principle component analysis. Depending on the approach and the level of processing, there are three different levels of fusion (Pohl & Van Genderen, 1998). They are Pixel level, Feature level, and Decision level fusion techniques.

Pixel level refers to the lowest processing level of image fusion by merging the measured physical parameters. Fusion at feature level requires the extraction of objects recognized in the various data source. Decision level fusion represents a method that uses value-added data where the input images are processed individually for information extraction. There are several objectives and achievements that can be attained using multi sensor image fusion techniques.

The main goals of applying fusion techniques could be to sharpen the image by improving the spatial and spectral resolution of the fused image, to enhance the extraction of certain features and information, for change detection which depends on the temporal aspects of the different sensors, for improving the classification by combining multiple source data for processing, to replace defective data as the images acquired by the satellites are influenced by numerous effects such as noise, cloud cover, blurred features etc. (Pohl & Van Genderen, 1998).

2.2. Pixel level fusion

The lowest processing level of fusion is the pixel level fusion where the measured physical parameters from two or more images are merged. As reviewed by Pohl & Genderen (2015) there are several pixel level fusion algorithms categorized in general as colour related and statistical related fusion techniques. The colour related techniques include the Intensity Hue Saturation fusion, Red Green Blue transformation fusion and YIQ fusion where Y represents the luma information that is the brightness of an image and I, Q represents the chrominance of the image. The statistical and the numerical methods include the Principal component analysis (PCA), Wavelet Transform, High pass filter (HPF), Regression variable substitution, Brovey transform and component substitution. . The PCA works on the principle of principal component transformation. The optical imagery is first resampled and transformed into principal components, and the first component is replaced with the panchromatic (PAN) image to fuse with the optical imagery using inverse PCA to get the fused product with high spectral and spatial content (Metwalli, Nasr, Allah, El-Rabaie, & El-Samie, 2010). Brovey transform is based on the arithmetic operations, wavelet fusion and high pass filter fusions are based on the extracting high frequency information content using filters and the component substitution is similar to the PCA method which works on the basis of forward transformation of the optical data and then follows the component substitution where the new data space is replaced with the high resolution band. Finally, the fused result is obtained by the inverse transform back to the original space. Regression variable based pixel level fusion was performed by Meng, Borders, & Madden,(2010) using Kriging. Here the correlation between the response variable (an image that needs to be fused) and the predictor variable (image with finer spatial resolution). Many types of research have been done in the past on pixel level fusion.

An improved Intensity Hue Saturation (IHS) transform based pixel level fusion was used by Ghanbari &

Sahebi (2014) in their research to fuse IKONOS multispectral and SAR HH band images. Both spectrally and spatially the fused image was comparatively good with other fusion techniques such as brovey and IHS. Amarsaikhan et al. (2010) compared the performances of different techniques such as PCA, brovey, Ehler's fusion and wavelet transform on fusing SAR and Optical imagery. The research resulted that the multi-sensor fusion could enhance the feature extraction. The IHS transformation was used by Chen, Hepner, & Forster (2003) to integrate the high spectral resolution, provided by hyperspectral data and the surface texture information derived from radar data into a single image of an urban area. Lu, Li, Moran, Dutra, & Batistella, (2011) have made a comparison of Radarsat 2 and ALOS PALSAR L fusion with Landsat TM mapper for land cover classification. Different pixel level fusion techniques such as wavelet fusion, High pass filter fusion, PCA and normalized multiplication. It was concluded that wavelet merge and high pass filter merge performed better in comparison with the other techniques.

Ehlers (1991)used IHS transform in the fusion of Landsat TM and pan SPOT data which proved successful in enhancing the spectral and spatial detail of the image. Experiment on Pixel level fusion of Landsat and Spot images, Landsat and Seasat SAR images, IR and visible images were conducted by Li, Manjunath, & Mitra, (1995) using wavelet transform technique and performed better than laplacian pyramid based methods due to the compactness, directional selectivity, and orthogonality of the wavelet transform. Image fusion using Ehler's spectral preserving algorithm was conducted by Klonus & Ehlers (2007). It was concluded that, for a multi sensor fusion, Ehler's fusion provided a better result when compared to other spectral characteristics preserving fusion techniques.

Advanced and complex pixel level fusion techniques like enhanced Gram-Schmidt spectral sharpening was performed by introducing a generalized intensity component for calculating a low resolution PAN image for the fusion process by Aiazzi, Baronti, Selva, & Alparone (2006). The results proved that the above method outperformed the regular Gram-Schmidt fusion in terms of spectral sharpness and high spatial quality. A comparative analysis of HIS, Brovey, and Ehler's fusion techniques were carried out by Abdikan, Sanli, Sunar, & Ehlers (2012) on the image and multispectral SPOT images and concluded that among the fusion techniques used, the Ehler's fusion produced a better result.

2.3. Feature level fusion

Feature level fusion involves the extraction of features from different data sources to form a single feature vector containing all the extracted features and then fused for further understanding (Pohl & Van Genderen, 1998). These extracted features correspond to the characteristics obtained from input images As reviewed by Zheng, Zhang, & Van Genderen (1998) in the feature level fusion different features are targeted by each sensor and feature extraction process in carried out to obtain a combined feature vector from each sensor. The resulted feature vectors are then fused together and forms a joint feature vector. The process of feature

extraction or feature selection plays a significant role in this level of fusion. There are different feature level fusion techniques as discussed by Zheng et al. (1998) which includes Neural networks, Dempster Shafer's theory, Expert systems, Logical templates, Bayesian inference and cluster analysis. Successful implementation of feature level fusion is possible only with the proper extraction and selection of features from the datasets.

There are two approaches defined by Bruzzone & Serpico (2000) for reducing the number of features. They are

(i) Extracting the information contained in the original features through the linear or nonlinear transformations to the original feature space. This method is usually termed as feature extraction

(ii) Derive a subset of the original set of features (bands) that allows separating the land cover classes. This process is commonly called as feature selection.

A high correlation occurs when a large number of features (bands) are obtained, and this leads to the redundancy of information. This occurs when the sensor has a high spectral resolution (Bruzzone & Serpico, 2000).

Research on kernel based feature selection approach was conducted by Persello & Bruzzone (2015) for the classification of hyperspectral data. This research focussed on selecting a subset of features from the hyperspectral image that helps in differentiating the defined classes and does not change across the source and target domains. This research was studied on two hyperspectral images to evaluate the domain stability in the kernel Hilbert space. Here the domain is referred to the images captured in the different geographical area or at different time period. The experimental results showed the improvement in classification accuracy with high generalization capabilities. Swain & Davis, (1981) suggested that the reduction in features helps in improving the classification accuracy by handling Hughes phenomenon and also reduces the computational burden.

Peli, Young, Knox, Ellis, & Bennett (1999) in their paper described that the extraction and selection of features from the data sets as the most important part of the feature-level fusion process for both spectral and SAR imagery that are used for target discrimination and to reduce the effects of registration error. They have also classified the extracted features into three categories as statistics based, Fractal based and correlation based features. The statistics based features use amplitude based statistics to target or characterize a particular area. Fractal-based features calculate the fractal behavior. The correlation-based features measure the level of correlation among the targets.

Another method of extracting features is through texture analysis. This is the way of extracting contextual information. The texture is one of the important parameters of SAR data. Texture based feature extraction was researched, and the fusion of SAR and multispectral imageries was performed by Byun (2014). The Grey level co-occurrence matrix approach was used by the author to extract texture information from SAR amplitude image. Another research on texture based fusion of SAR and multispectral images was performed by Kiema (2002). The author has used the homogeneity measure obtained from the GLCM method for the fusion approach. .

Very limited researches have been done in the past on feature level fusion of multiple sensors. Artificial neural network based feature level fusion was conducted by Giampouras, Charou, & Kesidis (2013). Here the authors used principle component analysis (PCA) as a feature extraction method and formed a feature vector along with the LIght Detection And Ranging (LiDAR) data which was then fused and classified using Bayesian regularization propagation algorithm. A conclusion was made that the classification could be done efficiently with the use of Artificial Neural Network (ANN). Using wavelet transform and neural network An efficient block based feature level image fusion technique was researched by Sheela, Vijayakumar, & Sujatha (2012).The feature extraction and selection was performed which was based on spatial frequency, Energy of Gradient, Edge information, Contrast visibility and variance. Research on feature level fusion was conducted by Huang, Zhang, & Li (2008) and used wavelet transform based feature extraction method and support vector machine for the classification of the formed feature vector using the extracted features. A review was done by Gamba (2013)on different feature level fusion approaches, status, and trends in remote sensing image fusion for urban areas. The author emphasized the growing importance of feature-based fusion and the high potential of spaceborne, airborne and ground-based sensors have in the extracting information of urban scenes.

2.4. Decision level fusion

Decision level fusion is the highest level of fusion among the three fusion levels. Decision level fusion represents a method that uses value-added data where the input images are processed and classified individually for information extraction. The obtained information is then combined applying decision rules to reinforce conventional interpretation and furnish a better understanding of the observed objects (Pohl & Van Genderen, 1998). Decision level fusion is one of the research areas in the field of multi-sensor image fusion and very few researches have been done in the past.

One of the research is in urban and industrial sites identification with the fusion of SAR and hyperspectral imageries. Three types of decision-level fusions namely the weighted majority vote, a method based on Support Vector Machines and based on a binary decision tree were implemented by Borghys et al. (2007) on SAR and hyperspectral imageries for improved object recognition in the region of urban and industrial

sites. It was concluded that the fusion based on decision tree provided a better result when compared with the other two fusion methods. Change detection in urban scenes with the fusion of SAR and Hyperspectral image was performed (Borghys et al., 2007). The expert classifier method was used to implement the decision level fusion and concluded that the adequate information of the changes in urban scenes was obtained.

Bigdeli, Samadzadegan, & Reinartz (2014) performed a decision based fusion of LiDAR and Hyperspectral using multiple support vector machine classifiers for individually classifying the input data sets. For the fusion of the classified outputs Bayesian classification method was used and the adopted method improved the classification accuracy and kappa value than the individual data sets. Another research on decision level fusion using SVM and Random forest as individual classifiers were performed on Landsat 8 and MODIS data by Wang, Li, & Gong (2015) and using the decision rules the images were fused.

Support vector machine based decision level fusion is also a standard method adopted by researchers for fusing multi-sensor datasets**.** Waske & Benediktsson (2007) used dual support vector machine based decision fusion of multi sensor images. Initially, the two sources were individually classified using SVM and then the feature vector was formed from the obtained rule images from both the classification. The rule images contain the distance of a pixel to the decision boundary of the SVM and the maximum value to the hyperplane determines the final class membership (Waske, Menz, & Benediktsson, 2007). Again a second SVM was used to classify the formed feature vector, and final class membership was decided. The research has concluded that the dual SVM based decision fusion of multi-sensor data outperforms other techniques such as majority voting, absolute maximum voting scheme and decision tree based fusion.

2.5. Multi component decomposition model

One of the important applications of polarimetric synthetic aperture radar is the terrain and land use classification. Polarimetric decomposition is the method to extract the ground features based on the scattering properties of the same. Zhang, Zou, Cai, & Zhang (2008) developed the multi component scattering model (MCSM) which consists of five scattering components namely the Surface scattering component, double bounce scattering component, Helix scattering component, Volume scattering component, and wire scattering component. This model is the extended version four component scattering model developed by (Wu, Yang, Zhu, & Zhang, 2014). Wire scattering component is the fifth component added to the MCSM model.

Each of the scattering components has significance in feature extraction. Double bounce scattering, Volume scattering, and Surface scattering are used to describe the polarimetric backscatter of naturally occurring scatterers that are from a pair of orthogonal surfaces (in urban regions), from a cloud of randomly oriented

dipoles and from moderately rough surface respectively and the Helix and Wire scattering is used to describe the polarimetric backscatter of scatterers from man-made objects in the urban areas (Zhang et al., 2008). Decomposition is an important process in case of classification of PolSAR image. MCSM, which is used to describe the polarimetric backscatter of both natural objects and man-made objects, proved useful in classification along with the texture parameter using SVM (Zhang, Zou, Zhang, & Zhang, 2009).

2.6. Support Vector Machines classification

Support vector machines is a non-parametric classifier which is being widely used in the classification of remotely sensed images. A critical review on the kernel methods on support vector machines was made by Bruzzone, Persello, & Chen (2010). The authors have mentioned the main properties of SVM which makes it to be used in most of the remote sensing applications are as follows,

1. The ability of the classifier to be robust in case of Hughes problem.
2. The use of kernel methods to solve the non-linearly separable classification problem.
3. Less time required for the learning process of the model.
4. There is no requirement for the statistical analysis of the training samples to perform the classification as it is a non-parametric method.

In comparison with the traditional and conventional classification methods like maximum likelihood, the minimum distance to mean classifier, etc., the SVM is more robust in handling complex data such as the high dimensionality high resolution satellite images and the Hyperspectral images. Dai, Huang, & Dong (2007) have proved that the support vector machines based classification is more efficient, better in the learning ability and in the expressing ability in the classification of hyperspectral data. Another research on the ability of SVM to classify the hyperspectral images was performed by Melgani & Bruzzone (2002) and they observed that the SVM is more efficient than the other non-parametric classifiers such as RBF Neural network and KNN classifiers, and less sensitive to Hughes phenomenon. As the SVM can handle more complex data, it is also widely used in the classification of SAR data.

Research on target recognition using SVM on SAR was performed by Zhao & Principe (2001) and have compared the SVM based target detection on SAR with other conventional classifiers. The results proved that the SVM outperformed all the other classifiers in target detection. Also, they have concluded that the SVM are able to form a locally bounded decision function for each of the classes. Fukuda, Hirosawa, & Ieee (2001) have performed classification of SAR using SVM on feature vectors such as the polarimetric parameters after the decomposition technique and also on the texture properties of SAR. This was performed by the authors on the high resolution data.

Next chapter deals with the study area of this research, datasets, and the tools used.

3. STUDY AREA, DATASETS, AND TOOLS USED

This chapter deals with the study area of the research, satellite imagery and the defined classes of the study area and the tools used.

3.1. Study area

For this research work, the study area selected was the in and around regions if Dhanbad city of Jharkhand state, India. The study area consists of complex urban and industrial areas, dense and sparse vegetation area, cropland, barren land, water and dry river bed and these are the potential classes on which the research work was carried out. Below is the figure of study and the figure 3-2 shows the different classes present in the study are on a Hyperion image of 30 meters resolution.

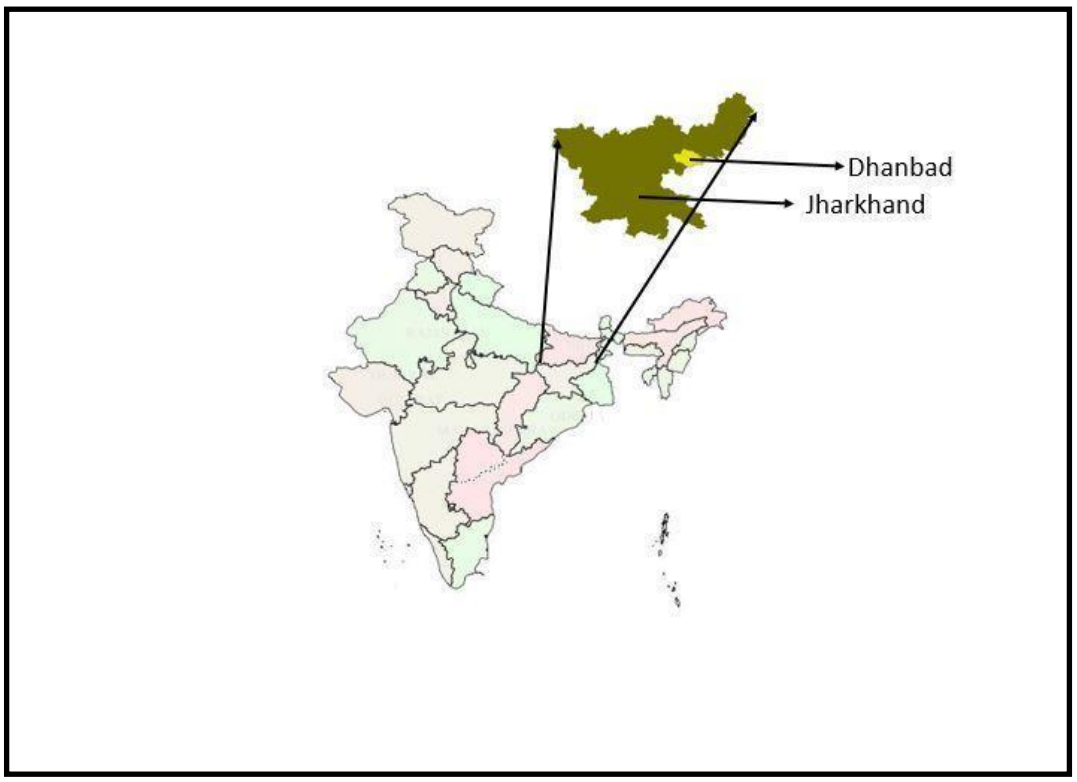

Figure 3-1 Study area, Source: http://bhuvan.nrsc.gov.in/bhuvan_links.php

3.1.1. Satellite view of the study area and the defined classes

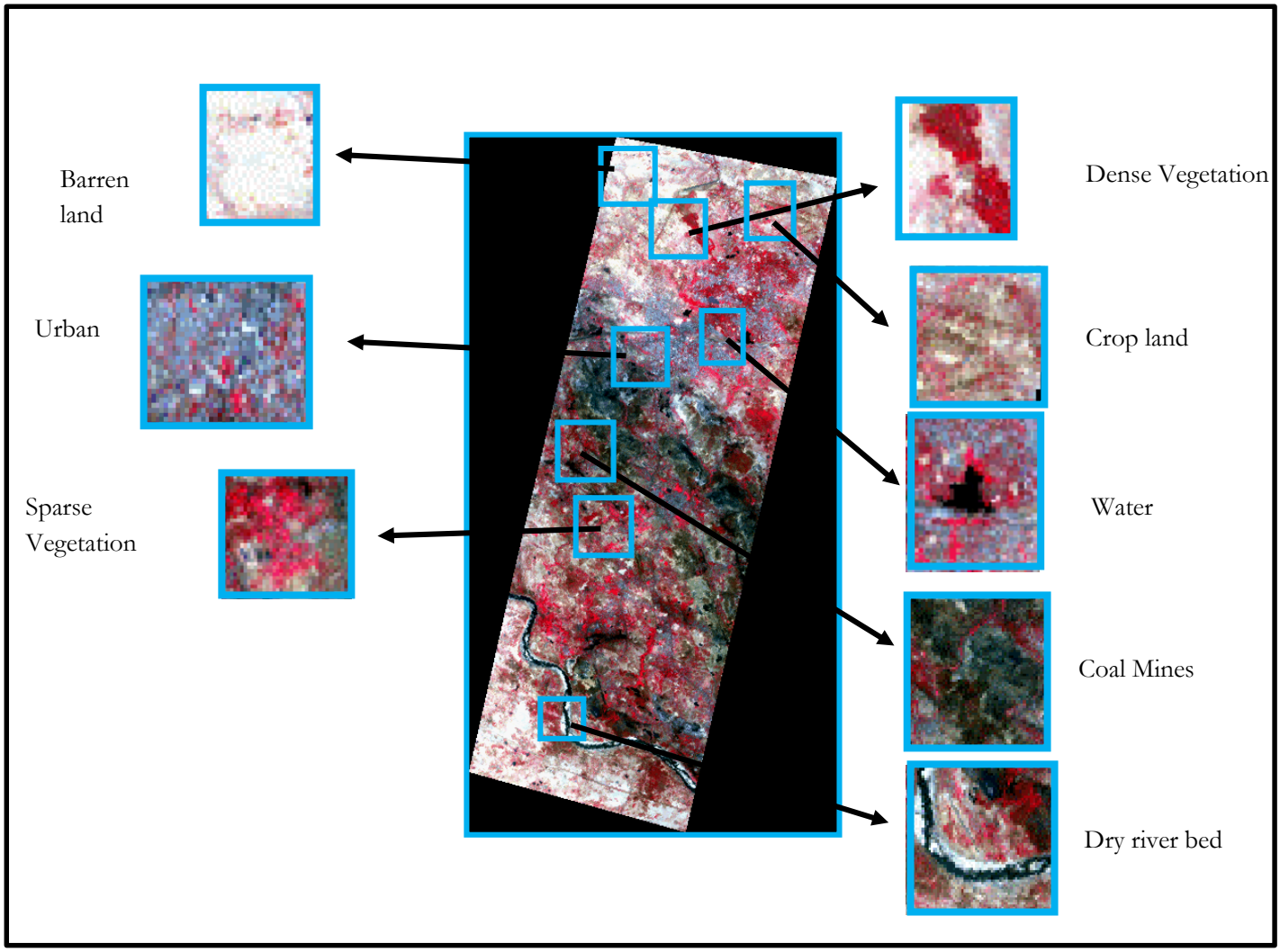

Figure 3-2 Hyperion (Spatial Res. 30 meters) and the defined classes

3.2. Datasets used

The datasets used for this research work used were,

EO-1 Hyperion data

Under the NASA's new millennium program in the year, November 2000 Hyperion the Earth Observation (EO-1) sensor was developed and provides data for improved characterization of the earth surface. Hyperion is a push broom based imaging instrument. The swath width of this instrument is 7.5 kilometres wide and consists of 220 unique spectral bands with the spectral range from 357nm-2576 nm.

Radarsat 2 data

Radarsat 2 data is a combinely funded mission of the Canadian Space Agency and MacDonald Dettwiler Associates Ltd. Of Richmond, BC in the year February 1998. The imaging frequency of Radarsat 2 is C-band at 5.405 GHZ and works in the fully polarimetric mode. The look direction of the Radarsat 2 antenna is left or right. Radarsat 2 offers data in all four polarization channels (HH, HV, VH, and VV)

ALOS PALSAR data

Japan Aerospace and Exploration Agency (JAXA) launched the Advanced Land Observing Satellite (ALOS) was launched in the year January 24, 2006. ALOS carried the PALSAR and was launched into the sun-synchronous orbit. The revisit time of this satellite was 14 times a day. The polarimetric mode of the PALSAR offers the complete polarimetry Of HH, HV, VV and VH polarizations

3.3. Dataset Specifications:

Table 3-1 Dataset specifications

Specifications	Hyperion	Radarsat 2	ALOS PALSAR
Spatial Resolution	30 meters	Range spacing – 3.125m Azimuth spacing – 3.125m	Range spacing – 6.25 m Azimuth spacing – 12.5m
Spectral Resolution	10 nm	-	-
Wavelength	220 bands (0.4 – 2.5 micrometer)	C band	L-band
Polarimetric mode	-	HH, HV, VH, VV	HH, HV, VH, VV
Incidence angle	-	27.6 degree	25.6 degree

Table 3-2 Tools Used

Tools	Purpose
PolSARPro Version	PolSAR Data processing
ENVI, ERDAS	Hyperspectral data processing, Data Fusion
ArcGIS	GIS related work
R	Classification and Accuracy Assessment

Next chapter is on the methodology adopted and the methods used to achieve the objective of the research.

4. RESEARCH METHODOLOGY AND METHODS

The purpose of this research is to enhance the land cover classification by fusing the fully polarimetric SAR data and Hyperspectral data. To achieve this goal, the methodology shown in the Figure 4-1 was adopted. . Initially, Hyperion (L1R data), Radarsat 2 (SLC) and ALOS PALSAR (SLC) were pre-processed and various polarimetric parameters polarimetric parameters were extracted from fully polarimetric data such as such as span, span, surface scattering, double bounce scattering, volume scattering, helix scattering and wire scattering. The extracted parameters were then co-registered with the atmospherically corrected Hyperion data. After the co-registration, pixel level, feature level and decision level fusion were performed and the classification and accuracy assessment of the fused products, as well as the individual datasets, were done. Comparative analysis was made between the accuracy results to obtain the optimal level and the fusion pair (Hyperion + RS2 or Hyperion + ALOS PALSAR) that gives the better overall accuracy.

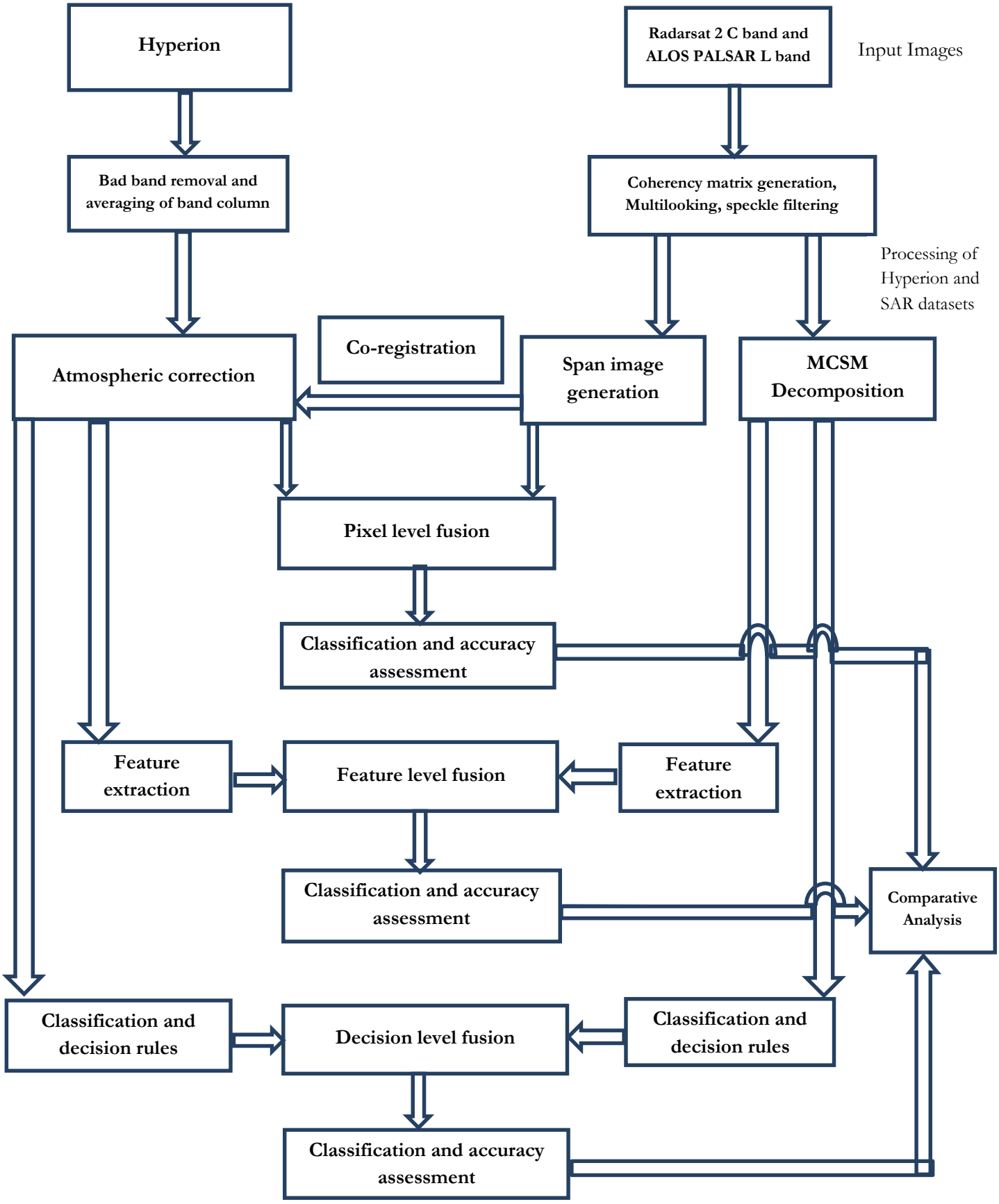

Figure 4-1 Research Methodology

4.1. Processing of the datasets

Pre-processing of the data is an important process in fusion. The quality of the fused image and further the accuracy of the classification of the fused image depends on how well the pre-processing has been done. The Hyperion image obtained was at level 1, and the fully polarimetric data (Radarsat 2 and ALOS PALSAR) were at level 1 single look complex (SLC).
The images underwent the pre-processing steps as follows.

- **Processing of Hyperion data**

The processing of Hyperion data required the bad band removal, averaging of the bad column and the atmospheric correction.

Bad band removal and averaging of bad column

Due to the atmospheric interference and water absorption, some bands of the Hyperion image appears to be black or very noisy as it has the low signal to noise ratio. Hence, those bands were removed manually. Total of 144 bands were obtained after the removal of non-informative bands. The scanner of the Hyperion sensor is the across track scanner which causes the stripping error due to its miss-calibration. This leads to the abnormal DN values in individual columns. Hence, those values are corrected using the averaging method.

Atmospheric correction

Atmospheric correction needs to be done as Hyperion was affected by the atmosphere which influences the radiation from ground to sensor. The primary objective of atmospheric correction is to find the actual surface reflectance of the objects by removing the atmospheric effects (Hadjimitsis et al., 2010). First Line of Sight Atmospheric Analysis of Hypercubes (FLAASH) model was used for the atmospheric correction of Hyperion data which is based on MODTRAN radiative transfer model.

- **Processing of PolSAR data**

The PolSAR data contains all the four polarization in the form of scattering matrix and its polarization state changes when it gets interacted with the target features. These backscatter responses from each of the polarization channels are stored in a scattering matrix. According to Verma (2014),

$$[S]=\begin{bmatrix} S_{HH} & S_{HV} \\ S_{VH} & S_{VV} \end{bmatrix} \quad \text{Equation 4-1}$$

where, S_{HH} = Backscatter response from HH Polarization channel
S_{HV} = Backscatter response from HV Polarization channel
S_{VH} = Backscatter response from HV Polarization channel
S_{VV} = Backscatter response from HV Polarization channel

The above matrix gives information only about the clear targets. But the earth surface has more complex structures and targets where the information provided by the scattering matrix is insufficient. Therefore, the second order statistics is calculated by making use of the vectorized form of the scattering matrix S. This is known as the coherency matrix. The vectorized form of scattering matrix using Pauli feature vector is given by,

$$K_p = \frac{1}{\sqrt{2}} \begin{matrix} S_{HH} + S_{VV} \\ S_{HH} - S_{VV} \\ 2S_{HV} \end{matrix} \quad \text{Equation 4-2}$$

The product of this vector with the transpose of itself form the coherency matrix and was converted from single look complex (SLC) to multilook complex image (MLC) to turn the slant range to ground range resolution. The coherency matrix is given as,

$$\langle [T] \rangle = \langle K_p K_P^{\dagger} \rangle = \begin{bmatrix} \langle |S_{HH} + S_{VV}|^2 \rangle & \langle (S_{HH} + S_{VV}) S_{HH} - S_{VV}) \rangle & 2\langle (S_{HH} + S_{VV}) S_{HV} \rangle \\ \langle (S_{HH} - S_{VV}) S_{HH} + S_{VV}) \rangle & \langle |S_{HH} - S_{VV}|^2 \rangle & 2\langle (S_{HH} - S_{VV}) S_{HV} \rangle \\ 2\langle S_{HV} (S_{HH} + S_{VV}) \rangle & 2\langle S_{HV} (S_{HH} - S_{VV}) \rangle & 4\langle |S_{HV}|^2 \rangle \end{bmatrix} \quad \text{Equation 4-3}$$

Where † represents the conjugate and the transpose and <> represents the averaging over the whole data. The sum of the diagonal elements gives the total backscatter intensity values called as **span**. The span images are shown in the Figure 4-2.

$$\textbf{Span} = \langle |S_{HH} + S_{VV}|^2 \rangle + \langle |S_{HH} - S_{VV}|^2 \rangle + 4\langle |S_{HV}|^2 \rangle$$

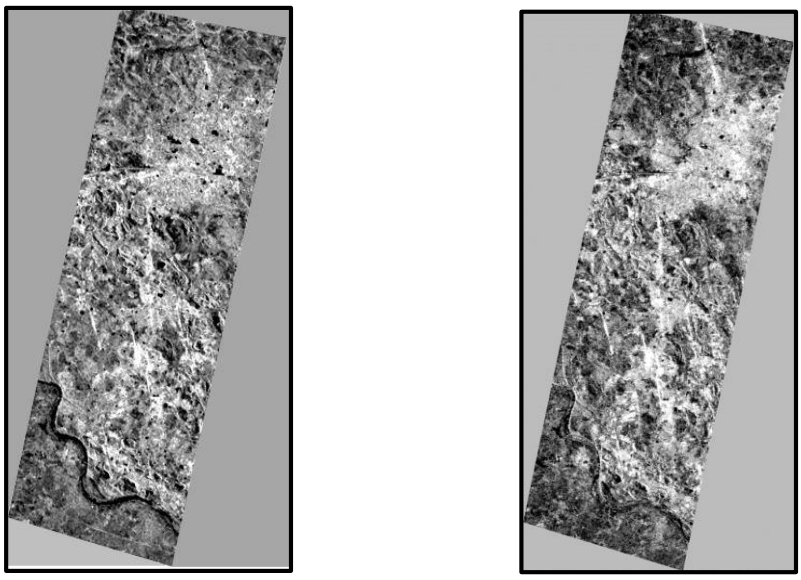

(A) (B)

Figure 4-2 Span images of Radarsat 2 (A) and ALOS PALSAR (B)

The SLC to MLC conversion is given as,

Slant range resolution to Ground resolution= $C\ \tau\ /2(1/sin\ \vartheta)$ Equation 4-3

where, C τ /2 = Pixel spacing in range direction and

Sin ϑ = Incidence Angle

Parameters	Radarsat 2	ALOS PALSAR
Ground range resolution	20 meters	20 meters
Incidence angle	27.6 degree	25.6 degree
Multilook factor	5,2	6,1

Various speckle filters namely the Gamma, box car filters Lee refined filter and Lee sigma filter were applied to reduce the speckles. It was observed that the Lee Refined filter with a window size of 3 provided a good result in terms of reduced smoothening of the image.

MCSM Decomposition

Multiple component scattering model decomposition was proposed by Zhang et al. (2008). It is an extension of the yamaguchi four component scattering model. Here, the fifth component known as the wire scattering is added to it. The wire scateering is very much prominent in urban areas. In the urban areas, the wire scattering is observed by the the canonical structures, walls, vertical buildings, etc. The total backscatter value is considered as the contribution of the five types of scattering mechanisms namely the Double bounce, Volume, Helix, Surface and Wire scattering. These scatterings depend on the scattering behaviour of the scatterers based on their orientation, shape, surface roughness, geometrical structure, etc. Zhang et al. (2008) explained that the MCSM decomposition as the linear combination of five scattering mechanisms which describes the total received backscatter.

Below description of the MCSM model is based on the work of Verma (2014).

The total coherency matrix of MCSM decomposition is given as,

$$[T] = f_s[T_s] + f_d[T_d] + f_v[T_v] + f_h[T_h] + f_w[T_w]$$ Equation 4-4

[T] = Total Coherency Matrix

$[T_s]$, $[T_d]$, $[T_v]$, $[T_h]$ and $[T_w]$ are the coherency matrices of the individual scattering components and f_s, f_d, f_v, f_h, f_w are the expansion coefficients of individual scattering components. The individual matrix elements of Surface, Volume, Helix, double bounce and wire scattering components are explained below.

Surface Scattering

The Surface scattering is prominent in the slightly rough surface regions where the cross polarization is negligible. For example, the road features, water bodies, barren land are the surface scatterers. The coherency matrix of the surface scattering is given as,

$$\langle [T_s] \rangle = \begin{bmatrix} 1 & \beta^* & 0 \\ \beta & |\beta|^2 & 0 \\ 0 & 0 & 0 \end{bmatrix}, Where\ \beta = \frac{R_H - R_V}{R_H + R_V}\ \ and\ \ |\beta| < 1 \qquad \text{Equation 4-5}$$

Where R_H and R_V are the Fresnel reflection coefficients

Double bounce Scattering

This type of scattering is displayed in the urban region where there are dihedral structures and also by the ground tree trunk. The coherency matrix is given S,

$$\langle [T_d] \rangle = \begin{bmatrix} |\alpha|^2 & \alpha & 0 \\ \alpha^* & 1 & 0 \\ 0 & 0 & 0 \end{bmatrix}, \text{where } \alpha = \frac{e^{2j\gamma_H} R_{TH} R_{GH} + e^{2j\gamma_V} R_{TV} R_{GV}}{e^{2j\gamma_H} R_{TH} R_{GH} - e^{2j\gamma_V} R_{TV} R_{GV}} \quad \text{and } |\alpha| < 1 \qquad \text{Equation 4-6}$$

where R_{TH}, R_{TV}, R_{GV}, R_{GH} reflection coefficients of ground and tree trunk surface for horizontal and vertical polarization. According to Woodhouse (2012), this particular model is generalized by adding the propagation factors as shown in the equation to represent any propagation attenuation and any phase change effects.

Volume Scattering

This type of scattering corresponds to the multiple scatterers for example the dense forest canopy. The coherency matrix is given as,

$$[T_V] = \begin{bmatrix} 2 & 0 & 0 \\ 0 & 1 & 0 \\ 0 & 0 & 0 \end{bmatrix} \qquad \text{Equation 4-7}$$

Helix Scattering

This type of scattering is prominent in the urban regions where there are complex man-made structures (Zhang et al., 2008). A left handed and a right handed circular polarization are generated by a helix target. The corresponding coherency matrix is given by,

$$[T_h] = \frac{1}{2} \begin{bmatrix} 0 & 0 & 0 \\ 0 & 1 & \pm j \\ 0 & \pm j & 1 \end{bmatrix} \qquad \text{Equation 4-8}$$

Wire Scattering

The thin canonical structures and the edges of the buildings contribute to the wire scattering (Zhang et al., 2008).

$$[S_w] = \begin{bmatrix} \gamma & \rho \\ \rho & 1 \end{bmatrix}, \text{Where } \gamma = \frac{S_{HH}}{S_{VV}}, \rho = \frac{S_{HH}}{S_{VV}} \quad \text{Equation 4-9}$$

The coherency matrix is given by,

$$\langle [T_w] \rangle = \frac{1}{2} \begin{bmatrix} |\gamma+1|^2 & (\gamma+1)(\gamma-1)^* & 2(\gamma+1)\rho^* \\ (\gamma-1)(\gamma+1)^* & |\gamma-1|^2 & 2(\gamma-1)\rho^* \\ 2(\gamma+1)^*\rho & 2\rho(\gamma-1)^* & 4|\rho|^2 \end{bmatrix} \quad \text{Equation 4-10}$$

From the above obtained coherency matrices of the individual scattering elements the total coherency matrix of the MCSM decomposition is given as,

$$[T] = f_s \begin{bmatrix} 1 & \beta^* & 0 \\ \beta & |\beta|^2 & 0 \\ 0 & 0 & 0 \end{bmatrix} + f_d \begin{bmatrix} |\alpha|^2 & \alpha & 0 \\ \alpha^* & 1 & 0 \\ 0 & 0 & 0 \end{bmatrix} + \frac{f_v}{4} \begin{bmatrix} 2 & 0 & 0 \\ 0 & 1 & 0 \\ 0 & 0 & 1 \end{bmatrix} + \frac{f_h}{2} \begin{bmatrix} 0 & 0 & 0 \\ 0 & 1 & \pm j \\ 0 & \mp j & 1 \end{bmatrix} + \frac{f_w}{2} \begin{bmatrix} |\gamma+1|^2 & (\gamma+1)(\gamma-1)^* & 2(\gamma+1)\rho^* \\ (\gamma-1)(\gamma+1)^* & |\gamma-1|^2 & 2(\gamma-1)\rho^* \\ 2(\gamma+1)^*\rho & 2\rho(\gamma-1)^* & 4|\rho|^2 \end{bmatrix} \quad \text{Equation 4-11}$$

The individual scattering powers of the five scattering elements are obtained as follows,

$$P_{s=} f_s(1+|\beta|^2)$$
$$P_{d=} f_d(1+|\alpha|^2) \quad \text{Equations 4-12}$$
$$P_v = f_v$$
$$P_h = f_h$$
$$P_w = f_w(1+|\gamma|^2+2|\rho|^2$$

The expansion coefficients present above in the equations can be obtained as follows,

From T23 element we get,

$$f_{h=2\,lm(T_{23})}$$

and $$f_w = \frac{Re(T_{23})}{(\gamma-1)\rho^*} \quad \text{Equation 4-14}$$

Therefore $$P_h = f_h$$

and $$P_w = \frac{Re(T_{23})}{(\gamma-1)\rho^*}(1-|\gamma|^2+2|\rho|^2) \quad \text{Equation 4-15}$$

The volume component is determined based on the copolarized components namely the HH and VV.

$$10\,log\left[\frac{\langle|S_{VV}|^2\rangle}{\langle|S_{HH}|^2\rangle}\right] = 10\,log\left[\frac{T_{11}+T_{22}-2Re(T_{12})}{T_{11}+T_{22}+2Re(T_{12})}\right] \quad \text{Equation 4-16}$$

$$For\ 10\log(\langle|S_{VV}|^2\rangle/\langle|S_{HH}|^2\rangle) < -2db, \langle|T_V|\rangle = \frac{1}{30}\begin{bmatrix} 15 & 5 & 0 \\ 5 & 7 & 0 \\ 0 & 0 & 8 \end{bmatrix}$$

$$For -2db < 10\log(\langle|S_{VV}|^2\rangle/\langle|S_{HH}|^2\rangle) < 2db, \langle|T_V|\rangle = \frac{1}{4}\begin{bmatrix} 12 & 0 & 0 \\ 0 & 1 & 0 \\ 0 & 0 & 1 \end{bmatrix}$$

Equations 4-1

$$For\ 10\log(\langle|S_{VV}|^2\rangle/\langle|S_{HH}|^2\rangle) > 2db, \langle|T_V|\rangle = \frac{1}{30}\begin{bmatrix}15 & -5 & 0\\ -5 & 7 & 0\\ 0 & 0 & 8\end{bmatrix} \quad \text{Equation 4-17}$$

Based on the coherency matrix of the volume scattering component the power of volume scattering is obtained as,

$$P_v = 4T_{33} - 2P_h - 8f_w|\rho|^2 \quad or\ P_v = \frac{15}{4}T_{33} - \frac{15}{8}P_h - \frac{15}{2}f_w|\rho|^2 \quad \text{Equation 4-18}$$

The equations containing the coefficient for surface and double bounce scattering is given as,

$$S = f_{s+}\, f_d|\alpha|^2 = T_{11} - \frac{P_v}{2} - \frac{f_w}{2}|\gamma + 1|^2$$

$$D = f_d|\beta|^2 + f_d = T_{22} - T_{33} - \frac{f_w}{2}(|\gamma - 1|^2 - 4|\gamma + 1|^2)$$

$$C = f_s\beta^* + f_d\alpha = T_{12} - \frac{f_w}{2}(\gamma + 1)(\gamma - 1)^* \quad \text{Equations 4-19}$$

Based on the sign of $\mathrm{Re}\langle S_{HH}S^*_{VV}\rangle$ the surface and double bounce scattering is estimated. In terms of coherency matrix elements, the $\mathrm{Re}\langle S_{HH}S^*_{VV}\rangle$ term is estimates as follows,

$$C_0 = T_{11} + T_{22} + T_{33} + P_h \quad \text{Equation 4-20}$$

If there is a dominance of surface scattering. Then $\mathrm{Re}\langle S_{HH}S^*_{VV}\rangle > 0$ i.e. $C_0 > 0$. In this case, the double bounce scattering is negligible. The surface and double bounce scattering power is given as,

$$P_s = f_s(1 + |\beta|^2) = S + \frac{|C|^2}{D}$$

$$P_d = f_d(1 + |\alpha|^2) = D - \frac{|C|^2}{D} \quad \text{Equations 4-21}$$

If $\mathrm{Re}\langle S_{HH}S^*_{VV}\rangle < 0$ the $\beta = 0$, the double bounce scattering is dominant. Then the power of the double bounce and the surface scattering is obtained as follows,

$$P_s = f_s(1 + |\beta|^2) = S - \frac{|C|^2}{D}$$

$$P_d = f_d(1 + |\alpha|^2) = D + \frac{|C|^2}{D} \quad \text{Equation 4-22}$$

Above are the power of different scattering elements.

Geocoding of extracted PolSAR parameters

The PolSAR data are captured on the side looking geometry which leads to distortions like shadow, layover, and foreshortening. To correct all these distortions and to Geo-Register the image, geocoding is required using Digital Elevation Model (DEM). The DEM used was the Shuttle Radar Topographic Mission (SRTM).

PolSAR parameters extracted from both Radarsat 2 and ALOS PALSAR data were geocoded to the projection UTM Zone 45 and Datum WGS 84.

Co-Registration and Subsetting of SAR and Hyperspectral Image

Co-registration is a vital step in the process of fusion as both the input images should precisely get overlaid on each other. The atmospherically corrected Hyperion was precisely co-registered with the geocoded Radarsat 2 and ALOS PALSAR and the common are from all three datasets were subsetted.

4.2. Pixel level fusion

Next step was the fusion at the pixel level. This is the lowest level of fusion where the images were fused pixel to pixel. In this study Hyperion image was fused with the span image of Radarsat 2 and ALOS PALSAR using three pixel level fusion techniques. They are,

1. High pass filter fusion,
2. Wavelet fusion
3. Gram-Schmidt fusion

The above methods were chosen to preserve the spectral property of the Hyperion image in the fused product. Later the SVM based classification and cross validation based accuracy assessment of the model was performed on the fused products. Finally, the optimal fusion technique and also the fusion pair that is either Hyperion and Radarsat 2 or Hyperion and ALOS PALSAR was found based on the overall accuracy and kappa. Individual class accuracies were also analyzed for each of the fusion techniques. Below Figure 4-2 represents the adopted pixel level fusion methodology.

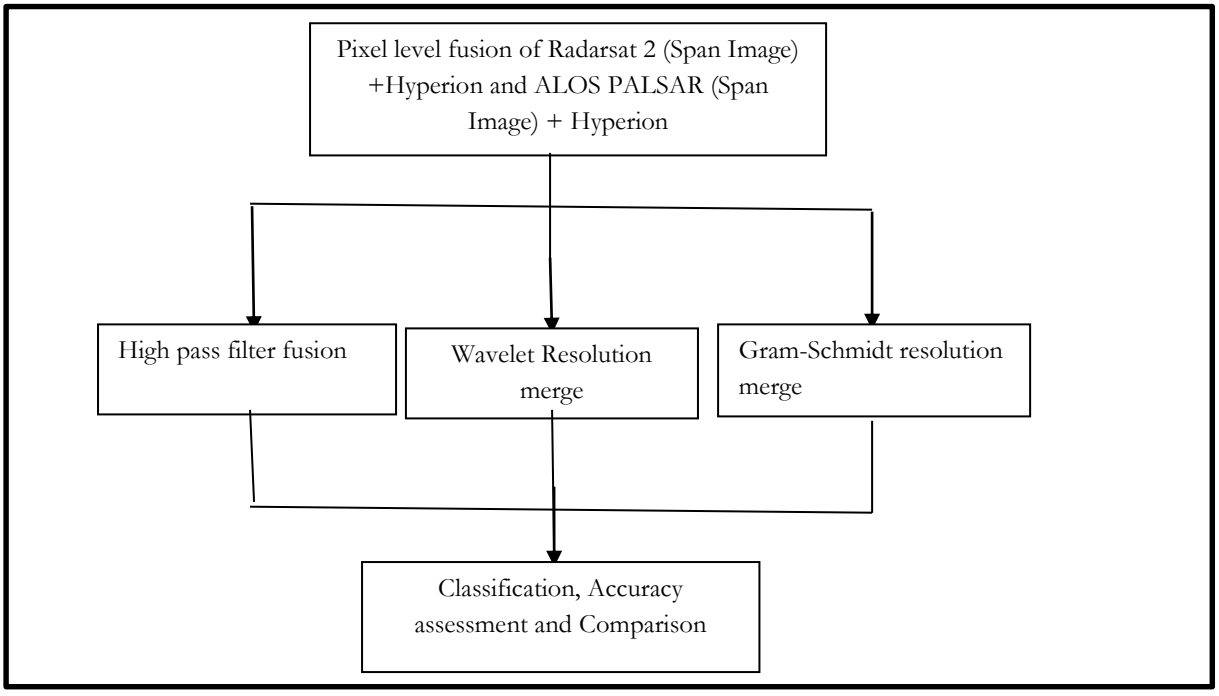

Figure 4-3 Pixel level fusion

Next heading of this section is about the working of the adopted pixel level fusion techniques.

- **High pass filter fusion**

In this method, the high spatial resolution image is filtered with a high pass filter. This results in the data containing high frequency information. Then it is added pixel wise to the low resolution bands (Pohl & Van Genderen, 1998). Below block diagram (Metwalli, Nasr, Allah, & El-Rabaie, 2009) shows the process of HPF fusion.

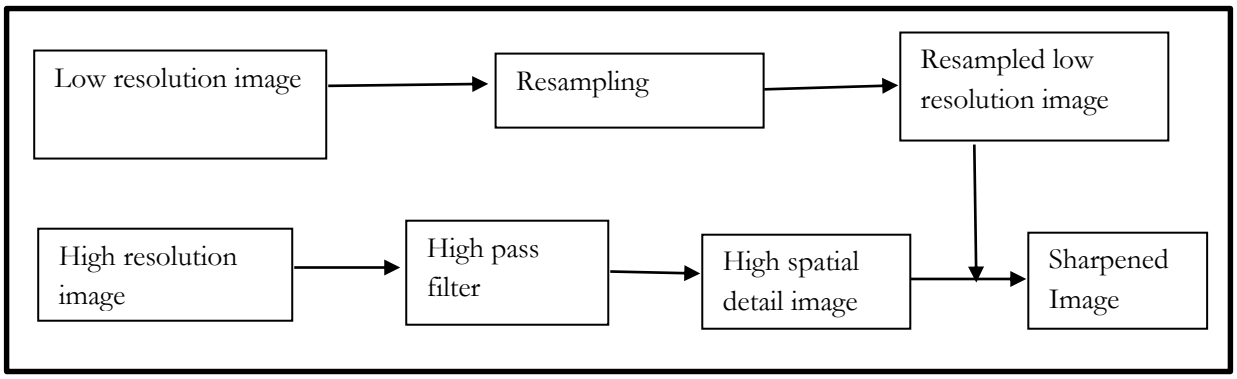

Figure 4-4 HPF fusion technique

The stepwise algorithm is as follows,

- ✓ Read pixel sizes from Image files and calculate R, where R is the ratio of low resolution cell size to high-resolution cell size.
- ✓ Apply the High-pass filter to the high spatial resolution.
- ✓ Using HPF Kernel, the high spatial resolution image is filtered which produces a high pass filtered image. The size of kernel depends upon the value of R.
- ✓ Resample the low resolution image to the pixel size of the high-pass image.
- ✓ Add the HPF image to each low resolution image band. The HPF image is weighted relative to the global standard deviation of the each low resolution band.
- ✓ Stretch the new fused image to match the mean and standard deviation of the original (input) low resolution image.

Therefore, the relevant parameters that need to be considered for the fusion using HPF are the R value, Kernel size and the weighting factor to determine the crispness of the output image. Table 4-1 shows the parameter values for the HPF fusion technique

Table 4-1 Parameter values for HPF fusion

Parameters	Hyperion + Radarsat 2 (SPAN) & Hyperion + ALOS PALSAR(SPAN)
R Value	1.55
Kernel size	5
Kernel centre value	24
Weighting factor	0.25

- **Wavelet Fusion**

Remotely sensed image analysis using wavelets is similar to Fourier transform analysis except the fact that in Fourier transform long continuous waves are used and in wavelet transform short continuous waves are used. The key element in wavelet transform is the selection of the base waveform to be used. This base waveform is called the mother wavelet, and it is used to represent the image. The input signal (image) is broken down into successively smaller multiples of this basis.

A signal is decomposed into a multi-resolution representation with both low detail and high detail information content using discrete wavelet transform (Li, Kwok, & Wang, 2002). When used for image fusion, the source images are first geometrically registered, and then decomposed by DWT to the same resolution. Corresponding wavelet coefficients are combined, and the fused image is obtained by performing the inverse wavelet transform (Li et al., 2002). Below diagram shows the discrete wavelet transform (DWT) of an input image. In the below image h_φ and h_ψ represents the low pass and high pass filters respectively. W_φ, W_φ^H, W^V_φ, W^D_φ are the approximation coefficients, horizontal coefficient, Vertical co-efficient, diagonal coefficients respectively (Gonzalez & Woods, 2001).

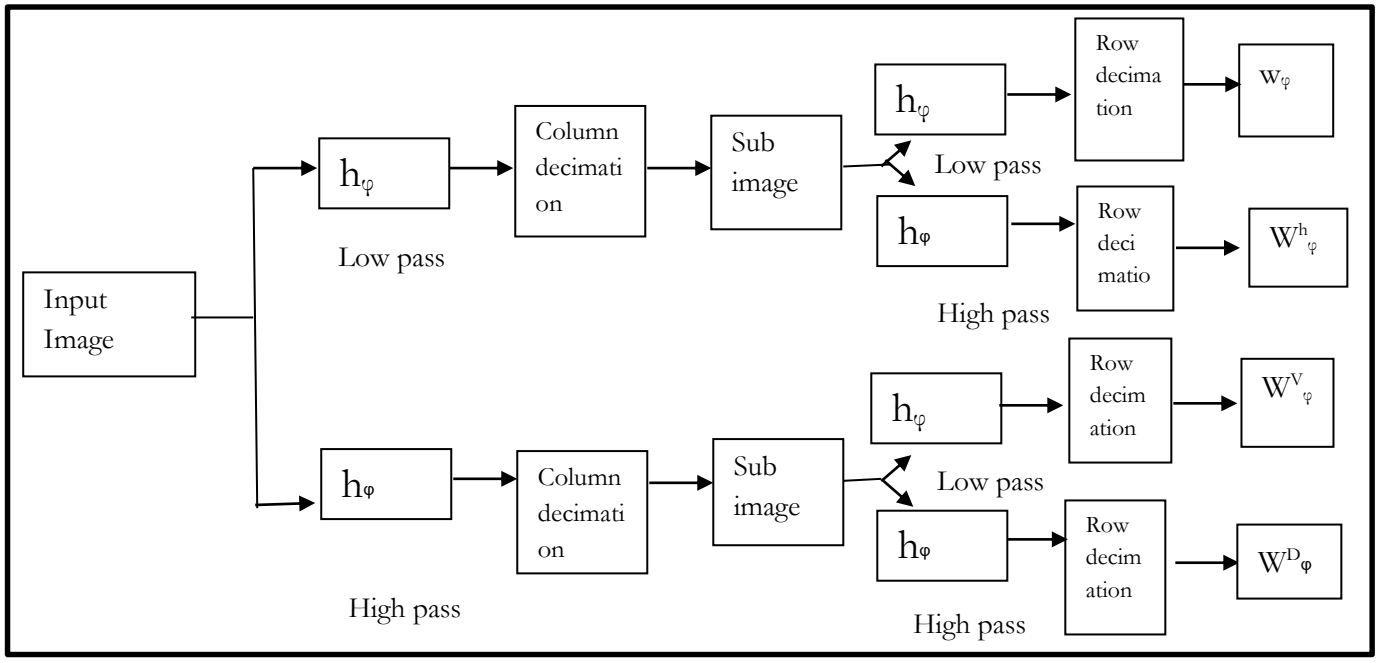

Figure 4-5 Discrete wavelet transform

In the inverse discrete wavelet transform (IDWT) the reduced images are then passed through the low pass and high pass reconstruction filters to obtain the output image. This process is the inverse of DWT where the sub images are upsampled along the rows and convolved along the columns with the filters. The obtained output are combined and upsampled along columns and then by row wise it is filtered to get the original image.

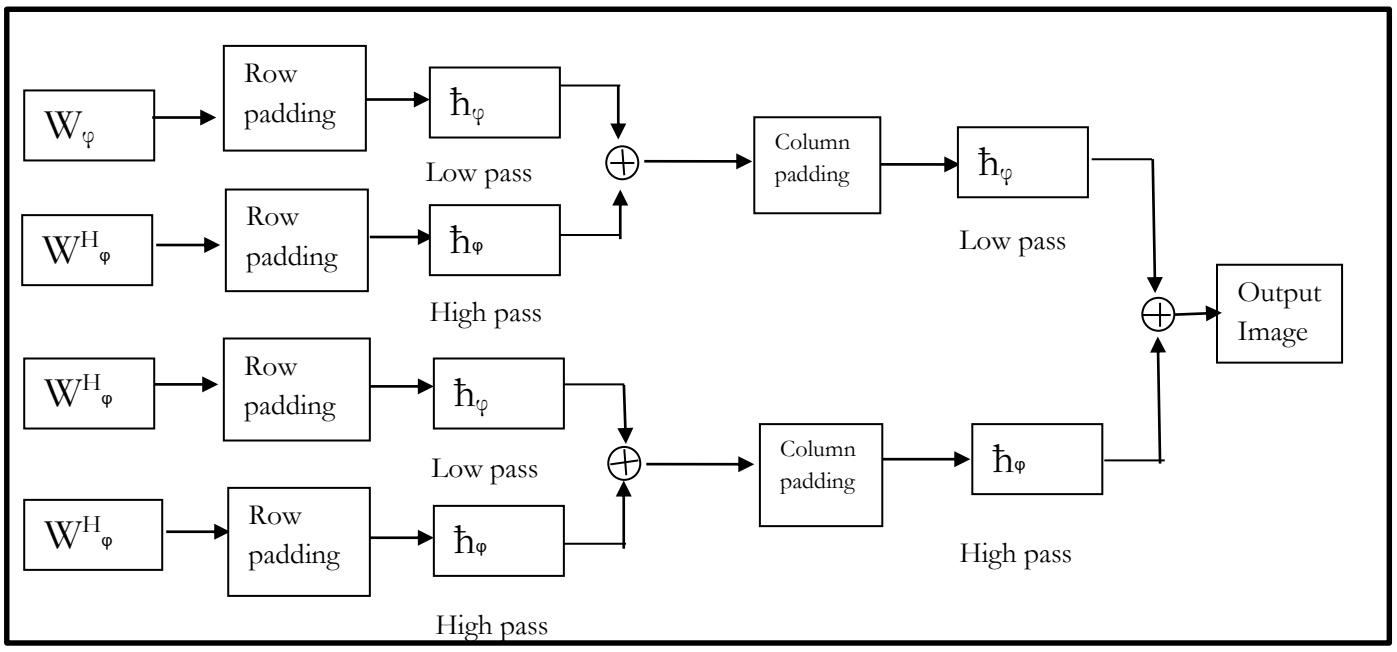

Figure 4-6 Inverse discrete wavelet transform

The algorithm of wavelet resolution merge (Li et al., 2002) is as follows,

- ✓ Decompose the high spatial resolution image through several iterations using the wavelets until low pass image is generated along with all the corresponding high pass images derived during recursive decomposition.
- ✓ The obtained low pass image from the high spatial resolution image is replaced with the low spatial resolution image
- ✓ Inverse decomposition takes place using the high pass images derived from the decomposition and high resolution image was obtained.

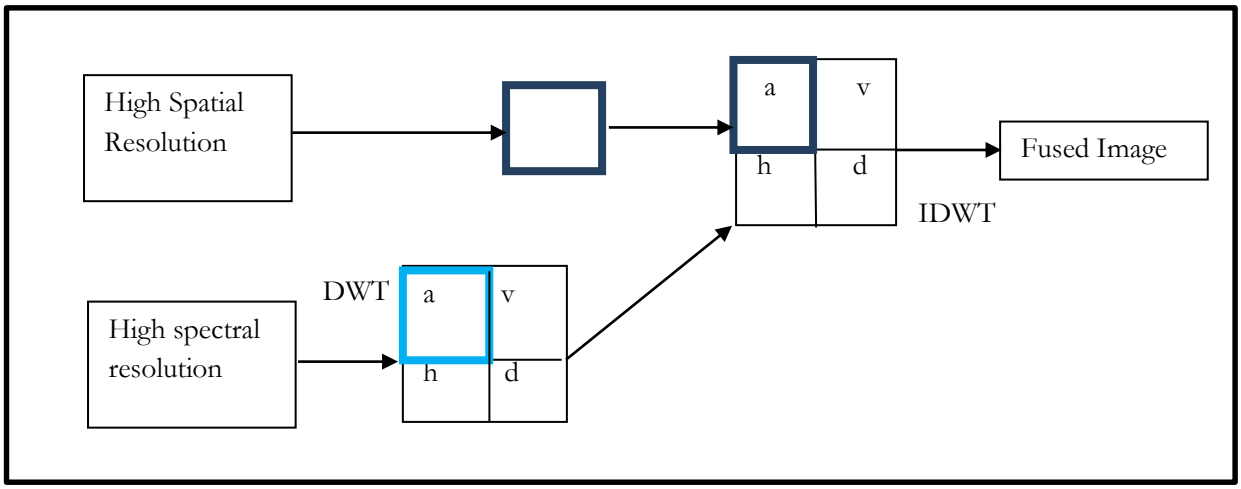

Figure 4-7 Wavelet fusion

- ➢ **Gram –Schmidt fusion**

The Gram-Schmidt merge is based on the Gram-Schmidt orthogonal transformation. Gram-Schmidt orthogonal transform is a common method which is being used in the multivariate statistics (Lu & Zhang, 2014). Conversion of non-orthogonal basis which is a set of linearly independent vectors to a set of orthonormal basis which is a set of orthogonal unit length vectors is the Gram – Schmidt process. The Gram-Schmidt process consists of taking each vector and then subtracting the elements in common with the previously obtained vectors (Klonus & Ehlers, 2007). The algorithm of Gram –Schmidt fusion process (Klonus & Ehlers, 2009) is as follows,

- ✓ A gray scale band from the lower spatial resolution spectral bands of spectral image is generated.
- ✓ Gram-Schmidt transformation is applied to the on the simulated gray scale band and the spectral bands, using the simulated gray scale band as the first band.
- ✓ Next step is to swap the high spatial resolution band with the first Gram-Schmidt band.
- ✓ Inverse Gram-Schmidt transformation is applied to form the fused image with high spectral and spatial resolution.

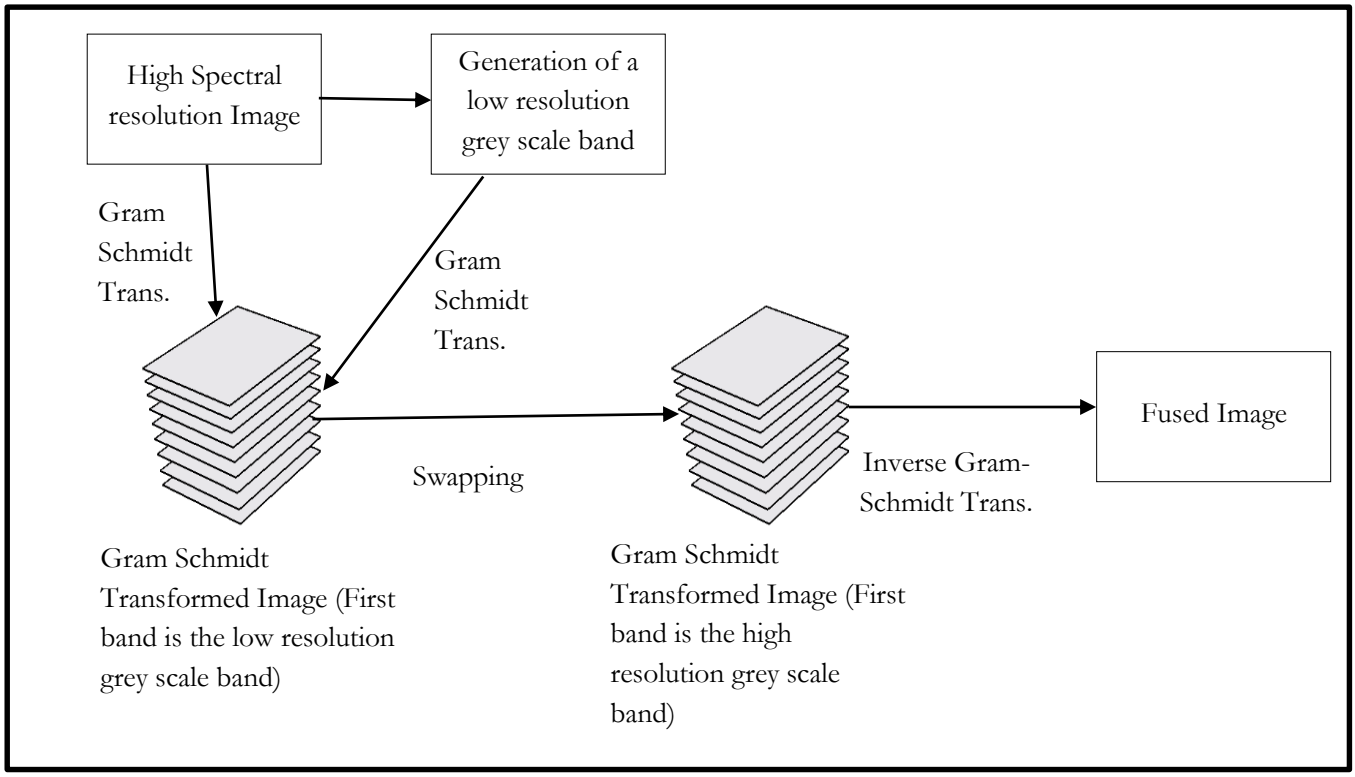

Figure 4-8 Gram Schmidt fusion

4.3. Feature level fusion

The second level of fusion performed was the feature level fusion. Here the features were extracted from different sources and then a feature vector was formed to perform SVM classification and accuracy assessment. The features from Hyperion was extracted using Kernel based principal component analysis method and the features from fully polarimetric SAR data was extracted using MCSM decomposition. The main purpose of KPCA is to generalize the PCA method for the nonlinear case as the higher dimensionality data is more sensitive to non-linearity. Also, KPCA considers the higher order information of the datasets and gives more principal components than the normal PCA. In the case of SAR images, MCSM decomposition was used to extract information. Decomposition of polarimetric SAR is useful in extraction of the features such as urban, vegetation, smooth surface features such as barren land, water, road features, etc. In the case of MCSM, it is useful in extracting the urban features prominently based on their scattering property. The Figure 4-8 shows the methodology and the methods adopted for performing feature level fusion.

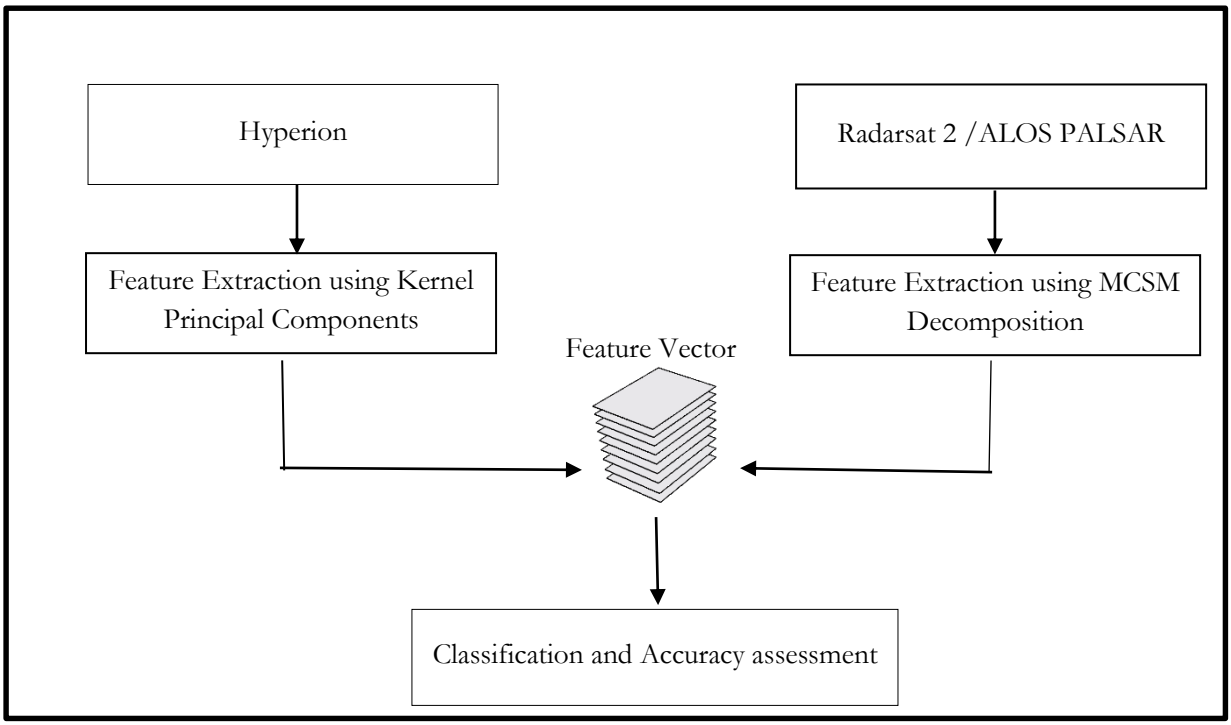

Figure 4-9 Feature level fusion

Below are explanation of feature extraction methods adopted for the feature level fusion.

- **Kernel Principal Component analysis based feature extraction in Hyperion**

Linear Principal component analysis is the linear dimensionality reduction and feature extraction technique which works on the second order statistics. In real, the data is not linear, hence, the use of kernel based principal component analysis which works on higher order statistics comes into the picture (Fauvel, Chanussot, & Benediktsson, 2006). Schölkopf, Smola, & Müller (1997) have shown that even if the mapped feature space F has arbitrarily large dimensionality the PCA can be performed for some choices of φ using the kernel functions. According to Schölkopf et al. (1997) a data x_k , where $k = 1, \dots, l$ is mapped to a high dimensionality feature space F as $\varphi(x_1) \dots \varphi(x_l)$ and, it is centered at

$$\sum_{k=1}^{l} \varphi(x_k) = 0 \qquad \text{Equation 4-23}$$

Here l is the total number of representative samples

After the mapping of data to a higher dimensional space F, to find PCA of the covariance matrix the necessary parameters called the Eigenvalues λ and the Eigenvectors V needs to be calculated. The covariance matrix is given as,

$$C = \frac{1}{l} \sum_{j=1}^{l} x_j x_j^T \qquad \text{Equation 4-24}$$

The Eigen vectors $V \in F \setminus \{0\}$ and the λ values ≥ 0 from which it is understood that,

$$\lambda V = CV \qquad \text{Equation 4-25}$$

Since the Eigen Vector lies in between φ (x_1)…….φ (x_k), the resulting equation is,

$$\lambda(\varphi(x_k).V) = C(\varphi(x_k).V) \text{ For all k=1….l}$$
$$V=\sum_{i=1}^{l} \alpha_i \ \varphi(x_i) \qquad \text{Equations 4-26}$$

where,

α_i =Co-efficient

By substituting V and C in the equation, we obtain,

$$l\lambda K\alpha = K^2\alpha \qquad \text{Equation 4-27}$$

Where K is the matrix of size l*l

The solution for the above equation is obtained by solving the Eigen value problem given below for the non-zero Eigenvalues.

$$l\lambda\alpha = K\alpha \qquad \text{Equation 4-28}$$

By normalizing the solutions of α^k which belongs to non-zero Eigen values and also the corresponding vectors in F is normalized we get,

$$1=\sum_{i,j=1}^{l} \alpha_i^k \ \alpha_j^k \left(\varphi(x_i).\varphi(x_j)\right) = \left(\alpha^k.K\alpha^k\right) = \lambda_k(\alpha^k.\alpha^k) \qquad \text{Equation 4-29}$$

To extract the principal components, the projections of the image at a point onto the Eigen vectors in F is computed as,

$$(V^k.\varphi(x)) = \sum_{i=1}^{l} \alpha_i^k \ (\varphi(x_i).\varphi(\mathrm{x})) \qquad \text{Equation 4-30}$$

Where,

V^k = Eigen Vectors

α = Column vectors.

Schölkopf et al. (1997) have found that the main advantage of using kernel based PCA is that it improves the recognition capability of the non-linear PCA components when compared with the linear PCA components.

- **MCSM based feature extraction in Radarsat 2 and ALOS PALSAR**

The extraction of features from the fully polarimetric data sets were performed using MCSM decomposition to obtain the Surface, Double bounce, Helix, Volume and Wire scattering parameters. The detailed description had been discussed earlier in this chapter.

Next section is about the decision level fusion.

4.4. Decision level fusion

The third and the highest level of fusion is the decision level fusion. Here the original source images namely the Hyperion, extracted MCSM polarimetric parameters from Radarsat 2 and the ALOS PALSAR were first classified and the obtained rule images were stacked together to form a feature vector. So there were two feature vectors formed, one was for the Hyperion and Radarsat 2 pair and the other one was for Hyperion and ALOS PALSAR pair. These rule images are the priori output of the classification. These rule images consist of the membership values of the belongingness of a pixel to a particular class based on the distance from the fitted decision line. In general, the SVM multiclass classification works on two types of strategies. They are

- ✓ One Against All (OAA)
- ✓ One Against One (OAO)

Since in this research, the SVM used was based on the "One Against All (OAA)" strategy, eight rule images were obtained for the eight defined classes and a second SVM classification was applied to the feature vectors to decide the final class membership of each pixel based on the fitted decision line. The one against all strategy was used in this research as it is computationally better than the one Against One (OAO)" strategy. Finally, the accuracy assessment was performed for the information fused outputs. The adopted methodology for the decision level fusion is shown in the figure 4-9.

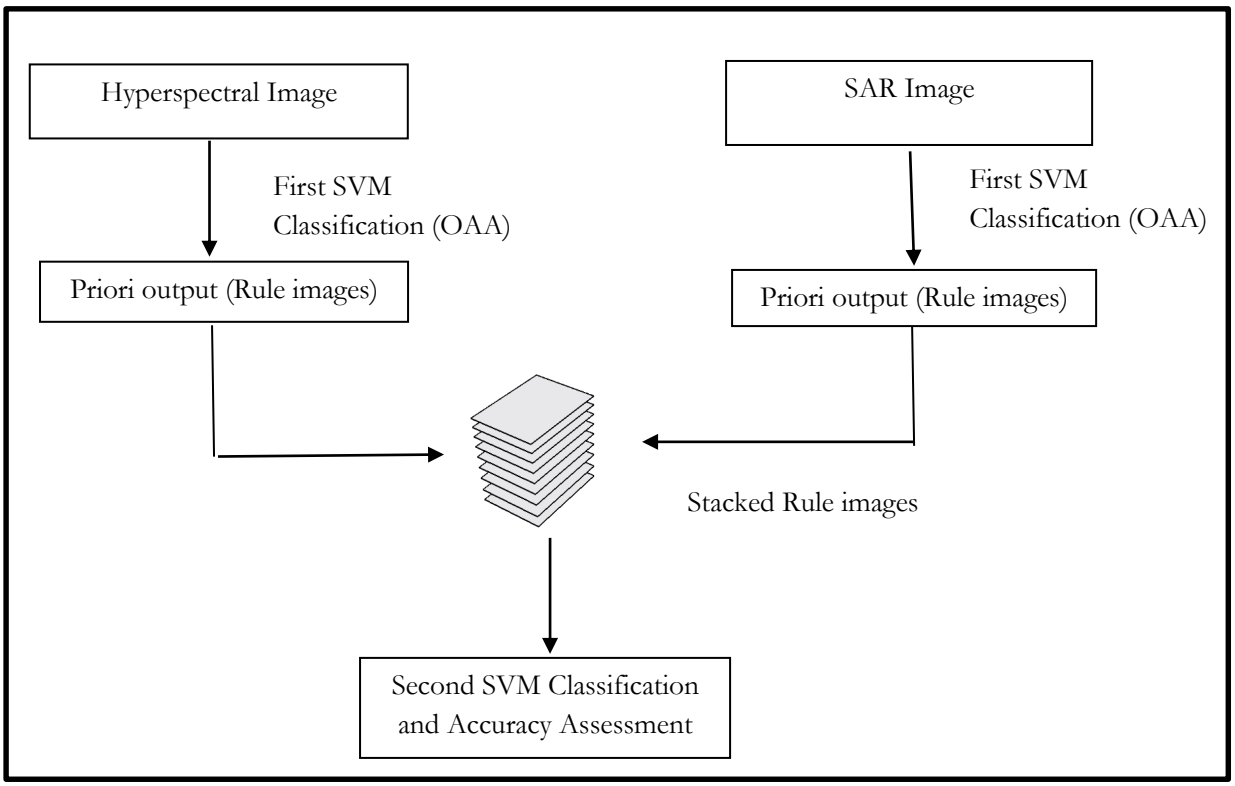

Figure 4-10 Decision level fusion

- **One Against All multiclass SVM classification**

Initially, the SVM were developed as a binary classifier. Now it's being used to solve the multiclass problems. There are two mostly used approaches namely One Against All and One Against One strategies being used to solve the above problem (Waske & van der Linden, 2008).. In the case of OAA strategy, there are a set of n binary classifiers are trained to separate each class from the remaining classes (Waske et al., 2007). Therefore n rule images are obtained which consists of the maximum distance from the fitted decision line, and this decides the final class membership of a pixel. Below is the depiction of OAA Aisen (2006)

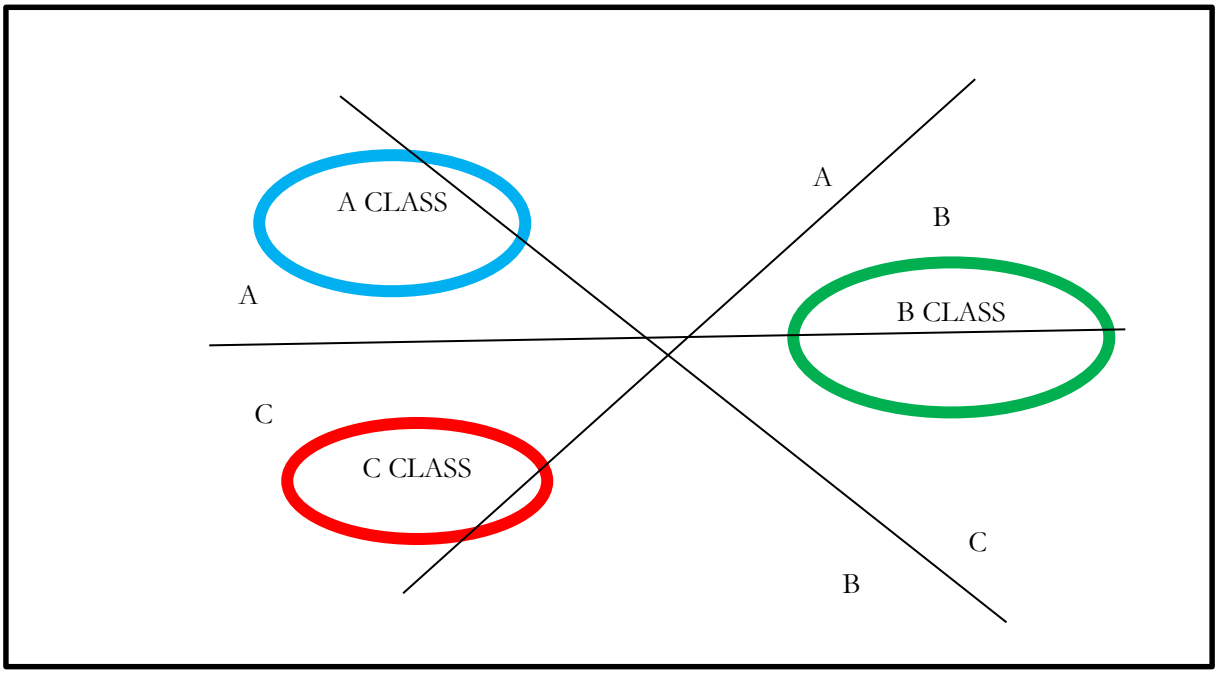

Figure 4-11 SVM - OAA Classification

4.5. Classification and Accuracy assessment

4.5.1. Classification

Classification using Support Vector Machine was performed after each level of fusion for the fused output from Hyperion + Radarsat 2 and Hyperion + ALOS PALSAR. Level 2 classification scheme of NRSC was adopted. The reason behind the choice of SVM classification was due to the high dimensionality of the hyperspectral dataset the well-known problem known as the Hughes phenomenon occurs. Hughes phenomenon is related to the number of training samples taken in relation to the dimensionality of the data. As the dimensionality of the data increases at a certain point, the prediction accuracy gets decreased. This is because of the less training samples with respect to the number of bands of the hyperspectral data. Generally, in this case, feature selection or extraction is applied to the high dimensional dataset but the SVM is more robust than any other classifier, and it is less sensitive to the Hughes phenomenon.

➢ Support Vector Machines and Kernels

Support vector machines is a supervised non-parametric and statistical learning technique. In this technique, there is no underlying assumption of the data (Mountrakis, Im, & Ogole, 2011). Given a set of labelled data, the SVM algorithm finds a hyperplane which separates the dataset into the defined classes. The optimal separation hyperplane indicates the decision boundary that helps in minimizing the miss-classifications. SVM classifier is a linear binary classifier in its simplest form. In the linear case of SVM, the assumption is that the data are linearly separable in the input space (Mountrakis et al., 2011).

Below explanation of the support vector machines is described based on the work of Melgani & Bruzzone (2004).

Let us consider a set of training samples i=1, 2…, N in a feature |space X_i and there are two classes which are linearly separable. Hence, it is possible to find an optimal hyperplane that separates the two classes. Therefore, the discriminant function is given as,

$$f(x) = W.x + b \qquad \text{Equation 4-31}$$

Where,

W = Vector that defines the hyperplane,

b = bias that can separate two classes without errors.

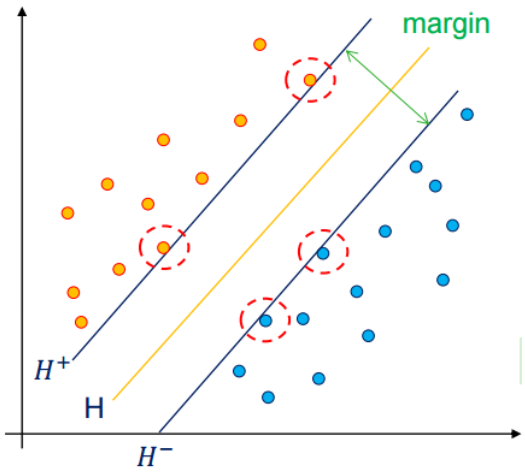

H – Hyperplane
H+ and H- are the
Two classes

Figure 4-12 SVM Linear classification (Bruzzone et al., 2010)

To get the optimal hyperplane, the parameters such as W and b has to be found. This is given as,

$$yi(W.Xi + b) > 0 \qquad \text{Where } i = 1, 2 \ldots, N \qquad \text{Equation 4-32}$$

The primary objective of SVM is to find the maximum distance between the training samples that are available closely and to the hyperplane that is separating. This distance is given a equal to 1/||W|| such that,

$$\min i\ (\ \ y_i(W.X_i + b)) \geq 1 \text{ Where } i = 1, 2, \ldots\ldots, N \qquad \text{Equation 4-2}$$

Therefore, the geometrical margin between the two classes can be given as 2/||W||, and the optimal hyperplane is found out by,

$$\begin{cases} \text{Minimize}: \dfrac{2}{||w||} \\ \text{Subject to: } y_i(W.X_i + b)) \end{cases} \qquad \text{Equation 4-33}$$

This optimization problem is translated into a dual problem using Lagrangian formulation AS

$$\begin{cases} \text{maximize: } \sum_{i=1}^{N} \alpha_i - \dfrac{1}{2}\sum_{i=1}^{N}\sum_{j=1}^{N} \alpha_i \alpha_j y_i y_j (\mathbf{x_i} \cdot \mathbf{x}_j) \\ \text{subject to: } \sum_{i=1}^{N} \alpha_i y_i = 0 \text{ and } \alpha_i \geq 0, \qquad i = 1, 2, \ldots, N. \end{cases} \qquad \text{Equation 4-34}$$

Where α_i is the Lagrange multiplier and now the discriminant function becomes dependent on both the Lagrange multiplier and also the training samples as,

$$f(X) \ = \ \sum_{I \in S} \alpha y_i (X_i . X) + b \qquad \text{Equation 4-35}$$

Corresponding to the non-zero Lagrange multipliers' S is then subset of training samples. In determining of the discriminant function the Lagrange multipliers weight each of the training sample according to the importance determining the discriminant function. Support vectors are the training samples associated to nonzero weights. These support vectors lie exactly at a distance 1/||W|| to from the optimal hyperplane. In real cases, it is not possible that there are linearly separable cases. In the case of non-separable data, the solution is that expresses the combination of two criteria. The criteria are the margin maximization as in the previous case and the error minimization to penalize the wrongly classified samples. Hence, the new function is given as,

$$\psi(W, \xi) = 1/2(||W||)^2 + C\sum_{i=1}^{N} \xi_i \qquad \text{Equation 4-36}$$

In the above equation, ξ_i called the slack variable is introduced to account for the non-separability of the data and C is the regularization or the cost parameter that allows to control the penalty assigned for the mis-

classification of the samples. It is to be noted that the larger the C value larger is the penalty associated with the miss-classification and vice-versa.

To improve the above method of separating the two inseparable classes is to generalize the above method to non-linear discriminant function using kernels. In general, a kernel corresponds to the inner dot product of two features in a feature space based on some mapping.

$$K(xi, xj) = \varphi(xi).\varphi(xj)$$ Where φ is the mapping term. Equation 4-37

According to mercer's theorem, every semi-positive definite function is a kernel. To be a valid kernel in SVM, the kernel function needs to fulfill mercer's theorem (Scholkopf & Smola, 2002). Most standard kernel functions used in SVM are Polynomial, Sigmoid and Radial basis function kernels.

Linear Kernel:

$$K(x, xi) = x.xi$$ Equation 4-38

Polynomial Kernel:

This kernel computes the inner product of all monomials up to degree p

$$K\ (x, xi) = (x.xi + 1)^{P}$$ Equation 4-39

Radial Basis Function Kernel:

$$\mathrm{K}\ (\mathrm{x}, \mathrm{xi}) = \frac{exp(-\|x-xi\|)^2}{2\sigma^2}$$ Equation 4-40

Sigmoid Kernel:

$$K(x, xi) = tanh\,(x.xi + 1)$$ Equation 4-41

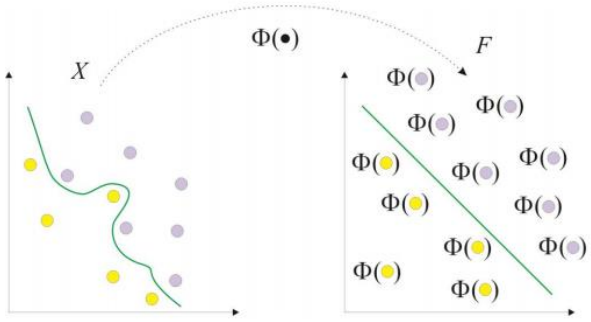

X is the input space
F is the high dimensional feature space
Φ is the mapping function

Figure 4-13 Nonlinearity mapping in high dimensional feature space using Kernel (Bruzzone et al., 2010)

Therefore using of the kernel can avoid the computation effort and solve the dual problem, as it avoids the computation of the inner products in the transformed space. Hence, the final discriminant function is expressed as,

$$f(X) = \sum_{i \in S} \alpha_{iy_i} k(X_i, X) + b \qquad \text{Equation 4-42}$$

4.5.2. Accuracy assessment

Accuracy assessment is one of the necessary steps in validating the methods and methodology adopted. In this research the cross-validation based model evaluation and accuracy assessment was adopted. In particular, the hold-out method of cross validation was performed with Training set, Test set and validation set. Following is the explanation of cross validation in general, holdout method of cross validation and optimization of kernel parameters.

- **Cross Validation**

Cross-validation, is also called as rotation estimation (Kohavi, 1995), is a model validation technique which is used to evaluate the results of how the analysis based on statistics will generalize to an independent data set. The basic idea of cross validation is to train the classifier with the training set and test it with the entirely new test dataset. The different methods of cross-validation are,

- ✓ Holdout cross validation
- ✓ K-fold cross validation
- ✓ Leave one out cross validation

In this research Hold out method cross validation was used and spatially uncorrelated samples were taken as training, validation, and test sets. Below is the description of the method.

- **Hold out method with parameter tuning**

This the simplest method of cross-validation. Hold out method was performed for this research to train the SVM classifier and to test it. This method is also called as the test sample estimation method as the data is divided into two mutually exclusive subsets of the training set and a test set or a holdout set (Kohavi, 1995). Additionally, a validation set was used to fine tune the kernel parameters.

Figure 4-14 Samples for cross validation

The validation set is used to fine tune the kernel parameters. In case of radial basis function the parameter is gamma (ɣ) and the SVM cost parameter C. In polynomial kernel the parameters are degree, gamma, coefficient and the SVM parameter C. In sigmoid kernel it is gamma and coefficient along with the SVM parameter C. A grid search is one of the methods to define a set of candidate values for the parameter which is to be optimized. These parameters were tested, and the optimum values of the parameters were obtained based on the higher accuracy on the validation set. Below is an example of assigning values for each parameter in a grid search.

Cost C ϵ {1, 50, 100, 150, 200, 250, 300}

Degree p ϵ {1, 2, 3}

Co-efficient C0 ϵ {1, 5, 10}

Gamma γ ϵ {0.05, 0.10, 0.15, 0.20,…, 1}

The parameters have to be well optimized and if not the overfitting or the under fitting problem of the model occurs.

4.6. Comparative Analysis

Finally, a comparative analysis was made between the three levels of fusion and the two pairs of the products. The optimum level of fusion and also the pair was chosen based on the accuracy of the classification.

5. RESULTS AND DISCUSSION

5.1. Results

5.1.1. Results of Pixel level fusion

At this level of fusion, a comparative analysis was made for different pixel level fused products of Hyperion and SPAN data extracted from PolSAR data (Radarsat-2 & ALOS PALSAR) and their classified outputs. The results of the classified outputs of the fused products are shown in the Figure 5-1. The summary of the classification parameters and the accuracy is given in the Table 5-1

High pass filter fusion

The fusion of Hyperion+Radarsat 2 (span) and Hyperion+ALOS PALSAR (span) preserved the spectral characteristics of Hyperion with minimal spatial distortion. The fused products are shown in the Figure 5-1 (A and B).

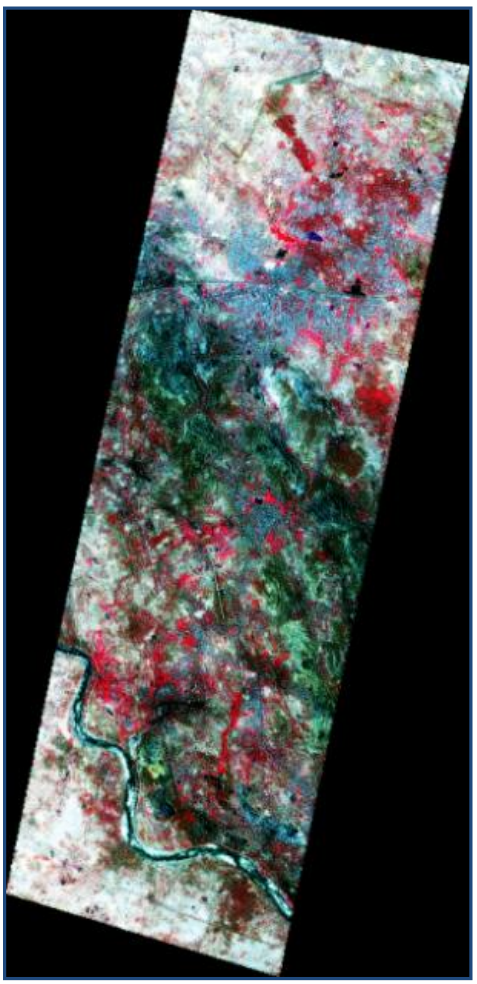

(A)

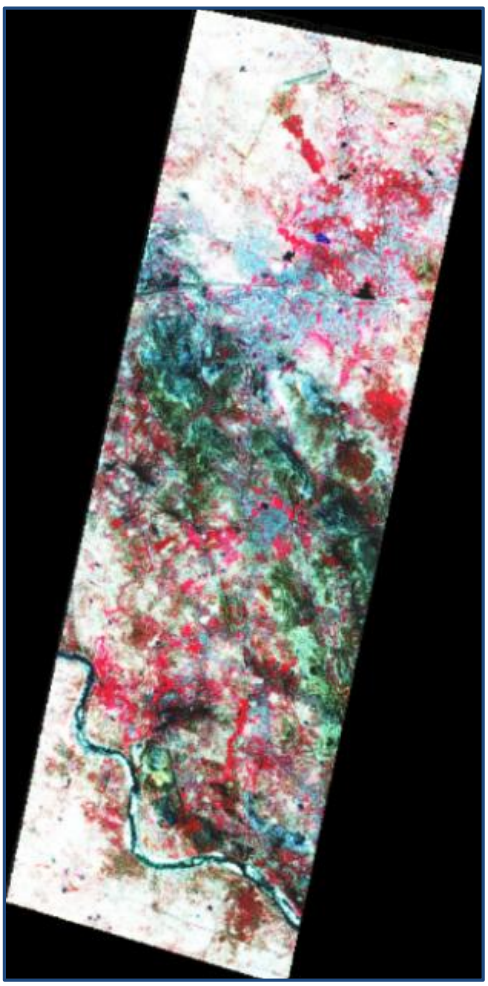

(B)

Wavelet fusion

Wavelet fusion of Hyperion+Radarsat 2 and Hyperion+ALOS PALSAR preserved the spectral property of Hyperion to a certain extent, but there were spatial distortions in both the fused products. The fused images are shown in the figure 5-1 (B and C).

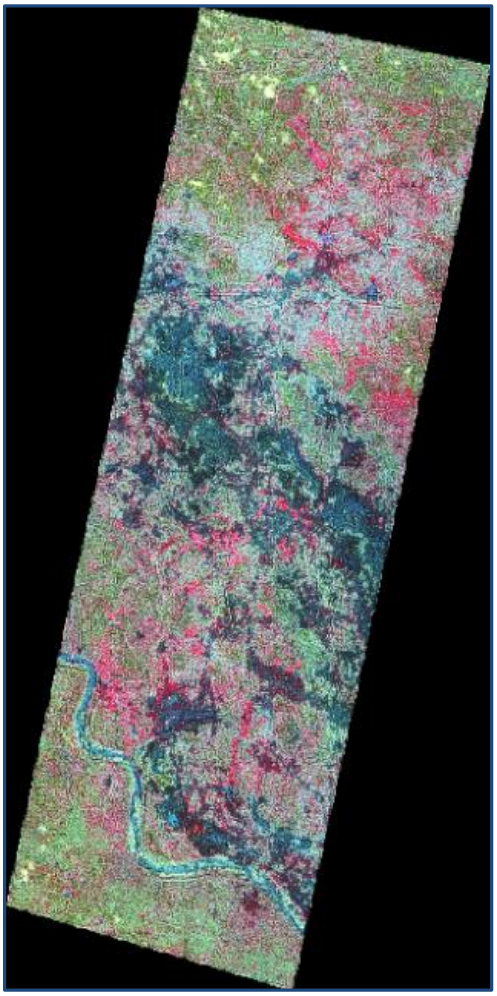

(C)

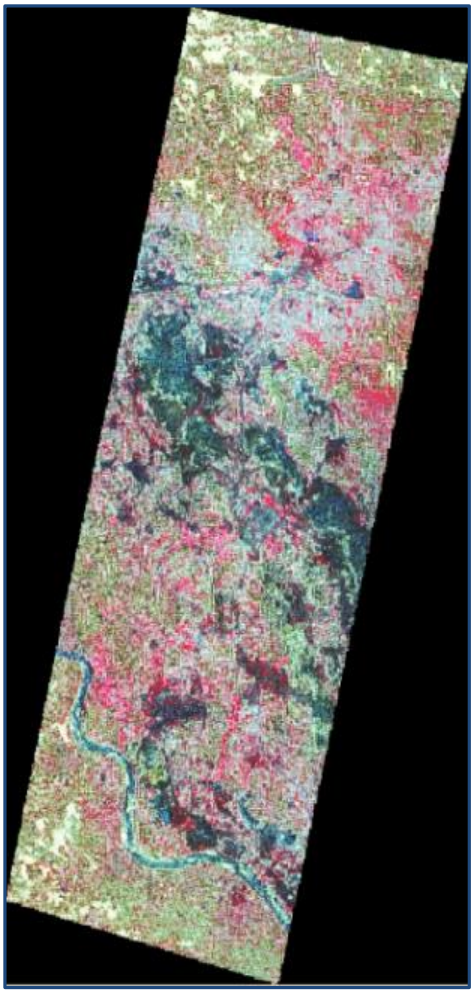

(D)

Gram-Schmidt Fusion

In this fusion, the spectral properties were not well preserved. It produced a spectrally distorted image as shown in the Figure 5-1(E and F).

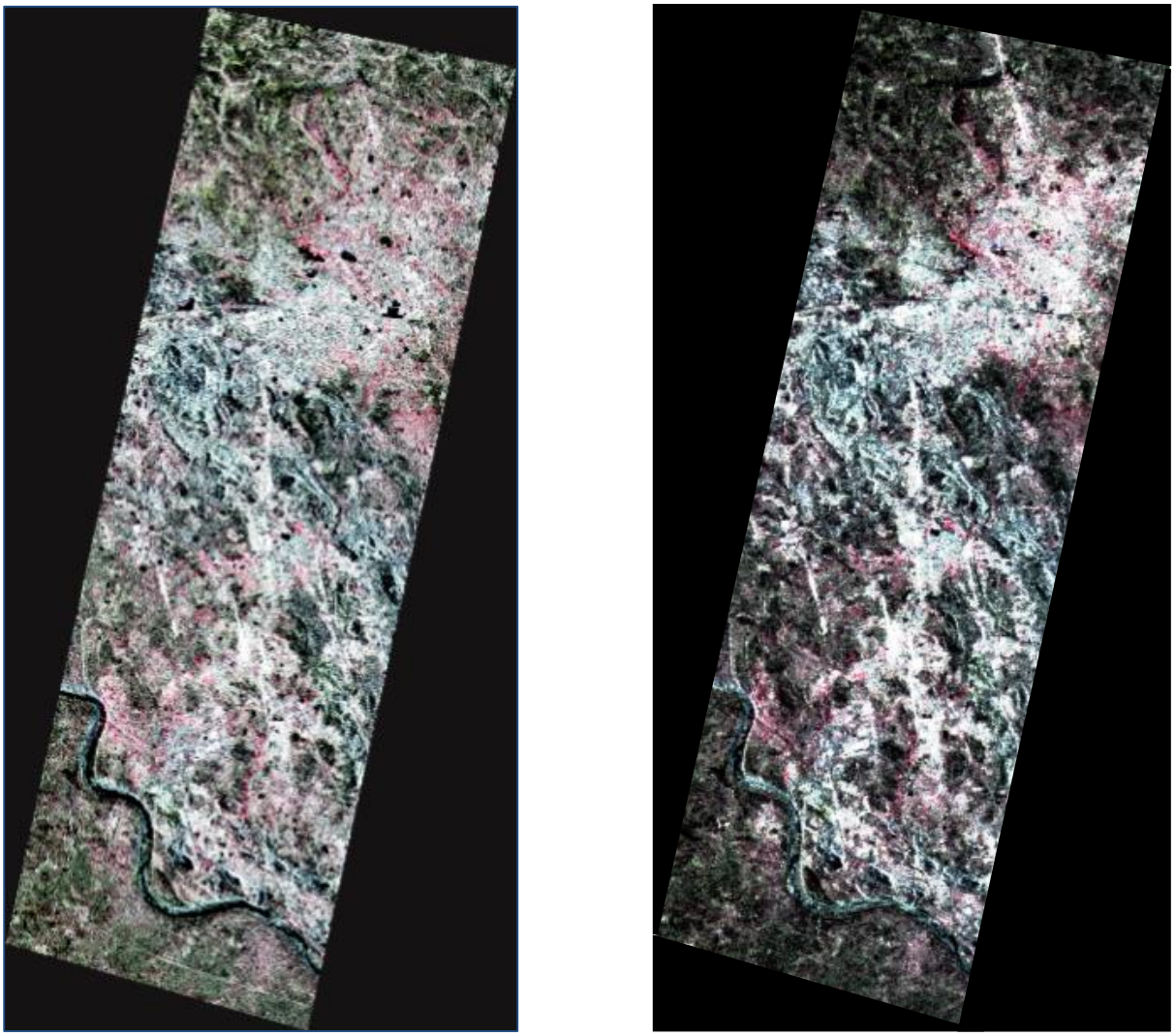

(E) (F)

Figure 5-1 Fused results of pixel level fusion - (A) - HPF fusion of Hyperion and Radarsat 2 (B)- HPF fusion of Hyperion and ALOS PALSAR (C) – Wavelet fusion of Hyperion and Radarsat 2 , (D) – Wavelet fusion of Hyperion and ALOS PALSAR, (E) – Gram-Schmidt fusion of Hyperion and Radarsat 2, (F) – Gram-Schmidt fusion of Hyperion and ALOS PALSAR.

- **Classification and the accuracy assessment of the fused products**

The classification was performed on all the pixel level fused products using non-linear support vector machines. The kernel function used for SVM was the radial basis function. Further the accuracy assessment was carried out using cross-validation based hold out method. Based on the ground truth data, the spatially uncorrelated pixels were taken as the training set, test set and validation set for each of the fused products and also for the original Hyperion. The SVM model was fine-tuned based on the accuracy obtained using validation set and the kernel parameter gamma and the SVM parameter C were chosen. Table 5-1 shows the summary of the parameter values chosen and the accuracy obtained for the classification of the fused products. Below are the classified images of the fused products and the original Hyperion image.

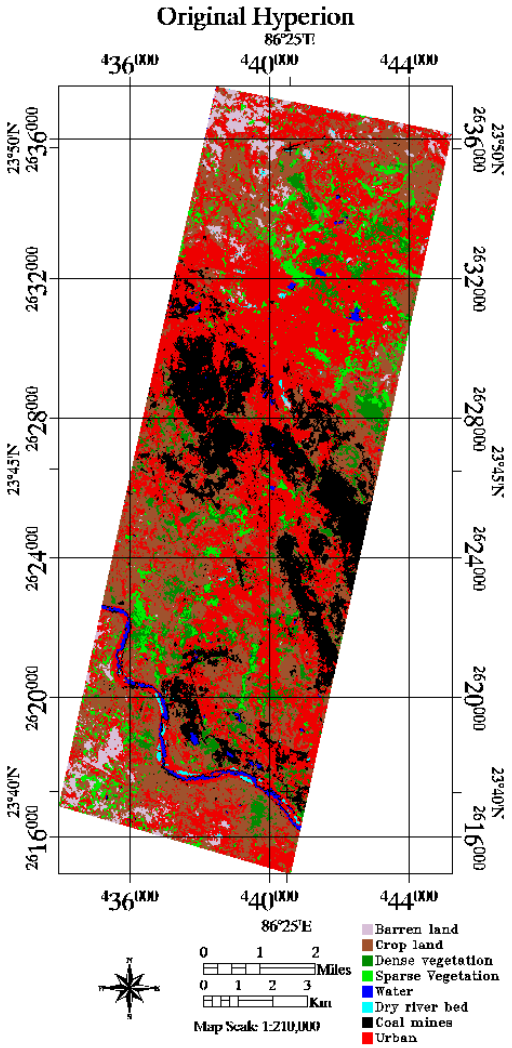

(A)

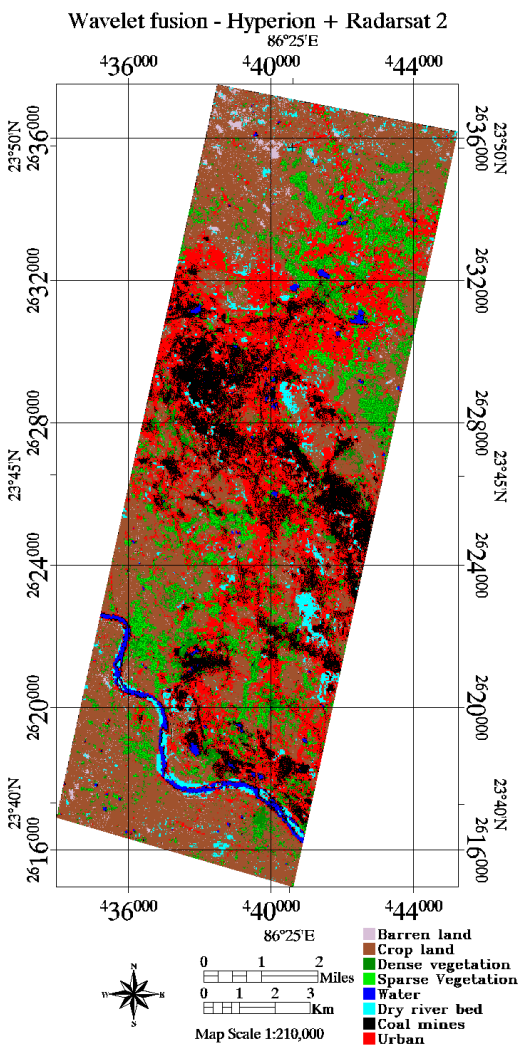

(B)

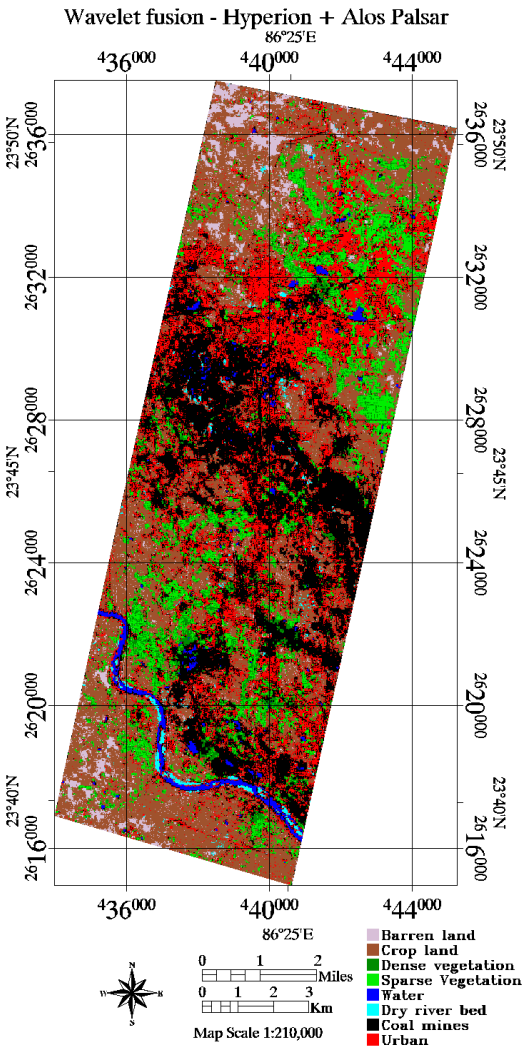

(C)

Barren land | Crop land | Dense Veg. | Sparse Veg. | Water | Dry river bed | Coal mines | Urban

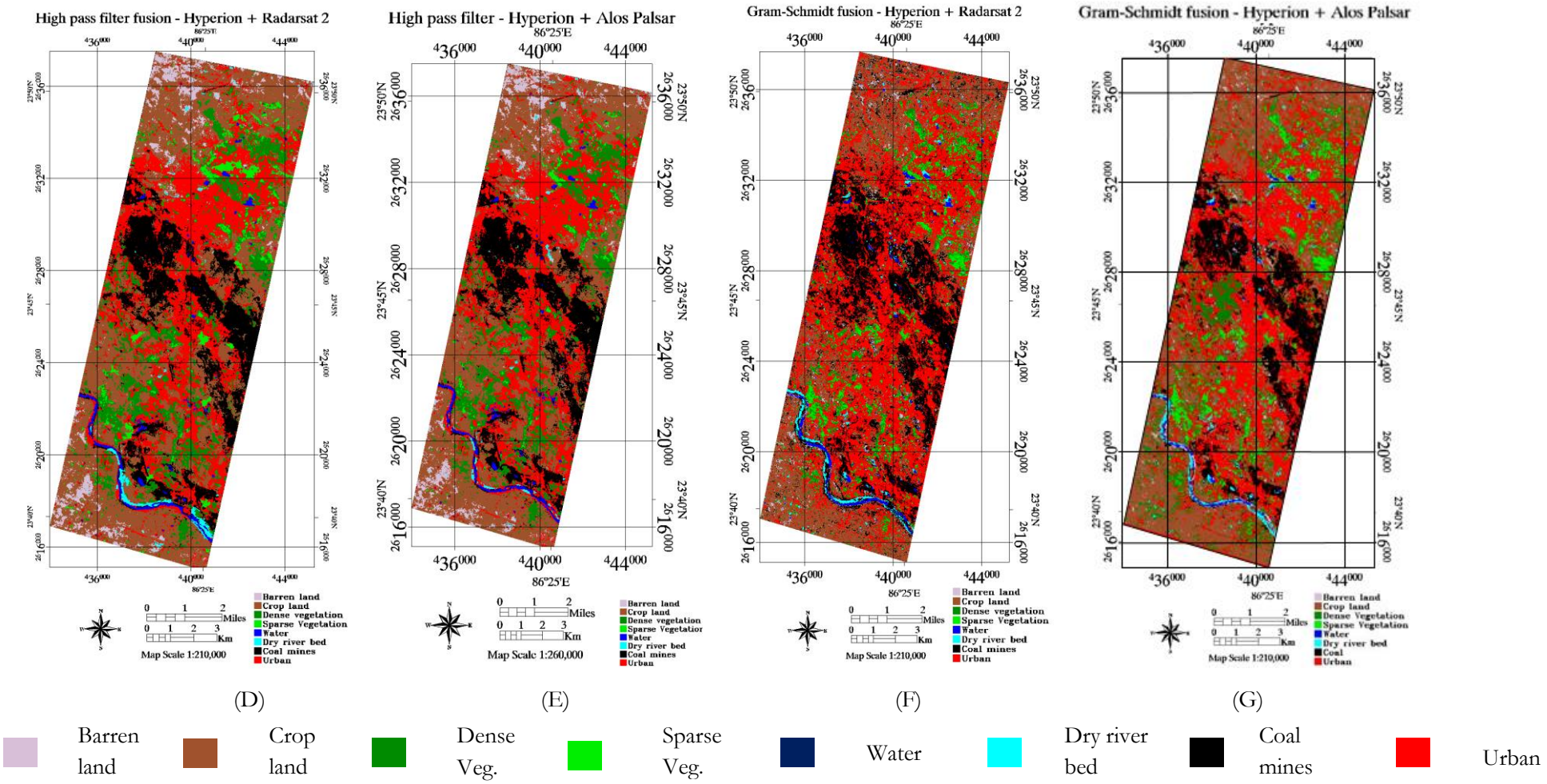

Figure 5-2 Classified images of pixel level fusion - (A)-Original Hyperion image, (B) - Wavelet fusion (Hyperion+Radarsat 2), (C)-Wavelet fusion (Hyperion+ALOS PALSAR), (D)-HPF fusion (Hyperion+Radarsat 2), (E)-HPF fusion (Hyperion+ALOS PALSAR), (F)-Gram-Schmidt fusion (Hyperion+Radarsat 2), (G) – Gram-Schmidt fusion (Hyperion+ALOS PALSAR.

Table 5-1 Summary of the classification parameters, and the accuracy assessment – Pixel level fusion

Data set / Classification and Accuracy Parameters	Hyperion	Wavelet fusion		High pass filter fusion		Gram-Schmidt fusion	
		RS2+HSI	AP+HSI	RS2/HSI	AP+HSI	RS2+HSI	AP+HSI
Cost Parameter	100	180	230	120	25	200	180
Gamma	0.75	0.20	0.40	0.25	0.85	0.95	0.95
Kernel	RBF	RBF	RBF	RBF	RBF	RBF	RBF
Total Support Vectors	385	1949	953	948	385	1889	514
OA	66.599	64.293	65.261	70.661	67.274	51.862	51.273
Kappa	0.565	0.561	0.568	0.635	0.601	0.328	0.305

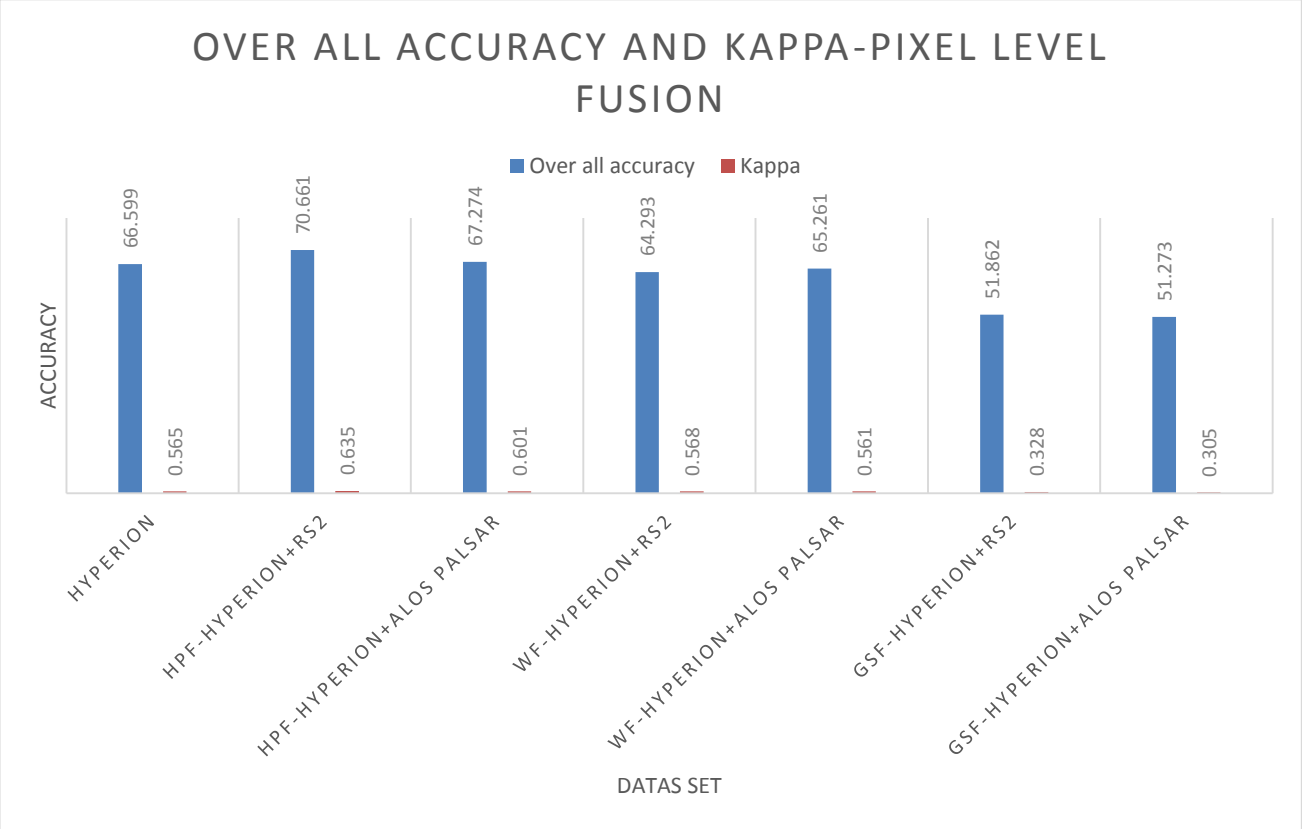

Figure 5-3 Comparison of overall accuracy and kappa of pixel level fusion techniques

The graphs (Figure 5-4 and Figure 5-5) represents the individual class accuracies for the defined land cover classes.

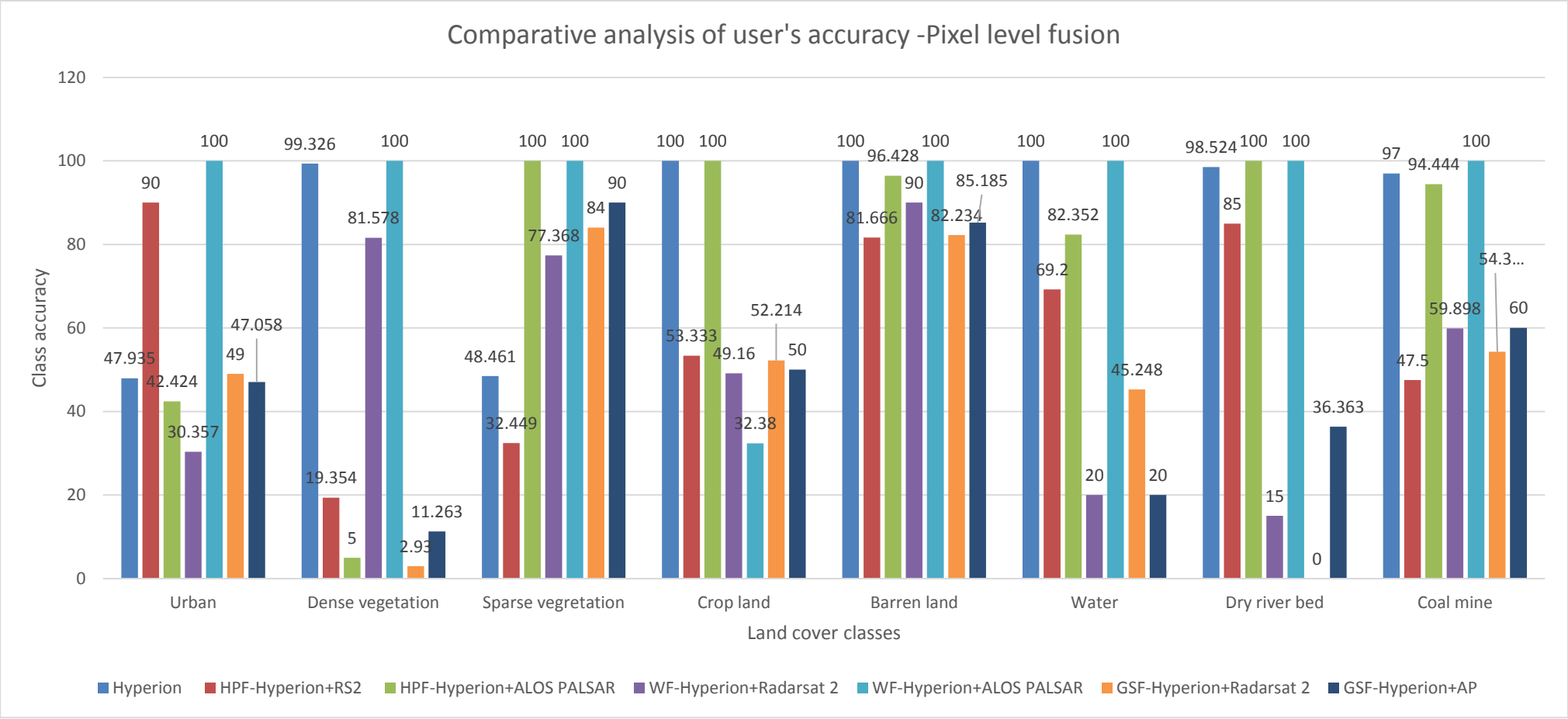

Figure 5-4 User's accuracies of the defined classes from the classified outputs of the Hyperion and Pixel level fused products

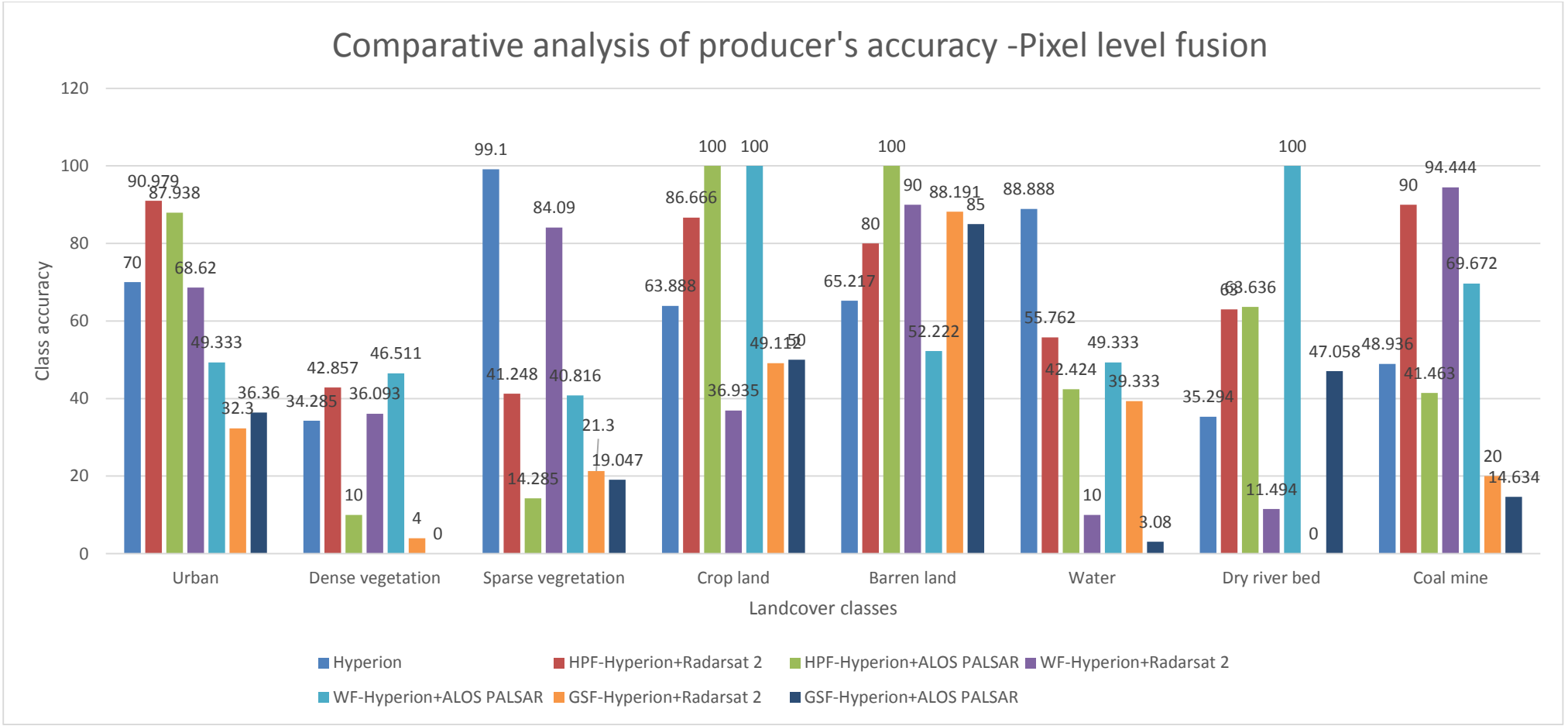

Figure 5-5 Producer's accuracies of the defined classes from the classified outputs of the Hyperion and Pixel level fused products

5.1.2. Results of Feature level fusion

The results obtained after feature level fusion performed by forming a feature vector of KPCA components extracted from Hyperion and the MCSM parameters extracted from the fully polarimetric SAR data.

- **Feature extraction from Hyperion using KPCA**

The kernel based PCA was performed using the radial basis function with a gamma value of 0.583. Unsupervised K-means was performed using random training samples. The distance between the training samples were considered for choosing the gamma value. Below are the obtained principal components using kernel method.

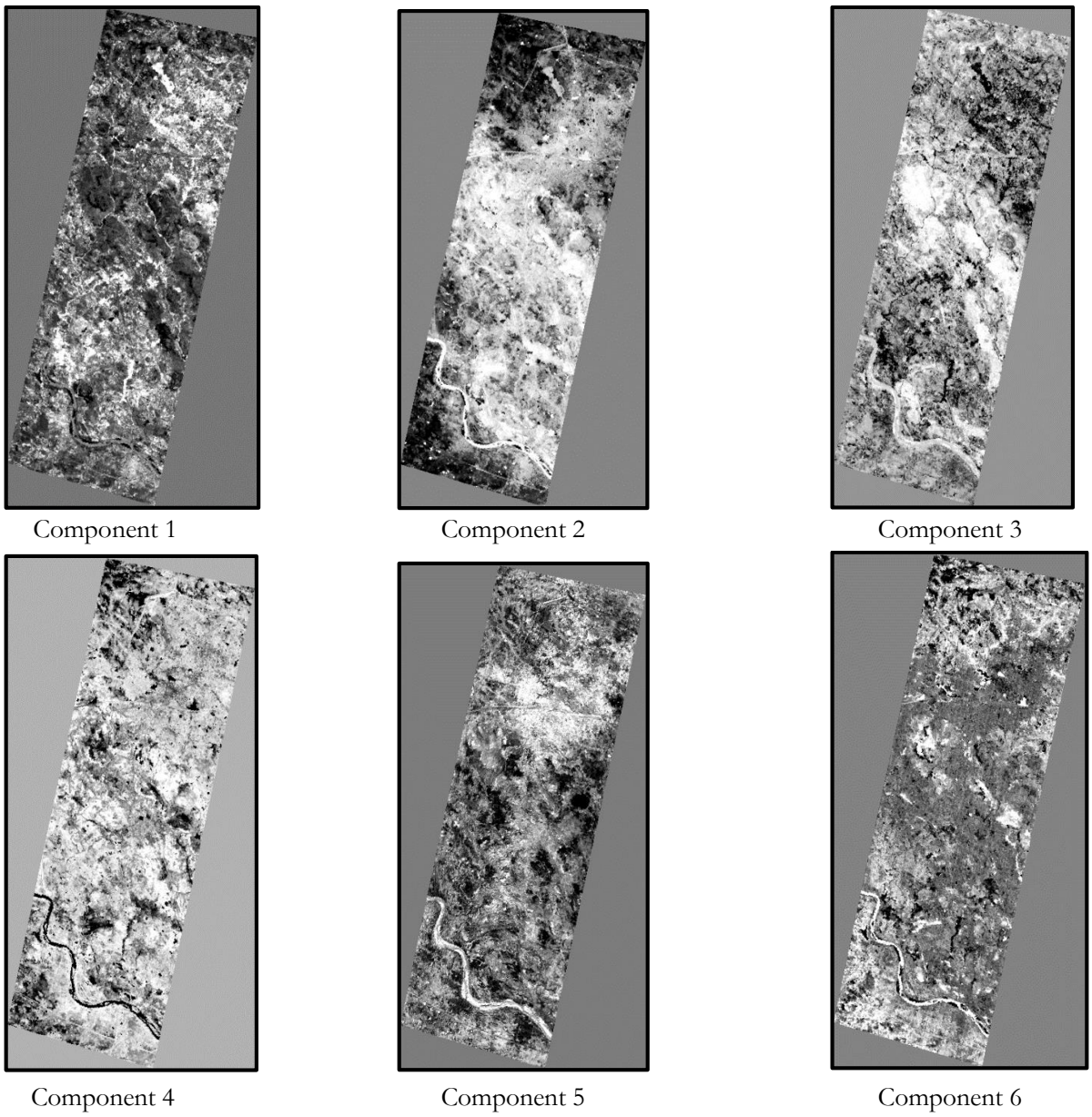

Figure 5-6 Principal components using KPCA

- **Multicomponent scattering model parameters**

The Multicomponent scattering model decomposition was performed on the fully polarimetric SAR data to extract the information using different scattering mechanisms such as the Double bounce scattering and Helix scattering for the extraction of urban features, Volume scattering for extracting the vegetation cover, Surface scattering for the moderately smooth scatterers and the wire scattering for extracting the thin canonical objects in the urban region. Below are the obtained MCSM components of RS2 and ALOS PALSAR images. The spatial resolution of the obtained images were at 20 meters.

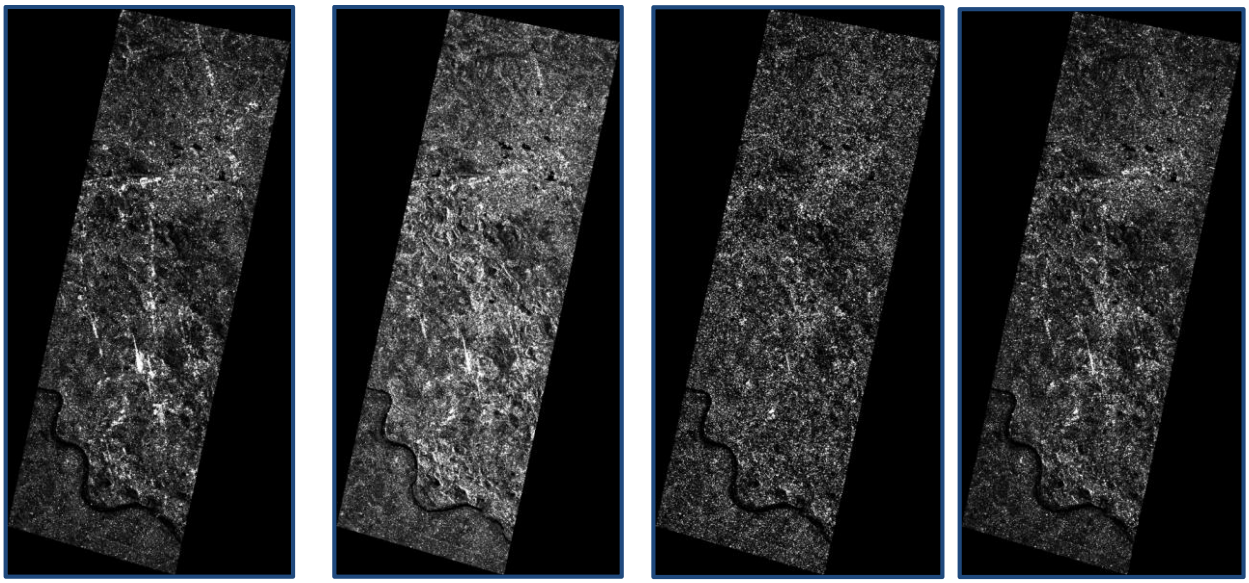

Double Helix Scattering Surface Scattering Volume Scattering Wire Scattering

Figure 5-7 MCSM parameters of Radarsat 2

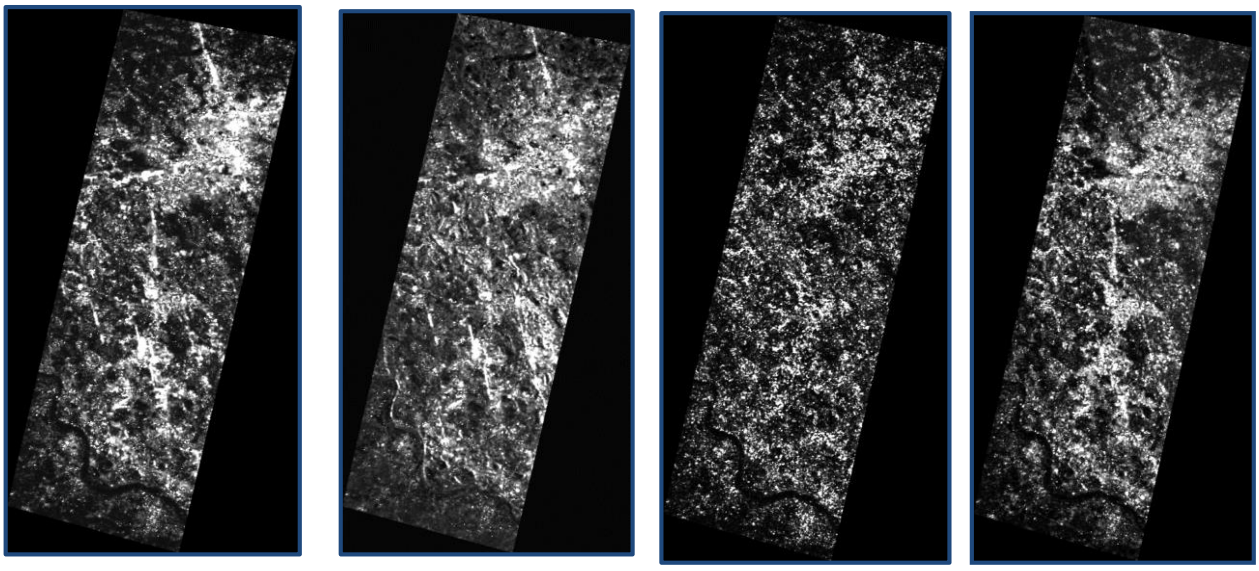

Double Helix Scattering Surface Scattering Volume Scattering Wire Scattering

Figure 5-8 MCSM components of ALOS PALSAR

False colour composite of the feature vectors formed using KPCA and MCSM components

Hyperion + Radarsat 2 **Hyperion + ALOS PALSAR**

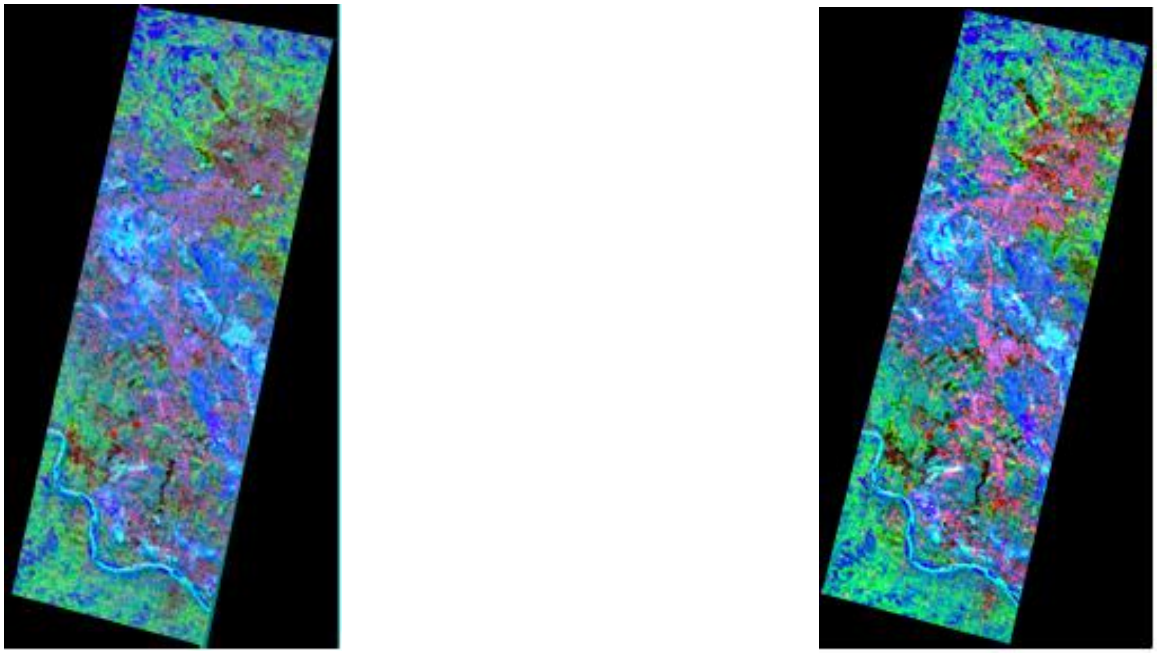

(A) (B)

Figure 5-9 False colour composite of the feature vectors R-Double Helix Scattering, G – KPCA component 6, B – KPCA component, (A)-Hyperion and Radarsat 2 (B) - Hyperion and ALOS PALSAR

- **Classification and accuracy assessment of the feature vectors and the SAR datasets**

After extracting the feature vectors from hyperspectral and PolSAR data the classification was performed using non-linear support vector machines. The kernel function used was the radial basis function for the classification of Hyperion and the feature vectors and polynomial kernel for the individual PolSAR datasets. In the case of the accuracy assessment was performed using cross-validation based hold out method. The spatially uncorrelated pixels were taken as the training set, test set and validation set for each of the feature vector and the fully polarimetric SAR datasets. The SVM model was fine-tuned based on the accuracy obtained using validation set and the kernel parameter gamma and the SVM parameter C were chosen. Table 5-2 shows the summary of the parameter values chosen and the accuracy obtained for the classification of the fused products. Figure 5-13 shows the classified images of the Hyperion, individual PolSAR data and fused products at feature level fusion.

In the below images RS2 indicates Radarsat 2

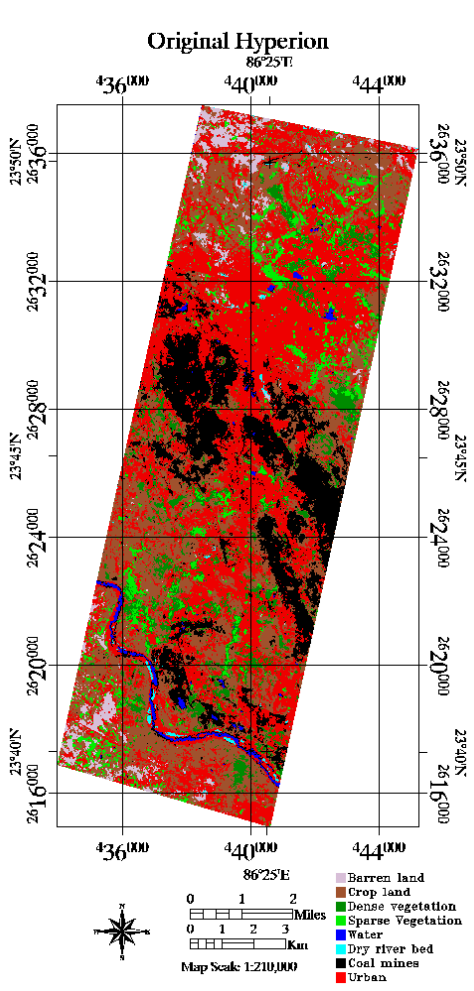

(A)

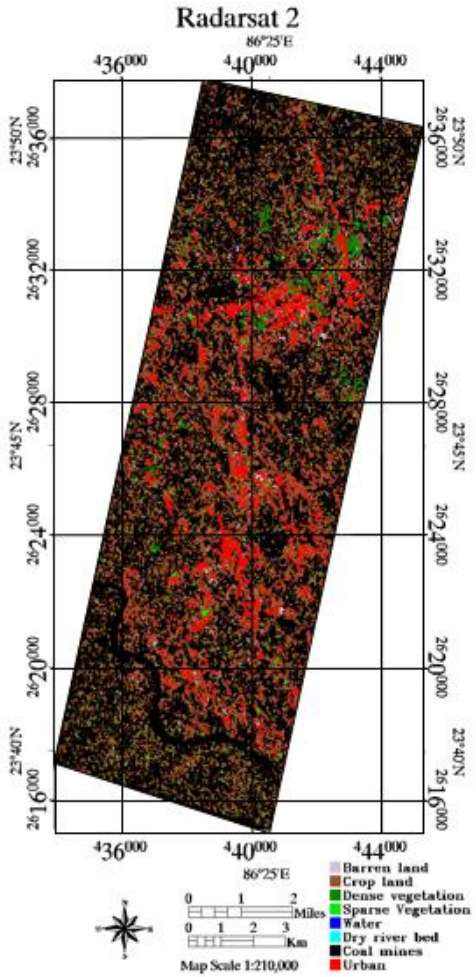

(B)

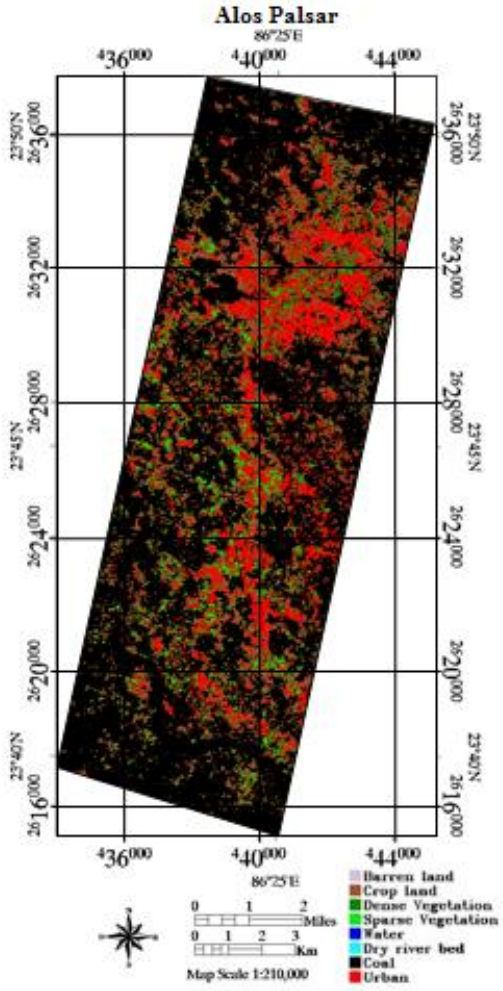

(C)

Barren land | Crop land | Dense Veg. | Sparse veg. | Water | Dry river bed | Coal mines | Urban

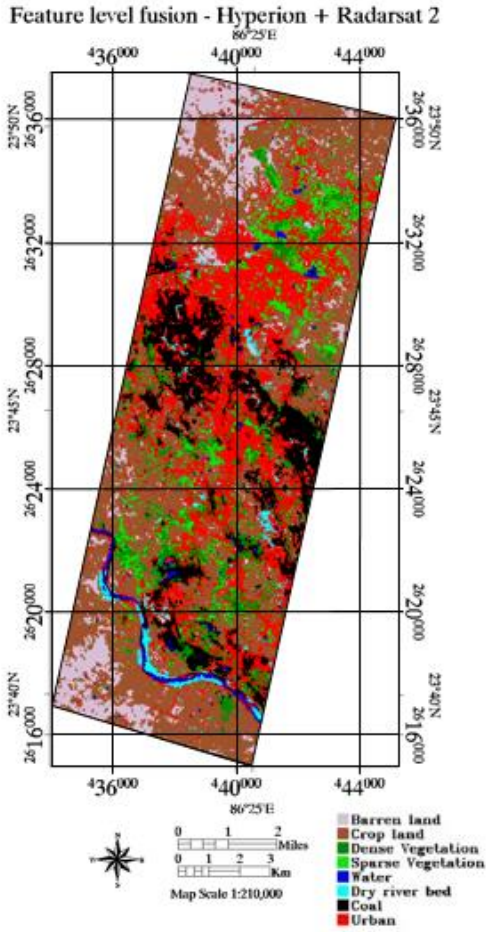

(D)

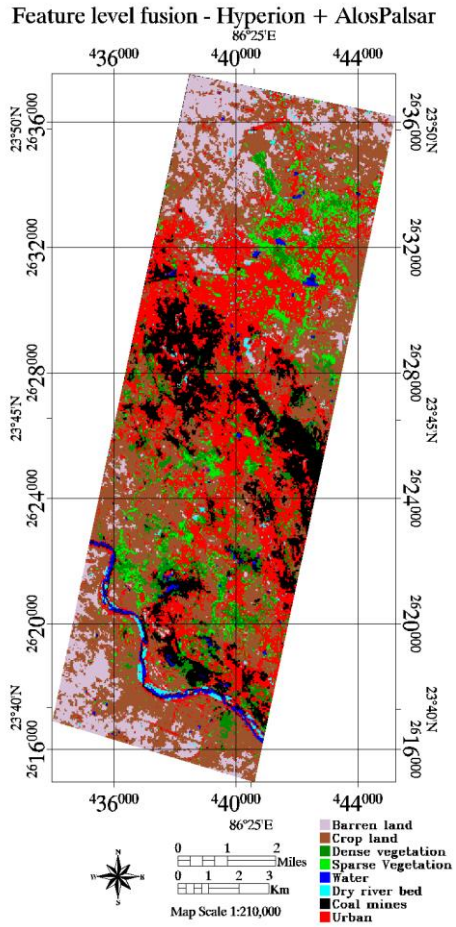

(E)

Barren land | Crop land | Dense Veg. | Sparse veg. | Water | Dry river bed | Coal mines | Urban

Figure 5-10 Feature level fusion - (A)- Hyperion, (B)- Radarsat 2, (C)- ALOS PALSAR,(D)-Hyperion+Radarsat 2, (E)-Hyperion+ALOS PALSAR

Table 5-2 Summary of the classification parameters, and the accuracy assessment – Feature level fusion

Dataset / Classification and Accuracy parameters	Hyperion Image	Radarsat 2 Image	ALOS PALSAR Image	Hyperion + Radarsat 2 using KPCA and MCSM	Hyperion + ALOS PALSAR using KPCA and MCSM
Kernel	RBF	polynomial	polynomial	RBF	RBF
Cost Parameter	100	230	320	270	290
Gamma	0.75	0.35	0.6	1.85	1.4
Degree	NA	2	2	NA	NA
Coeff0	NA	5	5	NA	NA
Total Support Vectors	385	557	970	623	381
OA	66.599	39.641	43.331	73.604	76.568
Kappa	0.565	0.279	0.376	0.679	0.713

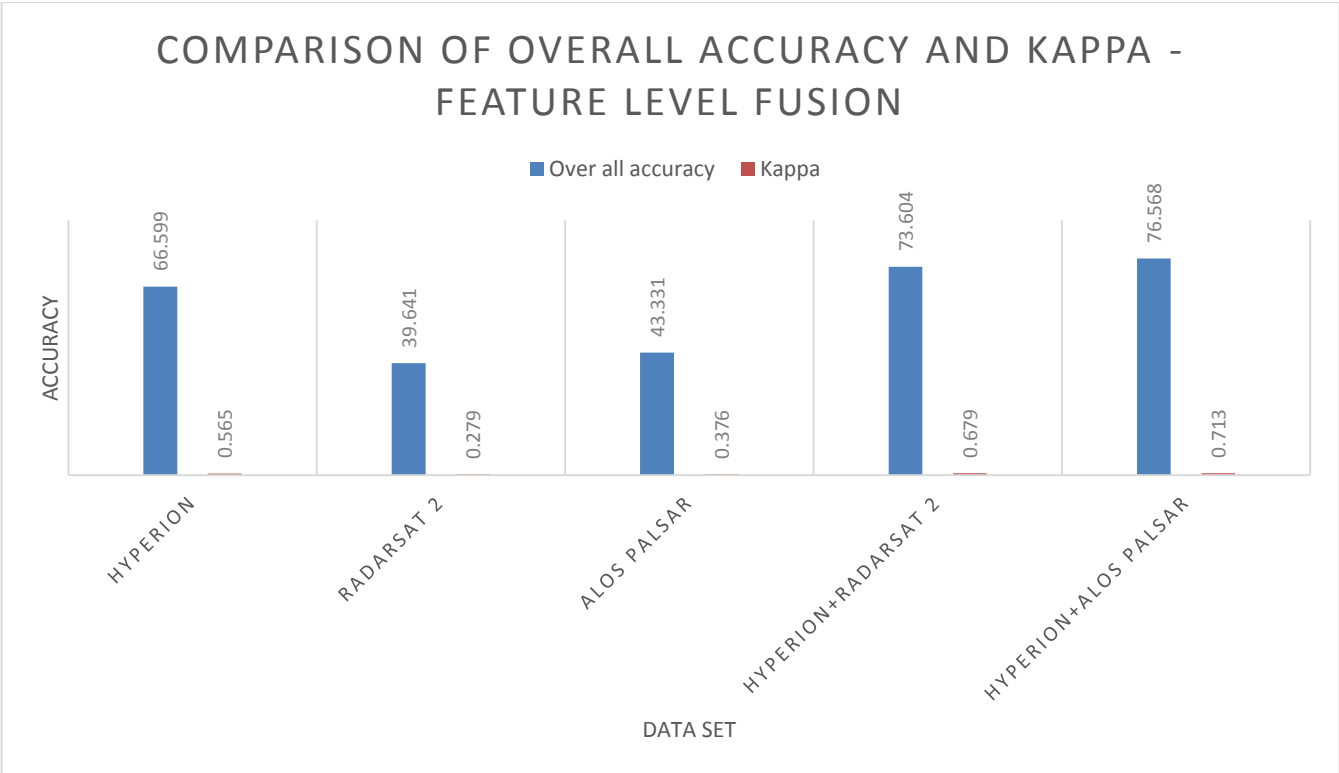

Figure 5-11 Comparison of overall accuracy and kappa - Feature level fusion

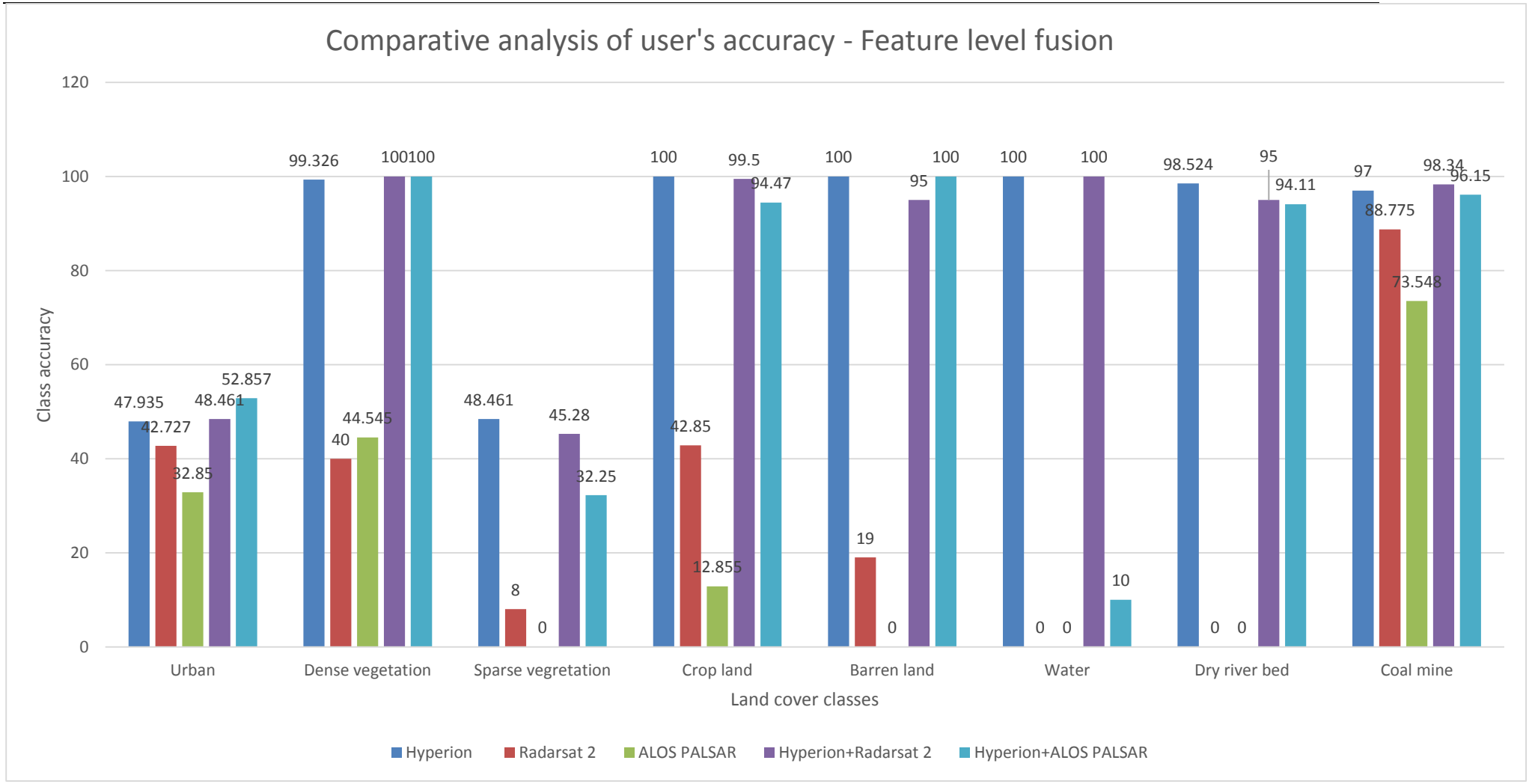

Figure 5-12 Userr's accuracies of the defined classes from the classified outputs of the Hyperion, Radarsat 2, ALOS PALSAR and Feature level fused products

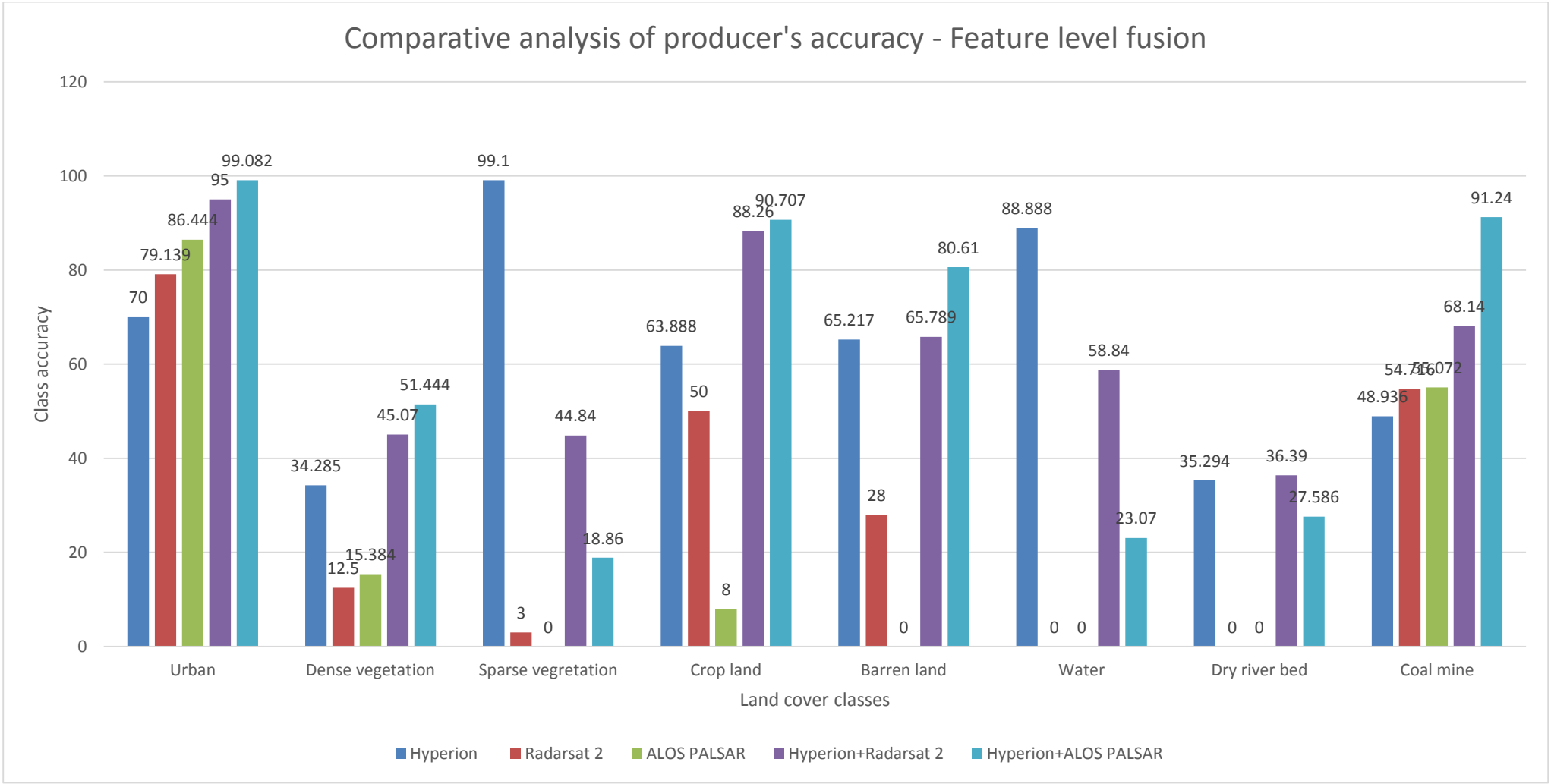

Figure 5-13 Producer's accuracies of the defined classes from the classified outputs of the Hyperion and Feature level fused products

5.1.3. Results of Decision level fusion

Decision level fusion was performed on the rule images which were the priori output of the SVM classification of Radarsat 2, ALOS PALSAR and the Hyperion images. Total 8 rule images were obtained for each of the classes for all the three datasets. The feature vector formed using the obtained rule images is shown in Figure 5-16

True colour composite of the feature vectors formed using the rule images

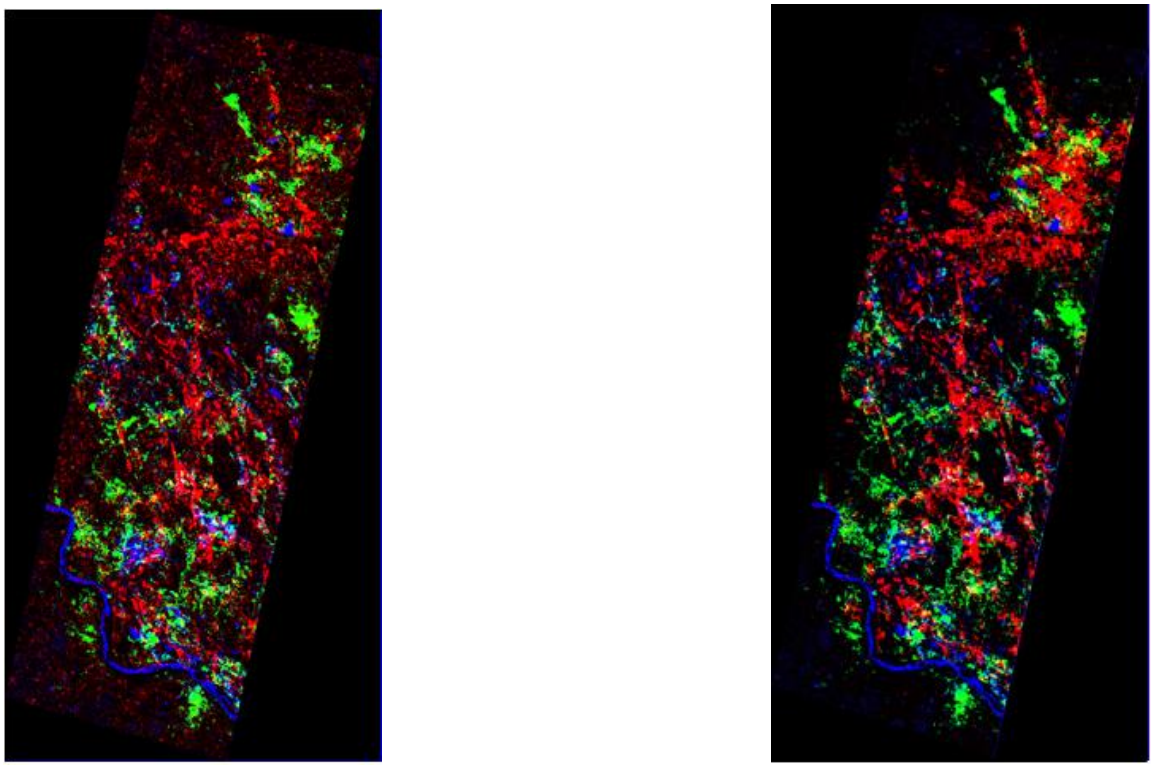

(A) (B)

Figure 5-14 False colour composite of the feature vector, R-Rule image of Urban class – Fully polarimetric data, G – Rule image of Dense vegetation class – Hyperion, B- Rule image of Water class – Hyperion - (A)-Hyperion and Radarsat 2, (B)-Hyperion and ALOS PALSAR,

- **Classification and accuracy assessment of the feature vectors and the SAR datasets**

The feature vectors obtained using the rule images were classified using the SVM second time to obtain the final class membership of the pixels. The training, test, and validation samples were taken based on the membership values of each pixel belonging to a particular class. The value ranges from 0 to 1. The values indicate the distance of the pixels to the fitted hyperplane of the SVM model. Lower the value closer is the pixel to the fitted hyperplane and vice-versa. A decision was made in a way that a range was set from 0.80 to 1, and the pixels belonging to this specified range was considered as the training, test, and validation samples. Different kernels such as radial basis function, polynomial and sigmoid were tried, and the optimal kernel was chosen based on the overall accuracy. Figure 5-15 shows classified images of the original data sets and the information fused datasets at decision level fusion. Summary of the classification parameters and the accuracy is shown in the Table 5-3 and Table 5-4.

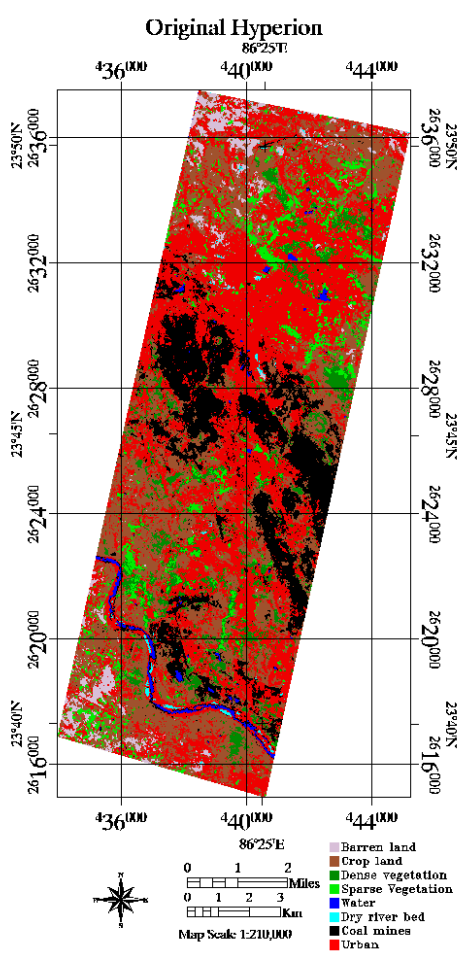

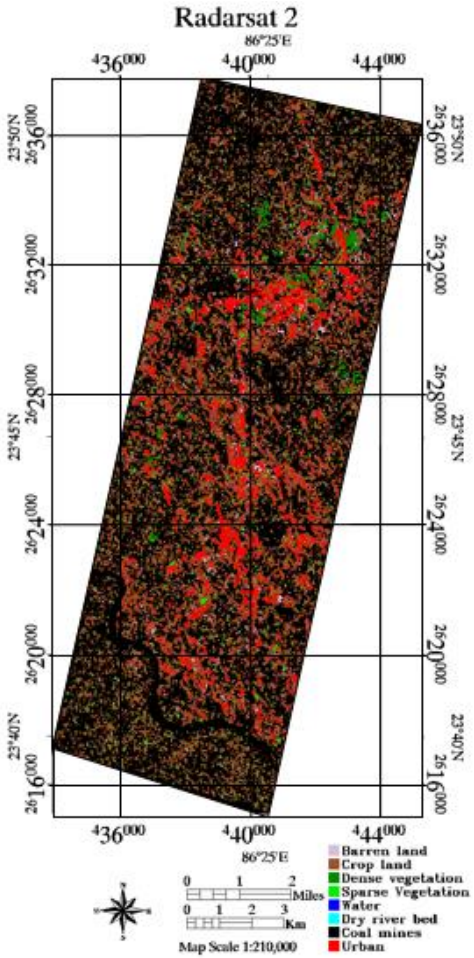

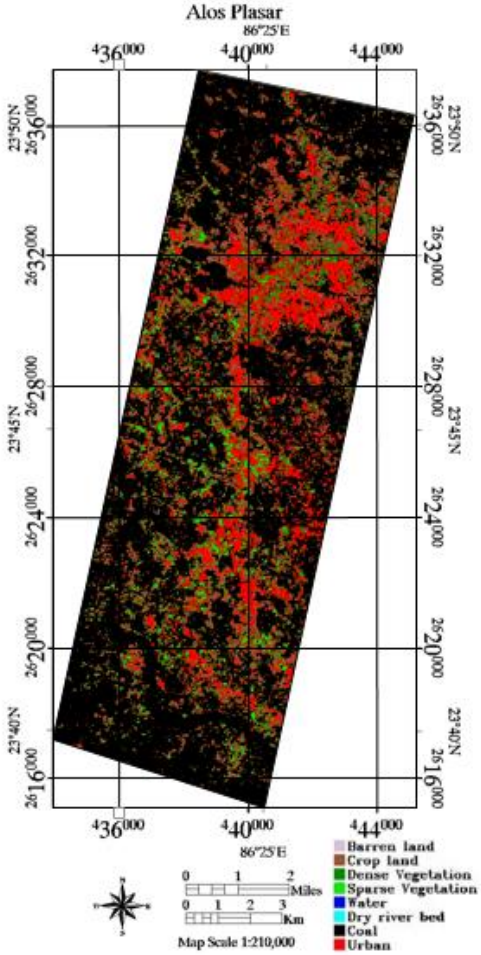

Barren land | Crop land | Dense Veg. | Sparseveg. | Water | Dry river bed | Coal mines | Urban

(A) (B) (C)

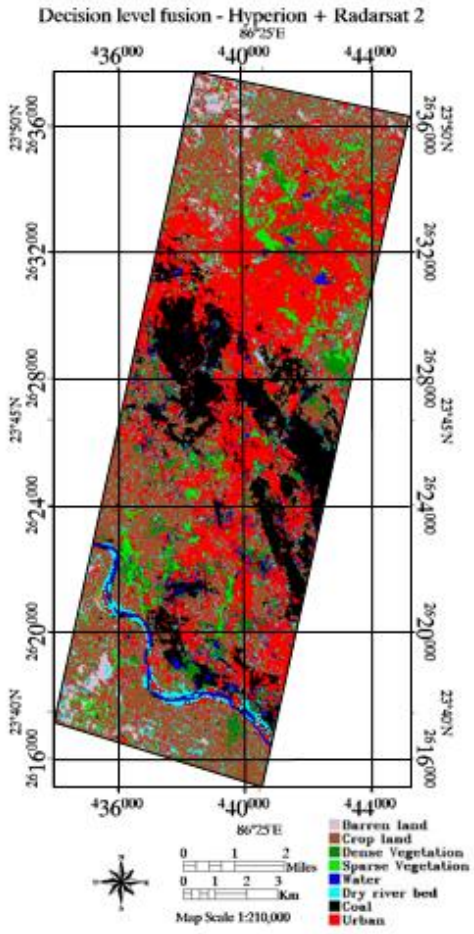

(D)

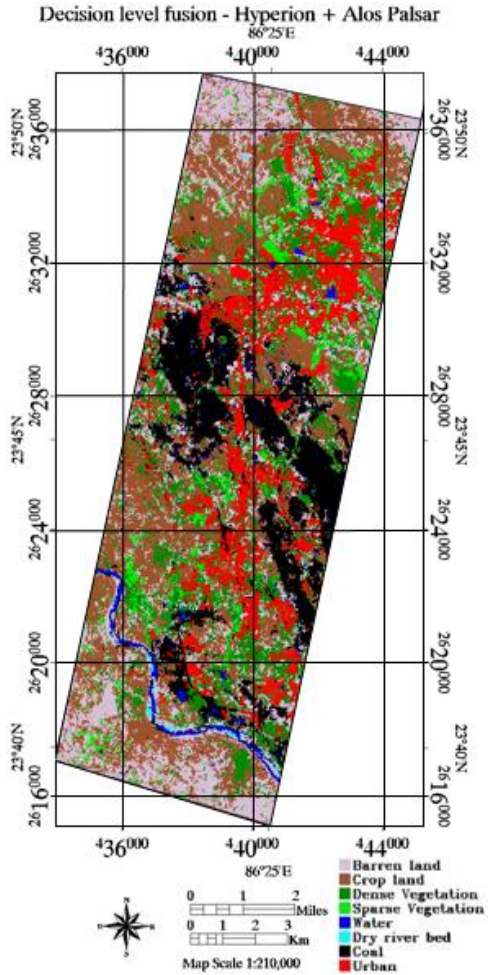

(E)

Barren land | Crop land | Dense Veg. | Sparse veg. | Water | Dry river bed | Coal mines | Urban

Figure 5-15 Decision level fusion- (A)-Hyperion, (B)-Radarsat 2, (C)-ALOS PALSAR, (D)-Hyperion+Radarsat 2, (E)-Hyperion+ALOS PALSAR

Table 5-3 Summary of the classification parameters, and the accuracy assessment – Decision level fusion (Hyperion + Radarsat 2

Data set / Classification parameters and Accuracy	Hyperion	Radarsat 2			Decision level fusion		
Kernel	RBF	Poly	RBF	Sigmoid	Poly	RBF	Sigmoid
C-Parameter	100	230	470	530	210	320	510
Gamma	0.75	0.35	1	0.25	0.9	0.65	0.9
Degree	NA	2	NA	NA	2	NA	NA
Coeff0	NA	5	NA	5	5	NA	5
Total Support Vectors	385	474	557	498	642	723	694
Overall Accuracy	66.599	39.641	38.499	36.723	61.253	67.521	48.443
Kappa Value	0.565	0.279	0.281	0.253	0.521	0.584	0.41

Table 5-4 Summary of the classification parameters, and the accuracy assessment – Decision level fusion (Hyperion + ALOS PALSAR)

Data set / Classification parameters and Accuracy	Hyperion	Alos Palsar			Decision level fusion		
Kernel	RBF	Poly	RBF	Sigmoid	Poly	RBF	Sigmoid
C-Parameter	100	320	380	420	290	260	390
Gamma	0.75	0.6	0.45	0.1	0.9	0.85	0.65
Degree	NA	2	NA	NA	2	NA	NA
Coeff0	NA	5	NA	5	5	NA	5
Total Support Vectors	385	847	970	926	774	903	842
Overall Accuracy	66.599	43.331	42.301	34.127	60.584	68.085	49.213
Kappa Value	0.565	0.376	0.332	0.225	0.51	0.623	0.412

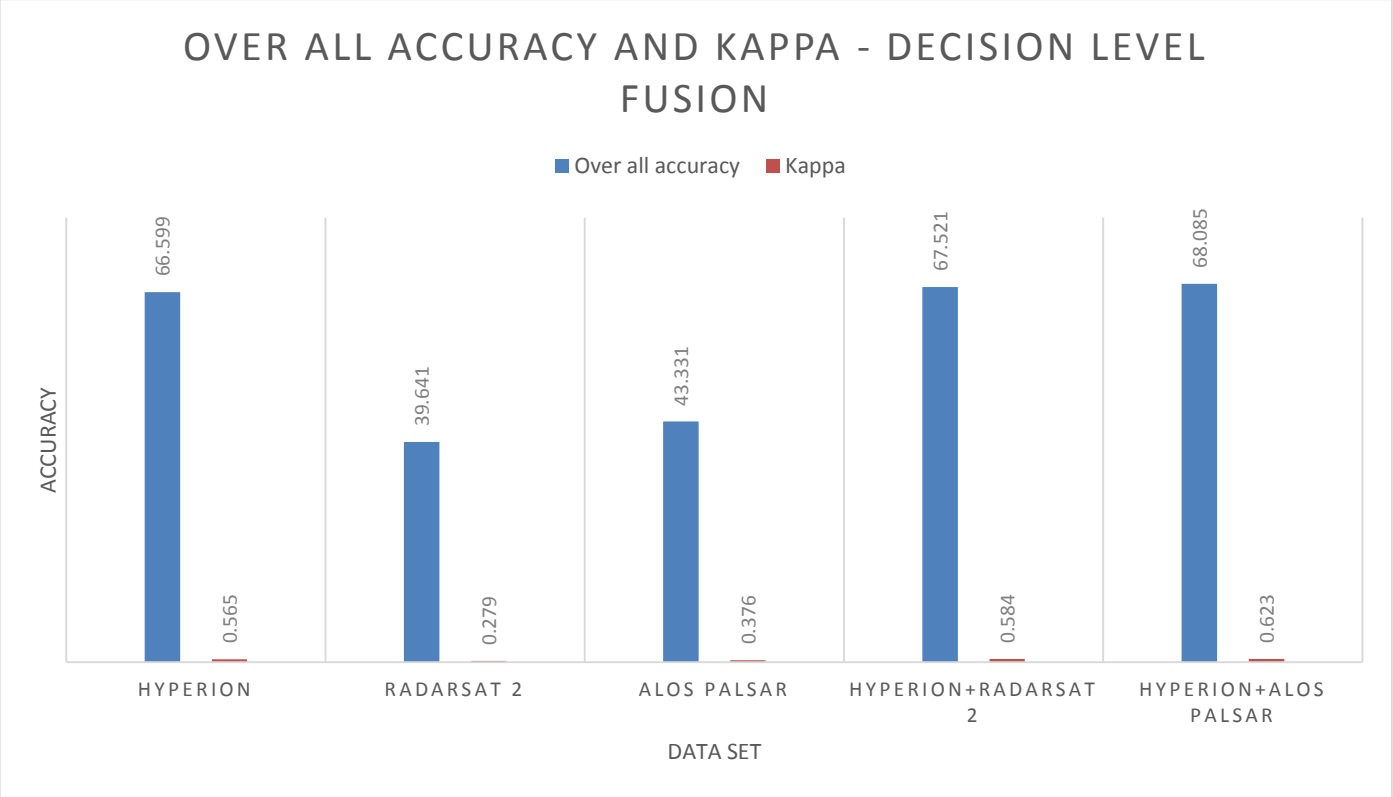

Figure 5-16 Comparison of overall accuracy and kappa - Decision level fusion

Figure 5-17 and Figure 5-18 shows the user and producer class accuracies for the defined classes at decision level fusion.

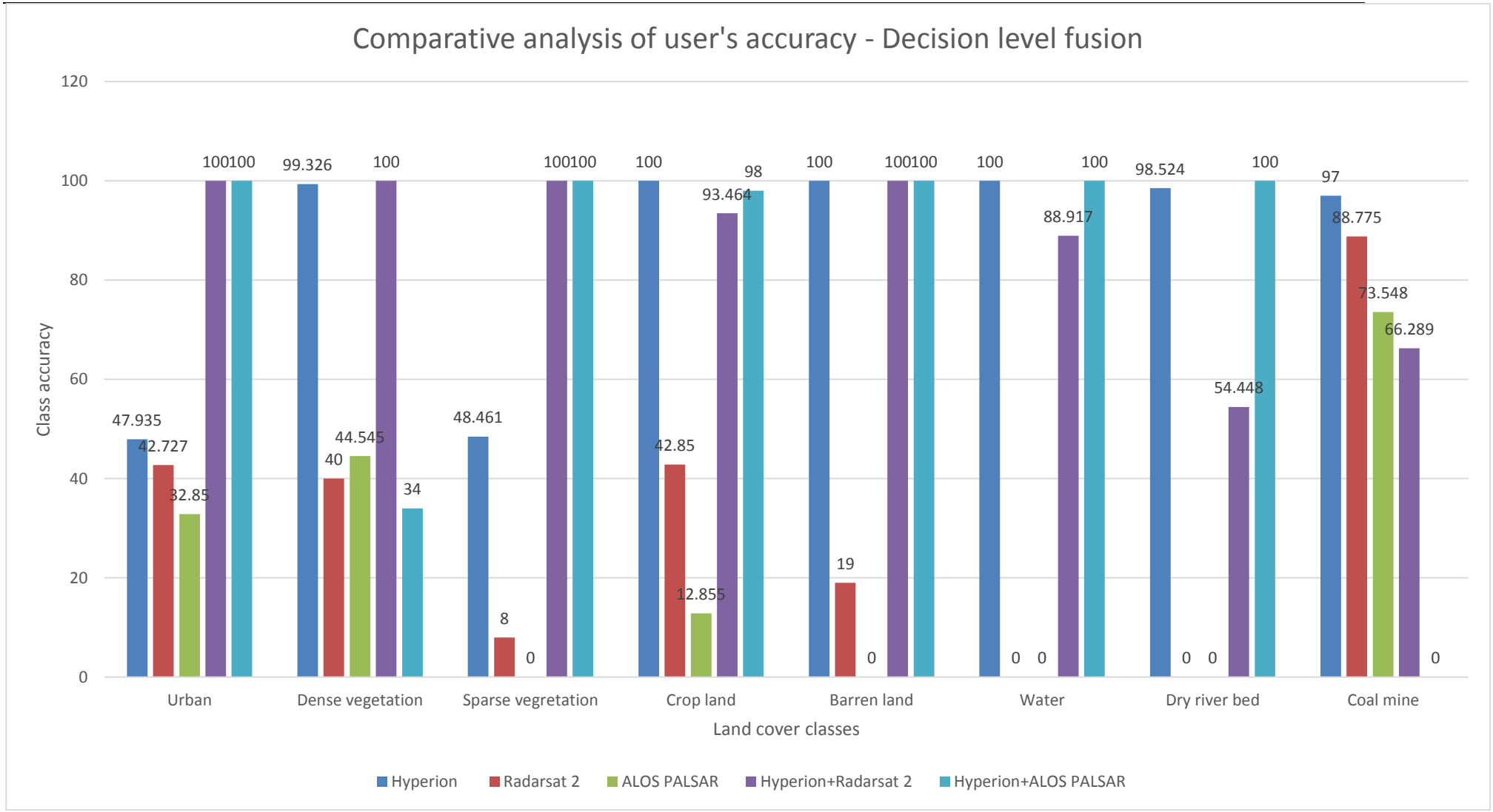

Figure 5-17 User's accuracies of the defined classes from the classified outputs of the Hyperion, Radarsat 2, ALOS PALSAR and Decision level fused products

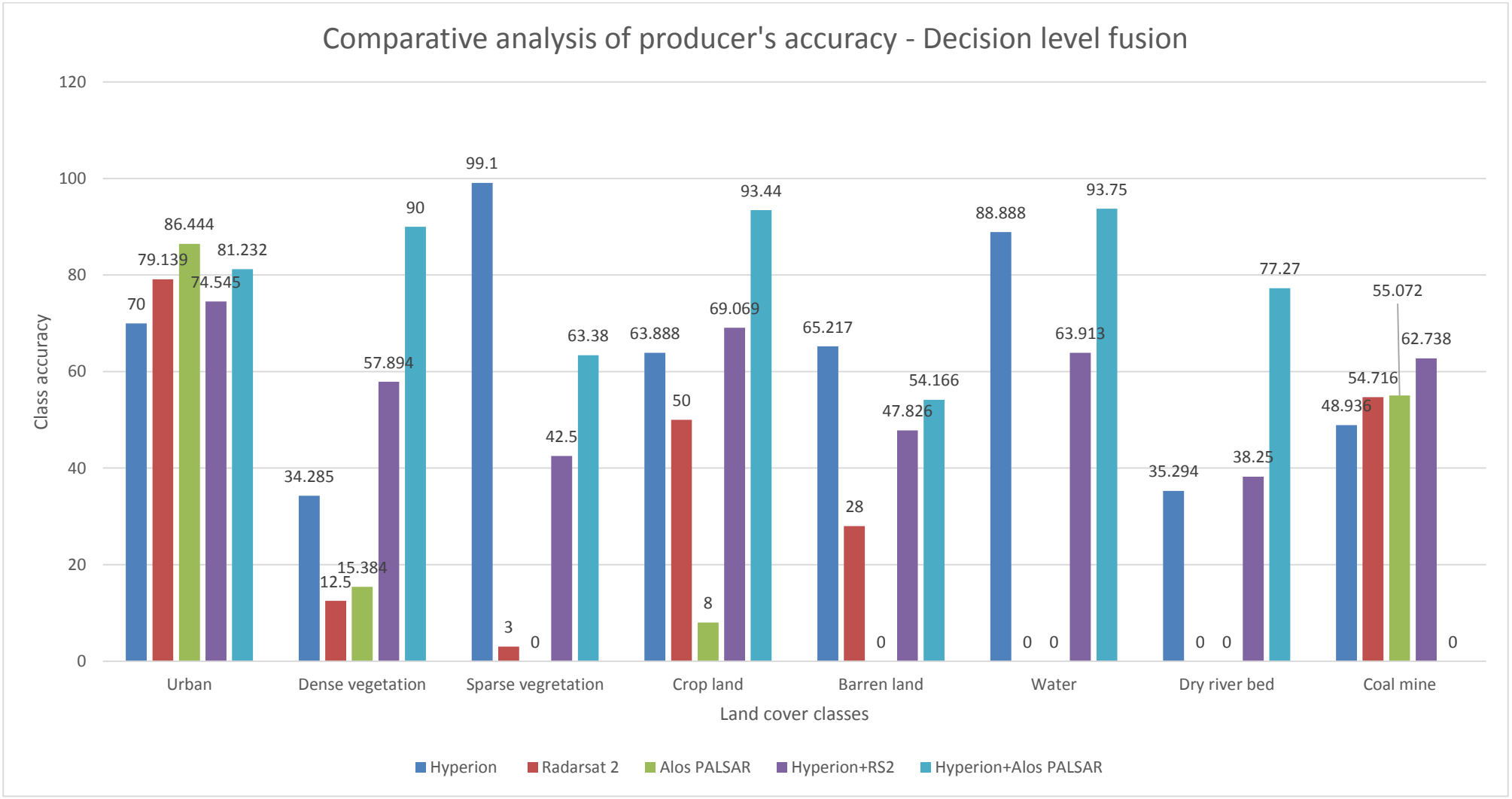

Figure 5-18 Producer's accuracies of the defined classes from the classified outputs of the Hyperion, Radarsat 2, ALOS PALSAR and Decision level fused products

5.1.4. Results of the comparative analysis of all the three levels of fusion

From the above obtained results of the three levels of fusion, the optimal combination of the fusion pair was chosen from each of the levels and then compared. The optimal pair was selected based on the overall accuracy and kappa. From the pixel level fusion technique, the optimal fusion pair was found to be Hyperion and Radarsat 2 for the high pass filter fusion technique. Similarly, for the feature level fusion and the decision level fusion, it was Hyperion and Radarsat 2. Figure 5-21 shows the comparative analysis overall accuracy and kappa at all the three fusion levels.

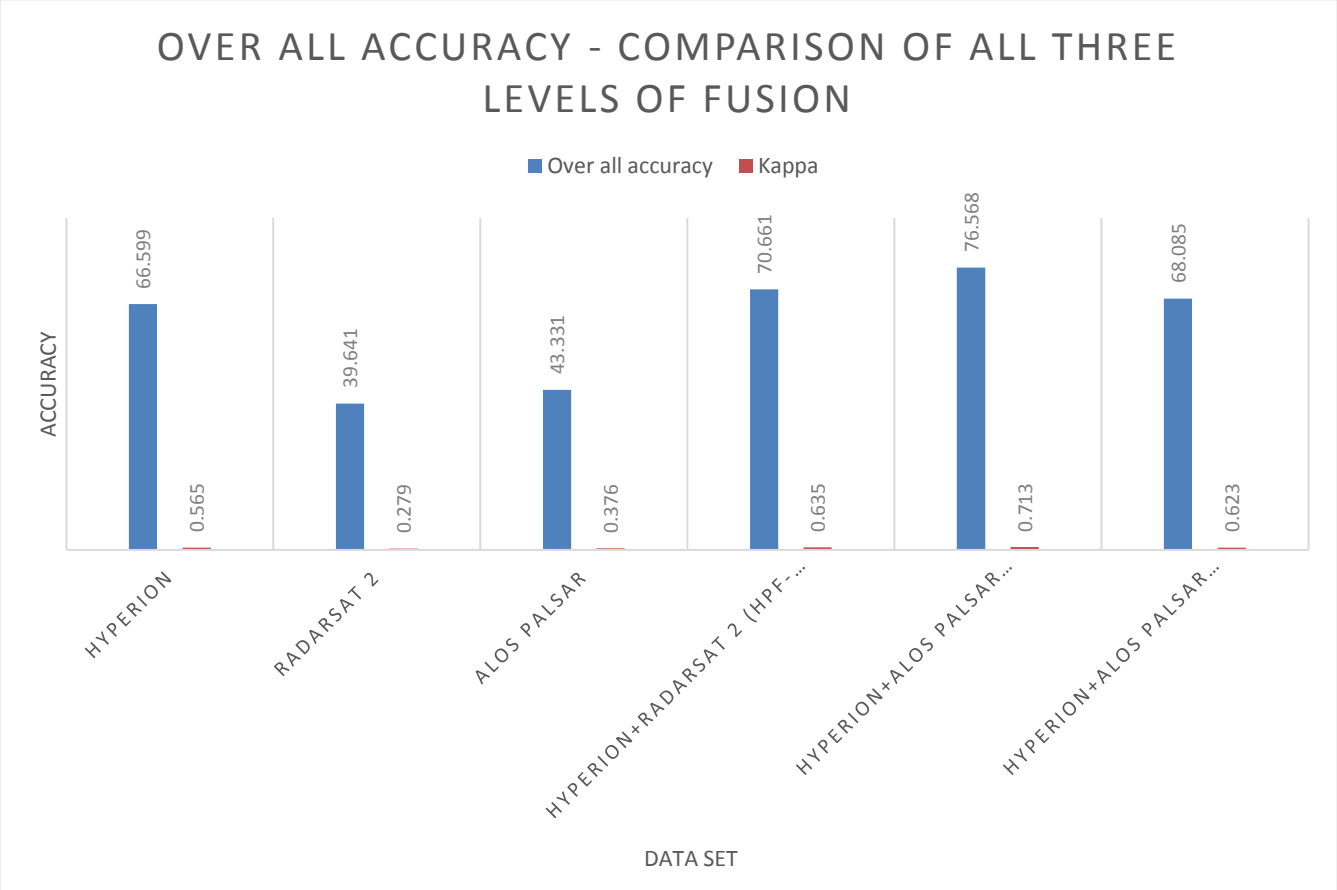

Figure 5-19 Comparison of overall accuracy and kappa - All three levels of fusion

Figure 5-20 and Figure 5-21 represents the individual class accuracies at all three fusion levels

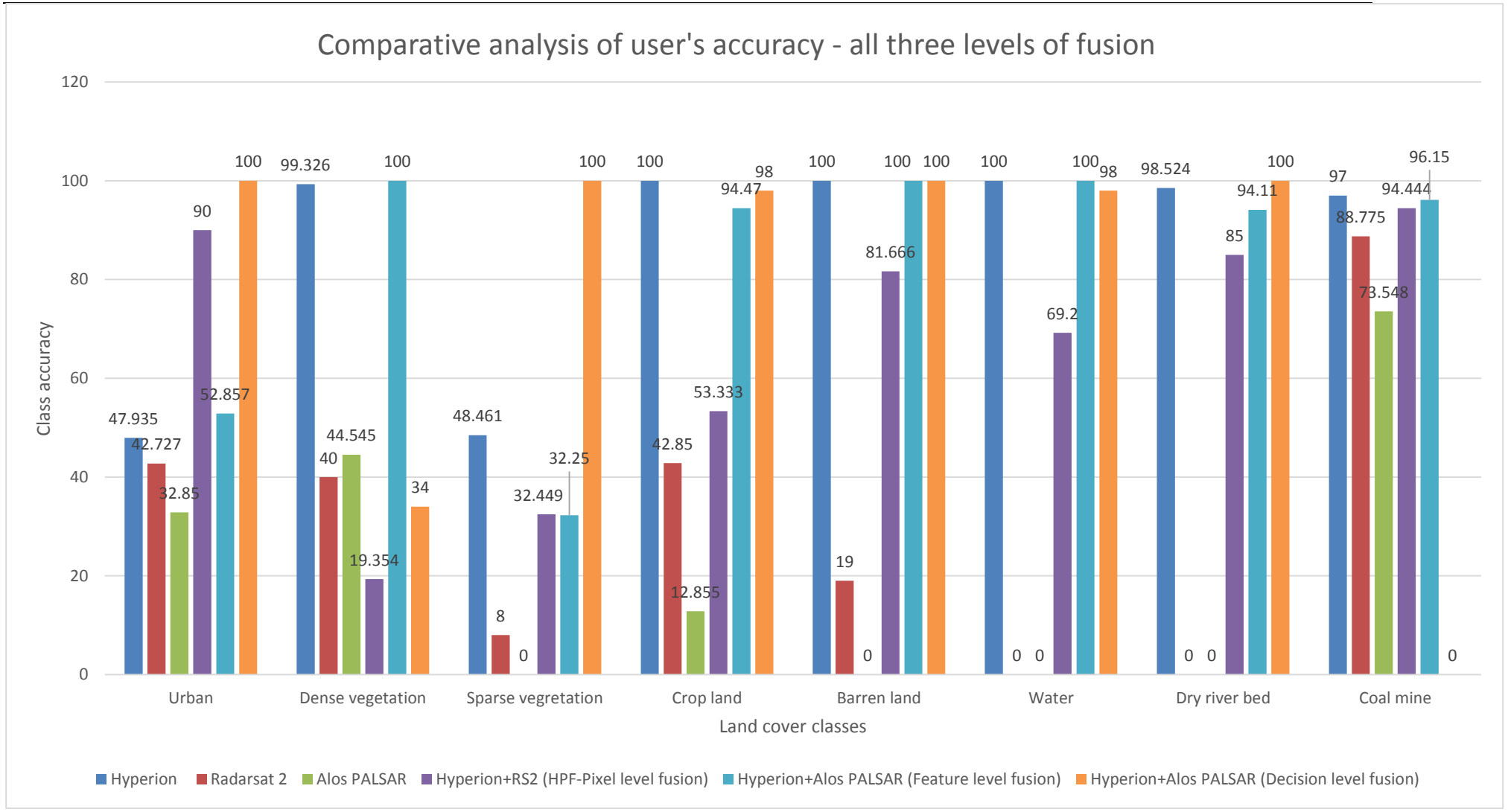

Figure 5-20 Userr's accuracies of the defined classes from the classified outputs of the Hyperion, Radarsat 2, ALOS PALSAR and fused products at all three levels of fusion

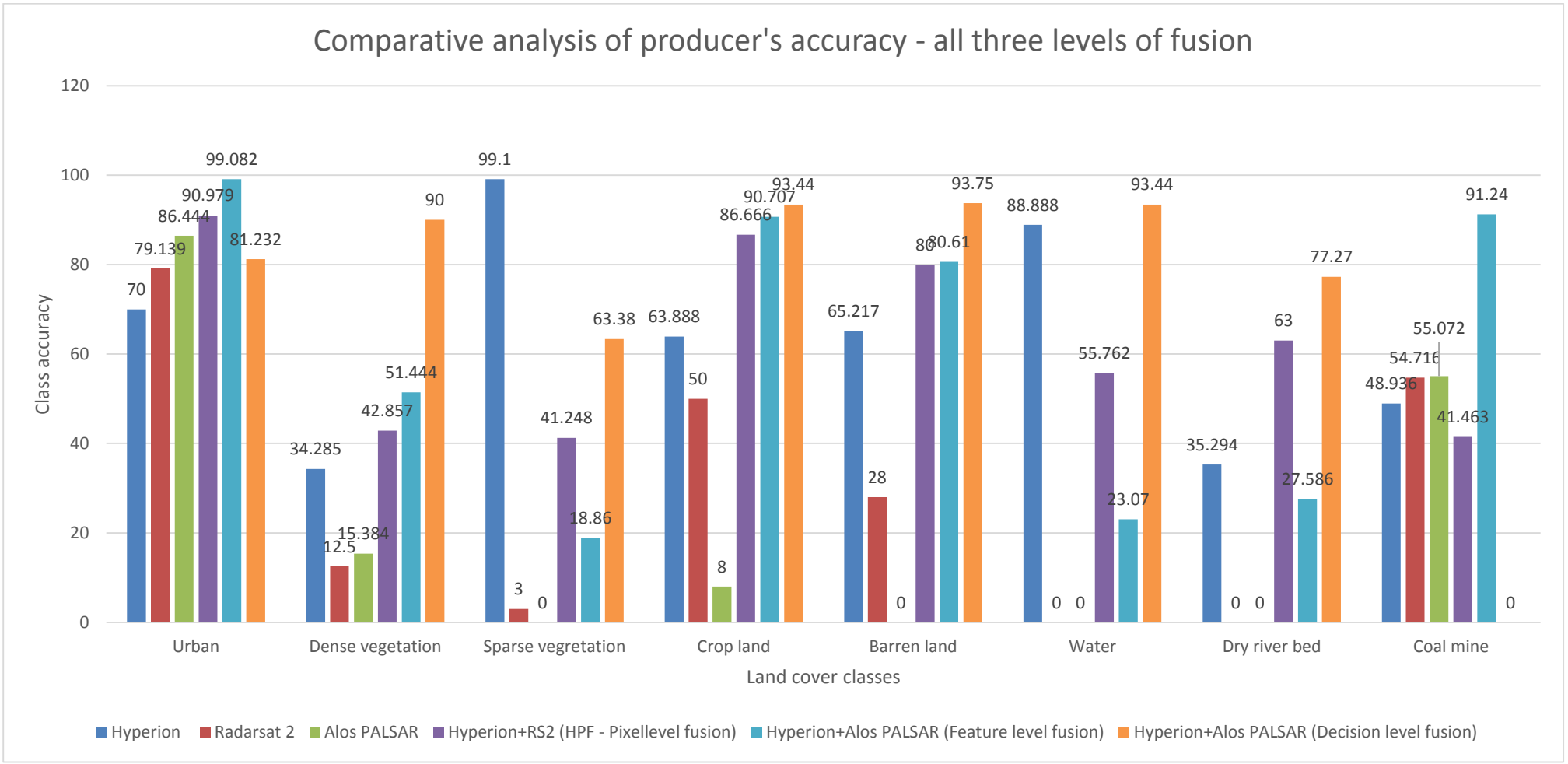

Figure 5-21 Producer's accuracies of the defined classes from the classified outputs of the Hyperion, Radarsat 2, ALOS PALSAR and fused products at all three levels of fusion

5.2. Discussion

This section deals with the discussions on the obtained results at pixel level, feature level and decision level fusions and the comparison of all three levels of fusion

5.2.1. Discussion on pixel level fusion results

The three pixel level fusion techniques namely the wavelet fusion, High pass filter fusion and Gram-Schmidt fusion were chosen because these techniques are highly suitable for preserving the natural spectral properties of the original Hyperion image and also improving the spatial resolution. Similarly, all the three fusion techniques have their own limitations. In case of wavelet resolution merge, due to the decomposition of the higher resolution image during the discrete wavelet transformation, the spatial distortion occurs in the fused image. In Gram-Schmidt fusion, it forms a low resolution grey scale image from the high resolution grey scale image and according to literature this method performs well for single sensor fusion. But it was used for this research to check how the fusion performs for the mentioned datasets. In the case of High pass filter fusion, the most important advantage is that it preserves the spectral properties of the original optical image. But in the case of higher spatial resolution, there are distortions in the spectral properties due to the improper selection of the parameters such as the kernel center value, filter size and added the weight of the high pass filtered image. A detail discussions on the pixel level fusion results are made below:

Based on the obtained results, it was observed that the high pass filter fusion of Hyperion and Radarsat 2 images (Figure 5-2 (D)) gave a better result in terms of overall accuracy and kappa value (Table 5-1) when compared with original Hyperion image and other fusion results. There was an improvement of around 3 % in the overall accuracy of the HPF fused image when compared with the original Hyperion image. To a certain extent the high pass filter fusion of ALOS PALSAR and Hyperion (Figure 5-2 (E)) improved the classification accuracy by 0.7 %. Also, the Kappa value of the high pass filter fusion of both Radarsat 2 and ALOS PALSAR images were better when compared with the other fused results. The main reason could be due to the ability of the fusion technique to preserve the spectral properties of the original Hyperion image with a minimal spatial distortions. The results of the accuracy assessment of the pixel level fusion is given in the Table 5-1.

In the case of Gram-Schmidt fusion, the results were comparatively poor which could be due to the multi-sensor fusion and overall accuracies of both Hyperion+Radarsat2 and Hyperion + ALOS PALSAR reduced by 14 % (Table 5-1). The classified images are shown in the Figure 5-2 (G and H).

It was found that the wavelet resolution merge for both the pairs provided nearly the same results and did not affect much in the improvement of the overall accuracy and kappa value(Table 5-1) when compared with the original Hyperion classified image. Also, one of the important observation was that there was spatial distortion in the fused image. This could be one of the reasons for the reduced classification accuracy.

Accuracy of the classification not only depend on the overall accuracy and kappa values. It also depends on the individual class accuracies. In different fused datasets some of the classes have showed an improved and better user and producer accuracy when compared with the other (Figure 5-4 & 5-5). Due to the longer penetration capability of Alos PALSAR, though the wavelet fusion of Hyperion and Alos PALSAR provided a slightly lesser accuracy when compared with Hyperion, the class accuracy of dense forest was much better than the other products. In case of barren land, due to surface scattering and high penetration power of Alos PALSAR the fusion with Hyperion gave a better interpretation of barren land region (Figure 5-2 B & D) Also the producer accuracy of the same class in Hyperion and Alos PALSAR fusion showed an improvement when compared with the other datasets (Figure 5-4 & 5-5). Due to the less penetration power of Radarsat 2 the sparse vegetation which includes the shrubs and grass lands showed a better producer accuracy in wavelet and HPF when compared with the other fused products but not better than Hyperion. Another important observation was in the case of dry river bed. Due to high penetration power of Alos PALSAR the dry river bed showed an improvement in the accuracy in wavelet and HPF fusion. Therefore due to the high spectral property of Hyperspectral the urban and dry river bed was able to get differentiated. The urban class showed a much better improvement in Radarsat 2 fusion with Hyperion using HPF. In case of cropland class the Radarsat 2 fusion with Hyperion using HPF and Alos PALSAR fusion with Hyperion using HPF and wavelet showed improvement in producer accuracies (Figure 5-5). But according to previous studies, the Radarsat 2 is better for crop land identification when compared with Alos PALSAR. But in this research, since the datasets acquired were consisting of harvested crop land both Radarsat 2 and Alos PALSAR fusion showed accuracy improvement.

Overall HPF fusion using Radarsat 2 and Hyperion gave an improved overall accuracy and Kappa value when compared with original Hyperion. The accuracy of RS2+Hyperion (HPF) was only slightly better by around 3% when compared with the Radarsat2 and Alos PALSAR (HPF). But when analysed on the individual class accuracies each of the fused product except the Gram Schmidt have some advantage in extracting information about each classes. Though there were only few percent of increase in the overall accuracy when compared with original Hyperion the individual class accuracies are important to obtain more information which were inferred in the fused products. One more important point here is that the accuracies of the fused products were compared with the original low spectral resolution Hyperion image and not with the SAR as the SAR data sets used were grey scale images and were not classified. Generally from the literatures, in case of pixel level fusion the classification accuracy of the fused product was compared only with the high spectral resolution image and not with the high spatial resolution PAN or the grey scale image.

Next section is about the discussions on the results obtained at feature level fusion.

5.2.2. Discussion on feature level fusion results

The results of feature level fusion were obtained through the information fusion of the extracted features Hyperion through kernel based principle component analysis (Figure 5-6) and SAR datasets through MCSM decomposition (Figure 5-7 and Figure 5-8). The feature vectors (Hyperion+Radarsat 2 and Hyperion + ALOS PALSAR) formed are shown in the Figure 5-9 (A and B). Classification after the information fusion of Hyperion+ RS2 and Hyperion+ ALOS PALSAR, have resulted in the increase in overall accuracy and kappa (Table 5-2). The classified images are given in the Figure 5-10 (D and E). There is an improvement of around 10 %and 33 % in the overall accuracy of Hyperion + ALOS PALSAR fusion when compared with the individual datasets namely the Hyperion and ALOS PALSAR. In the case of the other pair, there is around 7% and 36% improvement n in the overall accuracy in comparison with Hyperion and Radarsat 2 (Table 5-2). In the case of class accuracies, the urban class accuracy (both producer's and user's accuracy) was improved from the fusion of RS2 with Hyperion and ALOS PALSAR with Hyperion the fusion with ALOS PALSAR when compared with the individual datasets. The main reason could be the MCSM decomposition technique used for the extraction of features in SAR datasets. This decomposition technique is capable of extracting the urban region from the fully polarimetric data. The individual class accuracies of the dense vegetation and sparse vegetation also showed a good improvement in the case of Hyperion + ALOS PALSAR and Hyperion + Radarsat 2 respectively. A reason could be due to the high penetration power of ALOS PALSAR the dense vegetation could have been classified correctly. Since Radarsat 2 has a low penetration power the sparse vegetation is better in the fusion of latter. Due to the surface scattering which is prominent in the moderately rough surface regions, there was an increase in the both producer's and the user's accuracy of barren land in both the information fusion of Hyperion with RS2 and ALOS PALSAR. Also, the coal mining regions were classified, and the accuracy was improved which could also be due to the surface scattering parameter. The results of the accuracy assessment are given in the Table 5-2

Main reasons for the above results could be the feature extraction, in particular, the kernel based non-linear transformation of the Hyperion data played a significant role in improving the overall accuracy and also some of the class accuracies of the classified feature vectors namely the water and dry river bed which were not classified correctly in the individual ALOS PALSAR and RS2 images. Also the MCSM decomposition based feature extraction in SAR improved the class accuracy of the urban class.

The accuracies could have been further improved if the classification of the SAR datasets were performed better. Due to the surface scattering property of the coal mines class, dry river bed class, barren land class and also the water class were creating confusion and were miss-classified (Figure 5-10 (B and C)).

Overall the fusion of Hyperion and ALOS PALSAR comparatively gave a better result in terms of overall accuracy and kappa.

Next section is about the discussion on the decision level fusion results.

5.2.3. Discussion on decision level fusion results

In this level of fusion, different kernels such as radial basis function, polynomial and sigmoid were used to classify the Radarsat 2, ALOS PALSAR and the feature vectors of Hyperion + RS2 and Hyperion + ALOS PALSAR. The initial output of this level of fusion was the rule images of RS2, ALOS PALSAR, and the Hyperion images. These are the priori outputs of the SVM classification which consists of the membership values of the each pixel belonging to a particular class. Later the rule images of RS2 and ALOS PALSAR were stacked individually with the Hyperion (Figure 5-14 (A and B)). Second SVM was applied based on the training samples obtained from the stacked rule images and finally the class memberships were decided for each of the pixels. Different parameters such as gamma for RBF kernel, gamma, degree and Coeff0 for polynomial kernel and gamma and degree for sigmoid kernel were chosen based on grid search method on the validation set.

From the obtained results, the decision level fusion significantly improved the classification accuracy of the fused product when compared with the original RS2 and ALOS PALSAR by a greater margin, but very less improvement was found in comparison with Hyperion. It was observed that the ALOS PALSAR and Hyperion fusion was better when compared with Radarsat 2 and Hyperion in terms of overall accuracy and kappa (Table 5-3 & 5-4). The individual classification of the PolSAR images proved less useful in terms of the overall accuracy. The reasons could be due to the similar backscatter range values for coal, barren land, dry river bed and water because of the smooth surface scattering. Highest overall accuracy and kappa was obtained when the polynomial kernel was used for the individual SAR images. In the SVM applied to the feature vectors, it was found that the RBF kernel improved the overall accuracy. The summary of the accuracy results and classification parameters are given in the Table 5-3 & 5-4

In the case of individual class accuracies the urban, cropland, water, coal and dense vegetation classes of the fused images improved in terms of producer's accuracy in comparison with the individual images. The urban class improved due to the MCSM decomposition parameters extracted from PolSAR data. The accuracy of dense vegetation was high in Hyperion and ALOS PALSAR fusion result due to the higher penetration capability of ALOS PALSAR. The comparative analysis of the user and producer accuracies of the individual classes for decision level fusion is shown in the Figure 5-17 and Figure 5-18.
From the obtained results, there was no much improvement in the overall accuracy when compared with Hyperion. The reason could be due to the poor classification of the SAR datasets which were of coarser spatial resolution as well as the classes namely the coal, barren land, dry river bed and the water class were having the same range of backscatter values due to the surface scattering property. This lead to the misclassification of the classes.

Overall the fusion of Hyperion and ALOS PALSAR proved to be better in comparison with Hyperion and Radarsat which improved the classification accuracy by around 1.5% when compared with Hyperion and

the individual SAR dataset by around 28 % in comparison with Radarsat 2 and 29% in comparison with ALOS PALSAR.

5.2.4. Discussion on the results of the comparative analysis of all the three levels of fusion

Based on the obtained results of all the three levels of fusion, the optimal data pair which gave highest overall accuracy and the kappa at each level of fusion was found to be,

1. Hyperion and Radarsat 2 for the pixel level fusion (Table 5-1)
2. Hyperion and ALOS PALSAR for the feature level fusion (Table 5-2) and
3. Hyperion and ALOS PALSAR for the decision level fusion (Tables 5-3 and 5-4).

Comparative analysis was made in terms of overall accuracy and kappa (Figure 5-19) among the three and the optimal fusion pair along with the level of fusion was obtained. Based on the analysis, the Hyperion and ALOS PALSAR pair have the highest overall accuracy at the feature level of fusion. The overall accuracy obtained was 76.568 % which was greater than the original Hyperion, Radarsat 2. At decision level fusion Hyperion and ALOS PALSAR fusion have the better overall accuracy of around 68%.

The producer's accuracy of coal mines, cropland, and urban classes was improved at feature level fusion of Hyperion and ALOS PALSAR fusion pair (Figure 5-20 & 5-21).
The main reasons for the above obtained results on all three levels of fusion are,

- ✓ Effective feature extraction from both the datasets could have resulted in high accuracy at feature level fusion.
- ✓ The spectral preserving property of HPF is the main reason for improved accuracy at pixel level fusion.
- ✓ Thirdly at decision level, there was no much improvement in accuracy when compared with the original Hyperion and the other fusion levels. This could be due to the improper classification of SAR datasets which resulted in the ineffective decision making process.
- ✓ Coarser resolution of SAR datasets (20 meters resolution) was one of the important factors that had an effect on the obtained results.
- ✓ The penetration capability of each ALOS PALSAR and Radarsat 2
- ✓ MCSM decomposition which is prominent in extraction of the urban features but it was less effective in the classification process of the PolSAR datasets.

Above are the discussions on the obtained results using the adopted methodology and the methods.

6. CONCLUSION AND RECOMMENDATION

6.1. Conclusion

Land cover classification is one of the primary applications of the remotely sensed datasets. But due to the coarser spatial resolution or, the less spectral resolution of the space borne sensors, the interpretation of the features becomes difficult and affects the accuracy of classification. Hence, it is necessary to combine the complementary information from multiple sensors for better interpretation and classification. In this study, three levels of fusion namely the pixel level, feature level, and the decision level were performed using Hyperion data which has a high spectral resolution individually with Radarsat 2 C-band and ALOS PALSAR L-band which have a better spatial resolution and also contains polarimetric information. The main objective of this research work was to enhance and improve the land cover classification accuracy by the fusion of dual frequency fully polarimetric SAR and hyperspectral data.

At the pixel level, three fusion techniques namely the Gram-Schmidt, High pass filter and wavelet fusion methods were tested. In the case of feature level fusion Kernel based principal component analysis was used as a feature extraction process in Hyperion and Multi component scattering model decomposition based extraction of features was used in case of polarimetric data and then the information were combined. The OAA strategy of SVM based fusion was performed at decision level where the decisions to combine information from both the sensors were made from the obtained rule images of the individual classes.

Different kernels were tested apart from RBF for non-linear classification using SVM for ALOS PALSAR, Radarsat data and also for the classification of feature vectors at the decision level fusion. It was observed that the polynomial kernel gave a better overall accuracy when compared with the radial basis and sigmoid kernel as shown in the Table 5-5. For Hyperion and fused products classification at the pixel level and the feature vectors classification at feature level, the radial basis function was tested. In the case of accuracy assessment, cross validation based hold out method was performed. There was an increase in accuracy for the fusion of Hyperion and ALOS PALSAR at feature (Table 5-2) and decision level (Table 5-3 and Table 5-4), whereas the fusion of Hyperion and Radarsat 2 with High pass filter fusion gave an improved accuracy at pixel level fusion (Table 5-1).

From the comparative analysis, it was observed that the fusion of Hyperion and ALOS PALSAR L-band fusion at feature level provided an improved classification accuracy when compared to the Hyperion and Radarsat 2 C-band and the individual sources. Also, the kernel based support vector machine classification played a significant role in improving the classification.

6.1.1. Answers to the research questions

1. **How Multicomponent scattering model improves the feature extraction in fully polarimetric data?**

   From the obtained results there were 5 scattering parameters obtained from the MCSM decomposition technique. They are the Surface scattering, Double bounce scattering, Helix scattering, Volume scattering and Wire scattering. This decomposition is mainly for the efficient extraction of urban features as the double bounce scattering, helix scattering, and wire scattering are more prominent in urban regions. Wire scattering is noticeable where there are thin canonical structures, helix scattering is prominent to identify the complex helical structures and the tall buildings give rise to the double bounce scattering. Similarly, the surface scattering parameter identifies the smooth surface scatterers. In this research, the smooth surface scatterers included ere the water bodies, barren land, coal region, and the dry river bed. The volume scattering helps in the identification of the vegetation features. As this model is more suitable for extraction of the urban region, from the individual classification of ALOS PALSAR and Radarsat 2 fully polarimetric data it was found that the urban class gave a more improved class accuracy than the other classes.

2. **Which pixel level fusion technique could give a satisfactory result for fusing hyperspectral data and span data extracted from quadpol data?**

   There were three pixel level fusion techniques implemented namely the High pass filter fusion, Wavelet fusion, and Gram-Schmidt fusion. Among these three, the High pass filter fusion gave a satisfactory result by improving the overall accuracy of the fused product when compared with the original Hyperion image. Also, the spectral properties of the original Hyperion data was preserved to a greater extent in the fused product.

3. **How fusion of fully polarimetric SAR and hyperspectral data efficiently enhance the classification of urban and vegetation cover types?**

   In the case of fusion of multi-sensor data, the sensors must be complementary to each other in providing information about the land cover features. In this research, the Hyperion data consists of a high spectral resolution with a number of contiguous spectral bands. This helps in distinguishing the spectrally similar features. In this study, the spectrally similar classes included the dense vegetation and sparse vegetation, urban features and the dry river bed region. Similarly, the MCSM decomposition performed on the fully polarimetric data provides an enhanced information about the urban feature. Also the co-polarized channels namely the HH and VV enhance the urban features interpretation and cross-polarized channel such as HV and VH are for the interpretation of vegetation features. It is evident from the obtained results that, in many cases the individual class accuracies of urban, sparse vegetation dense vegetation and cropland of the fused products have

shown improved accuracy results when compared with the individual sources. Hence, the fusion of fully polarimetric SAR and hyperspectral can efficiently enhance the urban and vegetation cover types.

4. **Which level of fusion and also which band along with the hyperspectral data can give an enhanced land cover classification?**
   From the obtained results it was observed that the ALOS PALSAR L-band along with the Hyperion data can give an enhanced land cover classification at the feature level fusion. This was concluded based on the overall accuracy and the kappa value obtained after the support vector machines classification.

6.2. Recommendation

It is very important in any research to evaluate the quality of the resultant product. Though there has been an effective improvement in the accuracy of the fused product of Hyperion and ALOS PALSAR at feature level when compared with the individual sources and other levels of fusion, there are few important observations which could be taken into account for the future work. They are,

- ✓ Usage of very high resolution spaceborne polarimetric data and hyperspectral data could improve the fusion performance.
- ✓ Feature selection technique like kernel based Hilbert space independence criterion could be used to select the features based on the defined classes that are relevant for the classification process. This could further improve the performance of feature level fusion.
- ✓ Texture parameters based classification could be done if the polarimetric data is of high spatial resolution. This, in turn, would improve the classification of the individual SAR datasets as well as the performance of decision level fusion.
- ✓ Decision level fusion on the Usage of "One Against One" strategy based SVM classification could improve the decision making and classification accuracy as it performs a pairwise discrimination of each of the classes from the other which does a particular class differentiation. Though it is a time consuming process, it could prove effective in classification and fusion.

7. REFERENCES

Abdikan, S., Balik Sanli, F., Sunar, F., & Ehlers, M. (2012). A comparative data-fusion analysis of multi-sensor satellite images. *International Journal of Digital Earth*, *7*(8), 671–687. http://doi.org/10.1080/17538947.2012.748846

Aiazzi, B., Baronti, S., Selva, M., & Alparone, L. (2006). Enhanced Gram-Schmidt Spectral Sharpening Based on Multivariate Regression of MS and Pan Data. In *2006 IEEE International Symposium on Geoscience and Remote Sensing* (pp. 3806–3809). IEEE. http://doi.org/10.1109/IGARSS.2006.975

Aisen, B. (2006). A Comparison of Multiclass SVM Methods. Retrieved from http://courses.media.mit.edu/2006fall/mas622j/Projects/aisen-project/

Amarsaikhan, D., Blotevogel, H. H., van Genderen, J. L., Ganzorig, M., Gantuya, R., & Nergui, B. (2010). Fusing high-resolution SAR and optical imagery for improved urban land cover study and classification. *International Journal of Image and Data Fusion*, *1*(1), 83–97. http://doi.org/10.1080/19479830903562041

Bigdeli, B., Samadzadegan, F., & Reinartz, P. (2014). A decision fusion method based on multiple support vector machine system for fusion of hyperspectral and LIDAR data. *International Journal of Image and Data Fusion*. Retrieved from http://ezproxy.utwente.nl:2196/doi/full/10.1080/19479832.2014.919964#abstract

Borghys, D., Shimoni, M., Degueldre, G., & Perneel, C. (2007). Improved object recognition by fusion of hyperspectral and SAR data. In *Proceedings 5th EARSeL Workshop on Imaging Spectroscopy. Bruges* (pp. 1–14). Retrieved from http://citeseerx.ist.psu.edu/viewdoc/download?doi=10.1.1.158.1637&rep=rep1&type=pdf

Borghys, D., Shimoni, M., & Perneel, C. (2007). Change detection in urban scenes by fusion of SAR and hyperspectral data. In *Proceedings of SPIE* (Vol. 6749, p. 67490R–67490R–12). http://doi.org/10.1117/12.738767

Bruzzone, L., Persello, C., & Chen, C. H. (2010). APPROACHES BASED ON SUPPORT VECTOR MACHINES TO CLASSIFICATION OF REMOTE SENSING DATA. In *Handbook of Pattern Recognition and Computer Vision* (pp. 329–352). http://doi.org/10.1142/9789814273398_0014

Bruzzone, L., & Serpico, S. B. (2000). A technique for feature selection in multiclass problems. *International Journal of Remote Sensing*, *21*(3), 549–563. http://doi.org/10.1080/014311600210740

Byun, Y. (2014). A texture-based fusion scheme to integrate high-resolution satellite SAR and optical images. *Remote Sensing Letters*, *5*(2), 103–111. http://doi.org/10.1080/2150704X.2014.880817

Chandola, S. (2014). *Polarimetric SAR Interferometry for Forest Aboveground Biomass Estimation*. ITC, University of Twente.

Chen, C.-M., Hepner, G. F., & Forster, R. R. (2003). Fusion of hyperspectral and radar data using the IHS transformation to enhance urban surface features. *ISPRS Journal of Photogrammetry and Remote Sensing*, *58*(1-2), 19–30. http://doi.org/10.1016/S0924-2716(03)00014-5

Dai, C., Huang, X., & Dong, G. (2007). Support Vector Machine for Classification of Hyperspectral Remote Sensing Imagery. In *Fourth International Conference on Fuzzy Systems and Knowledge Discovery, 2007. FSKD 2007* (pp. 77 – 80). http://doi.org/10.1109/FSKD.2007.550

Dong, J., Zhuang, D., Huang, Y., & Fu, J. (2009). Advances in multi-sensor data fusion: Algorithms and applications. *Sensors*. http://doi.org/10.3390/s91007771

Ehlers, M. (1991). Multisensor image fusion techniques in remote sensing. *ISPRS Journal of Photogrammetry and Remote Sensing*, *46*(1), 19–30. http://doi.org/10.1016/0924-2716(91)90003-E

Fauvel, M., Chanussot, J., & Benediktsson, J. (2006). Kernel Principal Component Analysis for Feature Reduction in Hyperspectrale Images Analysis. In *Proceedings of the 7th Nordic Signal Processing Symposium - NORSIG 2006* (pp. 238–241). IEEE. http://doi.org/10.1109/NORSIG.2006.275232

Fukuda, S., Hirosawa, H., & Ieee, I. (2001). *Support vector machine classification of land cover: Application to polarimetric SAR data. Igarss 2001: Scanning the Present and Resolving the Future, Vols 1-7, Proceedings*. http://doi.org/10.1109/IGARSS.2001.976097

Gamba, P. (2013). Image and data fusion in remote sensing of urban areas: status issues and research trends. *International Journal of Image and Data Fusion*, *5*(1), 2–12. http://doi.org/10.1080/19479832.2013.848477

Ghanbari, Z., & Sahebi, M. R. (2014). Improved IHS Algorithm for Fusing High Resolution Satellite Images of Urban Areas. *Journal of the Indian Society of Remote Sensing*, *42*(4), 689–699. http://doi.org/10.1007/s12524-014-0364-x

Giampouras, P., Charou, E., & Kesidis, A. (2013). Artificial Neural Network Approach for Land Cover Classification of Fused Hyperspectral and Lidar Data. In H. Papadopoulos, A. S. Andreou, L. Iliadis, & I. Maglogiannis (Eds.), *Artificial Intelligence Applications and Innovations* (Vol. 412, pp. 255–261). Springer Berlin Heidelberg. http://doi.org/10.1007/978-3-642-41142-7_26

Gonzalez, R. C., & Woods, R. E. (2001). Digital Image Processing. Retrieved from http://dl.acm.org/citation.cfm?id=559707

Hadjimitsis, D. G., Papadavid, G., Agapiou, A., Themistocleous, K., Hadjimitsis, M. G., Retalis, A., … Clayton, C. R. I. (2010). Atmospheric correction for satellite remotely sensed data intended for agricultural applications: impact on vegetation indices. *Natural Hazards and Earth System Science*, *10*(1), 89–95. http://doi.org/10.5194/nhess-10-89-2010

Huang, X., Zhang, L., & Li, P. (2008). A multiscale feature fusion approach for classification of very high resolution satellite imagery based on wavelet transform. *International Journal of Remote Sensing*, *29*(20), 5923–5941. http://doi.org/10.1080/01431160802139922

Kiema, J. B. K. (2002). Texture analysis and data fusion in the extraction of topographic objects from satellite imagery. *International Journal of Remote Sensing*, *23*(4), 767–776. http://doi.org/10.1080/01431160010026005

Klonus, S., & Ehlers, M. (2007). Image Fusion Using the Ehlers Spectral Characteristics Preservation Algorithm. *GIScience & Remote Sensing*, *44*(2), 93–116. http://doi.org/10.2747/1548-1603.44.2.93

Klonus, S., & Ehlers, M. (2009). Information Fusion, 2009. FUSION '09. 12th International Conference on. *Information Fusion, 2009. FUSION '09. 12th International Conference on*.

Knödel, K., Lange, G., Voigt, H.-J., Abel, T., Tejedo, A., & Toloczyki, M. (2007). Data Fusion. In *Environmental Geology* (pp. 1053–1098). Berlin, Heidelberg: Springer Berlin Heidelberg. http://doi.org/10.1007/978-3-540-74671-3

Kohavi, R. (1995). A study of cross-validation and bootstrap for accuracy estimation and model selection, 1137–1143. Retrieved from http://dl.acm.org/citation.cfm?id=1643031.1643047

Lamei Zhang, Bin Zou, Hongjun Cai, & Ye Zhang. (2008). Multiple-Component Scattering Model for Polarimetric SAR Image Decomposition. *IEEE Geoscience and Remote Sensing Letters*, *5*(4), 603–607. http://doi.org/10.1109/LGRS.2008.2000795

Li, H., Manjunath, B. S., & Mitra, S. K. (1995). Multisensor Image Fusion Using the Wavelet Transform. *Graphical Models and Image Processing*, *57*(3), 235–245. http://doi.org/10.1006/gmip.1995.1022

Li, S., Kwok, J. T., & Wang, Y. (2002). Using the discrete wavelet frame transform to merge Landsat TM and SPOT panchromatic images. *Information Fusion*, *3*(1), 17–23. http://doi.org/10.1016/S1566-2535(01)00037-9

Li, T., Zhang, J., Zhao, H., & Shi, C. (2013). Classification-oriented hyperspectral and PolSAR images synergic processing. In *2013 IEEE International Geoscience and Remote Sensing Symposium - IGARSS* (pp. 1035–1038). IEEE. http://doi.org/10.1109/IGARSS.2013.6721340

Lu, D., Li, G., Moran, E., Dutra, L., & Batistella, M. (2011). A Comparison of Multisensor Integration Methods for Land Cover Classification in the Brazilian Amazon. *GIScience & Remote Sensing*, *48*(3), 345–370. http://doi.org/10.2747/1548-1603.48.3.345

Melgani, F., & Bruzzone, L. (2002). Support vector machines for classification of hyperspectral remote-sensing images. *IEEE International Geoscience and Remote Sensing Symposium*, *1*(5), 506–508. http://doi.org/10.1109/IGARSS.2002.1025088

Melgani, F., & Bruzzone, L. (2004). Classification of hyperspectral remote sensing images with support vector machines. *IEEE Transactions on Geoscience and Remote Sensing*, *42*(8), 1778–1790. http://doi.org/10.1109/TGRS.2004.831865

Meng, Q., Borders, B., & Madden, M. (2010). High-resolution satellite image fusion using regression kriging. *International Journal of Remote Sensing*, *31*(7), 1857–1876. http://doi.org/10.1080/01431160902927937

Metwalli, M. R., Nasr, A. H., Allah, O. S. F., El-Rabaie, S., & Abd El-Samie, F. E. (2010). Satellite image fusion based on principal component analysis and high-pass filtering. *Journal of the Optical Society of America. A, Optics, Image Science, and Vision*, *27*(6), 1385–94. http://doi.org/10.1364/JOSAA.27.001385

Metwalli, M. R., Nasr, A. H., Farag Allah, O. S., & El-Rabaie, S. (2009). Image fusion based on principal component analysis and high-pass filter. In *2009 International Conference on Computer Engineering & Systems* (pp. 63–70). IEEE. http://doi.org/10.1109/ICCES.2009.5383308

Mountrakis, G., Im, J., & Ogole, C. (2011). Support vector machines in remote sensing: A review. *ISPRS Journal of Photogrammetry and Remote Sensing*, *66*(3), 247–259. http://doi.org/10.1016/j.isprsjprs.2010.11.001

Peli, T., Young, M., Knox, R., Ellis, K. K., & Bennett, F. (1999). Feature-level sensor fusion. In *AeroSense '99* (pp. 332–339). http://doi.org/10.1117/12.341355

Persello, C., & Bruzzone, L. (2015). Kernel-Based Domain-Invariant Feature Selection in Hyperspectral Images for Transfer Learning. *IEEE Transactions on Geoscience and Remote Sensing*. http://doi.org/10.1109/TGRS.2015.2503885

Pohl, C., Munro, D., & van Genderen, J. L. (1997). Enhanced image analysis through multilevel data fusion techniques. In I. Kadar (Ed.), (pp. 32–39). http://doi.org/10.1117/12.280821

Pohl, C., & van Genderen, J. (2014). Remote sensing image fusion: an update in the context of Digital Earth. *International Journal of Digital Earth*, *7*(2), 158–172. http://doi.org/10.1080/17538947.2013.869266

Pohl, C., & van Genderen, J. (2015). Structuring contemporary remote sensing image fusion. *International Journal of Image and Data Fusion*, *6*(1), 3–21. http://doi.org/10.1080/19479832.2014.998727

Pohl, C., & Van Genderen, J. L. (1998a). Review article Multisensor image fusion in remote sensing: Concepts, methods and applications. *International Journal of Remote Sensing*. http://doi.org/10.1080/014311698215748

Pohl, C., & Van Genderen, J. L. (1998b, January 25). Review article Multisensor image fusion in remote sensing: Concepts, methods and applications. *International Journal of Remote Sensing*. Taylor & Francis Group. http://doi.org/10.1080/014311698215748

Rani Sheela, C. M., Vijayakumar, V., & Sujatha, B. (2012). An Efficient Block based Feature Level Image Fusion Technique using Wavelet Transform and Neural Network. *International Journal of Computer Applications*, *Volume 52*.

Scholkopf, B., & Smola, A. (2002). Support Vector Machines and Kernel Algorithms.

Schölkopf, B., Smola, A., & Müller, K.-R. (1997). Kernel principal component analysis. In *Artificial Neural Networks — ICANN'97* (pp. 583–588). http://doi.org/10.1007/BFb0020217

Swain, P. H., & Davis, S. M. (1981). Remote Sensing: The Quantitative Approach. *IEEE Transactions on Pattern Analysis and Machine Intelligence*, *PAMI-3*(6), 713–714. http://doi.org/10.1109/TPAMI.1981.4767177

Townshend, J., Justice, C., Li, W., Gurney, C., & McManus, J. (1991). Global land cover classification by remote sensing: present capabilities and future possibilities. *Remote Sensing of Environment*, *35*(2-3), 243–255. http://doi.org/10.1016/0034-4257(91)90016-Y

Verma, R. (2014). *polarimetric decomposition based on general characterization of scattering from urban areas and multiple component scattering model*. ITC, University of Twente. Retrieved from https://www.itc.nl/library/papers_2012/msc/gfm/verma.pdf

Wang, J., Li, C., & Gong, P. (2015). Adaptively weighted decision fusion in 30 m land-cover mapping with Landsat and MODIS data. *International Journal of Remote Sensing*, *36*(14), 3659–3674. http://doi.org/10.1080/01431161.2015.1047049

Waske, B., & Benediktsson, J. A. (2007). Fusion of Support Vector Machines for Classification of Multisensor Data. *IEEE Transactions on Geoscience and Remote Sensing*, *45*(12), 3858–3866. http://doi.org/10.1109/TGRS.2007.898446

Waske, B., Menz, G., & Benediktsson, J. A. (2007). Fusion of support vector machines for classifying SAR and multispectral imagery from agricultural areas. In *2007 IEEE International Geoscience and Remote Sensing Symposium* (pp. 4842–4845). IEEE. http://doi.org/10.1109/IGARSS.2007.4423945

Waske, B., & van der Linden, S. (2008). Classifying Multilevel Imagery From SAR and Optical Sensors by Decision Fusion. *IEEE Transactions on Geoscience and Remote Sensing*, *46*(5), 1457–1466. http://doi.org/10.1109/TGRS.2008.916089

Woodhouse, I. H. (2012). Polarimetric radar imaging: from basics to applications by Jong-Sen Lee and Eric Pottier. *International Journal of Remote Sensing*, *33*(1), 333–334. http://doi.org/10.1080/01431161.2010.519925

Wu, D., Yang, A., Zhu, L., & Zhang, C. (2014). *Life System Modeling and Simulation*. (S. Ma, L. Jia, X. Li, L. Wang, H. Zhou, & X. Sun, Eds.)*International Conference on Life System Modeling and Simulation and International Conference on Intelligent Computing for Sustainable Energy and Environment* (Vol. 461). Berlin, Heidelberg: Springer Berlin Heidelberg. http://doi.org/10.1007/978-3-662-45283-7

Xiaochen Lu, & Junping Zhang. (2014). Panchromatic and multispectral images fusion based on modified GS-SWT. In *2014 IEEE Geoscience and Remote Sensing Symposium* (pp. 2530–2533). IEEE. http://doi.org/10.1109/IGARSS.2014.6946988

Zhang, L., Zou, B., Zhang, J., & Zhang, Y. (2009). An extended multiple-component scattering model for PolSAR images. *International Journal of Remote Sensing*. http://doi.org/10.1080/01431160802653732

Zhao, Q., & Principe, J. C. (2001). Support vector machines for SAR automatic target recognition. *IEEE Transactions on Aerospace and Electronic Systems*, *37*(2), 643–654. http://doi.org/10.1109/7.937475

Zheng, Y., Zhang, J., & Van Genderen, J. L. (1998). COMPARISON AND ANALYSIS OF REMOTE SENSING DATA FUSION TECHNIQUES.